Comparison of the influence of CeYAG and MCM-41 as nanofillers on the properties of polycarbonate and poly(methyl methacrylate)

by

MOTSHABI ALINAH SIBEKO (M.Sc.)

Submitted in accordance with the requirements for the degree of

Philosophiae Doctor (Ph.D.) in Polymer Science

Department of Chemistry

Faculty of Natural and Agricultural Sciences

at the

UNIVERITY OF THE FREE STATE (QWAQWA CAMPUS)

SUPERVISOR: PROF AS LUYT

January 2016

DECLARATION

I, the undersigned, hereby declare that the research in this thesis is my own original work, which has not partly or fully been submitted to any other University in order to obtain a degree.

Sibeko MA (Miss)

DEDICATIONS

This work is dedicated to my late grandfather Tseko Fanyane Sibeko, my parents Matebesi Daniel Sibeko (father) and Mantseki Marie Sibeko (mother) for their understanding, patience, support and love that they showed me in my entire life.

To my lovely sisters and brothers Madika, Mantwa, Matseko, Manakedi, Tello, Tseko, Setjhaba, Manakedi, Mochakela and Tebello Sibeko for always believing in me and supporting me even through the difficult times.

To my nephews and nieces Nthabiseng, Tumelo, Maziya, Refilwe, Kamohelo, Retshidisitswe, Hlohonolofatso, Teboho and Rethabile.

ABSTRACT

This study reports on the morphology of poly(methyl methacrylate) (PMMA) and polycarbonate (PC) filled with mesoporous silica (MCM-41) and cerium doped yttrium aluminum garnet (Ce:YAG) at contents in the range of 0.1 to 5 wt.%. The interactions between the polymer and fillers in these composites, and their thermomechanical, mechanical and thermal degradation properties were studied. The techniques used were small angle X-ray scattering (SAXS), transmission electron microscopy (TEM), CP-MAS-NMR spectroscopy, X-ray diffraction (XRD), dynamic mechanical analysis (DMA), thermogravimetric analysis (TGA), impact testing and luminescence spectroscopy. The samples containing more than 0.5 wt.% of filler were less transparent than those containing smaller amounts, due to the presence of agglomerates. MCM-41 particles were well dispersed at low loadings, but formed agglomerates at higher loadings, while the Ce:YAG particles were not too well dispersed in both polymers at low loadings. Mixing with PMMA and PC did not alter the pore dimensions in the MCM-41 structure, and it maintained its hexagonal structure, even though the polymer chains partially penetrated the pores during composite preparation. Both polymers have carbonyl groups that had hydrogen bond interactions with the silanol group (Si-OH) on the surfaces of the MCM-41 particles. In the case of Ce:YAG the interaction was through electron donor-acceptor interaction between the carbonyl oxygen lone pair in the polymers and the yttrium cation (Y^{3+}). PMMA, however, showed a stronger interaction than PC. The addition of MCM-41 and Ce:YAG increased the storage and loss modulus of PMMA and PC above the glass transition temperature. In the presence of MCM-41 the increase in modulus was due to the interaction of the polymer chains with the porous filler which restricted the mobility of the polymer chains and increased the stiffness of the composites. The impact strength of the polymer increased with the addition of MCM-41 and Ce:YAG, but the concentration corresponding to the maximum increase depended on the type of filler. The combination of blue LEDs with the PMMA/Ce:YAG composites loaded with 5 wt.% and PC/Ce:YAG composites loaded with 2 wt.% gave off light in the white region, making them suitable for applications in white light emitting diodes.

TABLE OF CONTENTS

LIST OF TABLES

LIST OF FIGURES

LIST OF ABBREVIATIONS AND SYMBOLS

6-PAA	6-palmitate ascorbic acid
a_0	distance between the centers of two adjacent pores
AFM	atomic force microscopy
Ce:YAG	cerium doped with yttrium aluminium garnet
CP-MAS-NMR	cross-polarization magic-angle spinning nuclear magnetic resonance spectroscopy
CTAB	cetyltrimthylammonium bromide
CIE	Commission Internationale de l'Eclairage
d_{100}	interplanar distance
DMA	dynamic mechanical analysis
DSC	differential scanning calorimetry
EG	expanded graphite
E'	storage modulus
E"	loss modulus
E_a	activation energy
Ex	excitation
Em	emission
GNFs	graphite nanofibers
HEMA	hydroxyethyl methacrylate
HDPE	high-density polyethylene
H-H	head-to-head linkage
KH570	γ-methacryloxy-propyl trimethoxy silane
KH560	γ-glycidyloxypropyl trimethoxy silane
LEDs	light emitting diodes
LOI	limiting oxygen index
MAA	methacrylic acid
MFI	melt flow index
$\overline{M}_n$	number-average molecular weight
$\overline{M}_w$	weight-average molecular weight

MMT	montmorillonites
MWCNT	multiwalled carbon nanotubes
NR	natural rubber
NMR	nuclear magnetic resonance
OFW	Ozawa-Flynn-Wall
PAA	poly(acrylic acid)
PP-g-MA	polypropylene-grafted-maleic anhydride
PC	polycarbonate
PVPh	poly(vinyl phenol)
PDI	polydispersity index
PE	polyethylene
PET	poly(ethylene terephthalate)
PCNs	polymer-clay nanocomposites
PL	photoluminescence
PEG	poly(ethylene glycol)
PP	polypropylene
PVC	polyvinyl chloride
PMMA	poly(methyl methacrylate)
PNP	phosphorescent nanoparticles
PDMS	polydimethylsiloxane
PS	polystyrene
POSS	polyhedral oligomeric silsesquioxane
RDP	resorcinol bis(diphenyl phosphate)
SEM	scanning electron microscopy
SAXS	small angle X-ray scattering
TEOS	tetraethoxysilane
$(\tan\delta)_{max}$	maximum value of tan δ
T_{1p}	spin–lattice relaxation time in the rotating frame
$T_{1\rho}(H)$	proton spin lattice relaxation time
$T_{1\rho}(C)$	carbon spin lattice relaxation time

tan δ	damping coefficient
TGA	thermogravimetric analysis
TEM	transmission electron microscopy
T_g	glass transition temperature
T_{max}	maximum degradation temperature
VSL	variable spin lock
w/w	weight by weight
wt.%	weight percentage
XRD	X-ray diffraction
YAG	yttrium aluminium garnet
YAP	yttrium aluminium perovskite
YAM	yttrium aluminium monoclinic

Chapter 1: General introduction and literature review

1.1 General background

Reinforcement of polymer materials with inorganic fillers has been a common practice in the plastics industry for decades, because it improves mechanical properties, thermal stability, flame retardancy, gas barrier properties, biodegradation and abrasion resistance of polymers. These properties combine the advantages of the inorganic filler (i.e., rigidity, thermal stability) and that of the organic polymer (i.e., flexibility, ductility, processability). Thermoplastic polymers are usually reinforced with nanoclay, nanofiber, graphite, multiwalled carbon nanotubes (MWCNT) and silica [1-5]. The presence of nanofillers can strongly change the macroscopic properties of the polymer, even at very low concentrations, and the level of improvement depends on a number of factors which includes the preparation method, the dispersion of the nanofiller in the polymer and the interfacial adhesion between the polymer and the nanofiller. However, the full effect of nanofillers is reduced due to the tendency of the particles to agglomerate, which then forces nanofillers to behave like microfillers and serve as weak reinforcing particles. As a result it becomes crucial to produce polymer composites with uniformly dispersed particles in order to obtain maximum improvement in the mechanical and physical properties [1,6-8]. The presence of agglomerates can be minimised by modifying the surface of the filler or adding a compatibilizer in order to increase the interaction between the polymer and the filler. To further improve the properties of the polymer, a number of routes have been used. Firstly, the incorporation of two nanomaterials into polymer matrices, which will generate a more effective enhancement due to the expected synergistic effect. Secondly, polymer blending which provides materials with extended useful properties beyond the range that can be obtained from single polymers [9-12].

Polymer composites increase the application of polymers and they are widely used in housing materials, transportation, construction, electronics and food packaging [5,13-15]. Different fillers are added into specific polymers in order to increase their applications in their respected fields. The application of polymer-clay nanocomposites (PCNs) has contributed tremendously in our society. The most common use of PCNs has been in the mechanical reinforcement of thermoplastics like nylon-6 and polypropylene (PP). Toyota was the first

company to commercialise these nanocomposites and use them in one of their popular models [16]. They produced polyamide-clay nanocomposites and used them to replace a metal component near the engine block that caused some weight savings. In this application, clay improved the heat distortion temperature of the material and allowed it to be used in high temperature applications. They have also been used for automotive applications (fuel tanks, bumpers, interior and exterior panels) where the presence of the clay resulted in an increase in the flexural strength and modulus while maintaining impact performance [17,18]. PCNs were found to improve the flame-retardancy of polymers without degrading their properties, and the organoclays are also much cheaper than the flame retardants they are replacing. Another common application of clay nanocomposites is for gas-barrier materials. The clay nanoparticles create a complex network in the polymer matrix such that various gases either diffuse very slowly or not at all through the polymer chains. The success of clay nanocomposites for decreased diffusion of oxygen and water resulted in their application in food/liquid packaging in order to keep foods fresher for longer [18].

The addition of silica nanoparticles into polymers not only improves the physical properties, but also exhibits some unique properties which attract more interest in industries. A number of practical applications of polymer/silica nanocomposites have been reported, which include coatings, flame retardant materials, optical devices, electronics, and optical packaging materials, photoresist materials and sensors. The reinforcement of acrylates by surface modified nanosilica led to acrylate nanocomposite coatings with improved scratch and abrasion resistance. These coatings can be used on substances such as polymer films, metal, wood and engineering wood, and floors. Nowadays a variety of coatings are manufactured and used for decoration as well as protection applications. The need for industrial heavy duty flooring is increasing and epoxy based coatings have been used mainly as flooring compound, which are very useful especially for surface protection against mechanical damages. Silica nanoparticles have been incorporated into epoxy as reinforcing agent to improve the physical and mechanical properties and broaden their performance in the industry [19-21].

Over the past decade, optically transparent polymers attracted considerable attention in numerous applications, including protective face shields and eyewear, protective coatings, windows, high performance transportation glazing, and electronic display screens [22]. Poly(methyl methacrylate) (PMMA) and polycarbonate (PC) attracted attention due to their

inexpensiveness and fascinating properties i.e. optical, mechanical, viscoelastic and thermal degradation kinetics. PMMA is mostly applied in medical technologies and implants, while PC is applied mostly in electronic components and construction materials. Although their properties were found satisfactory in different applications, there are still important properties that need to be enhanced in order to extend the application of these engineering polymers. For instance, microbial adhesion onto PMMA has been a long standing drawback. Moreover, PC and PMMA have poor fatigue resistance, poor resistance to solvents, high moisture sorption and low thermal stability. In a bid to improve these drawbacks different nanofillers are incorporated into the matrices to form polymer nanocomposites [23,24].

Materials such as titania, zirconia, silica, clay and graphite were used as typical reinforcing agents. Mesoporous silica (MCM-41) and yttrium aluminium garnet doped with cerium (Ce:YAG) are of interest in this study because of their extensive advantages and their lack of use as polymer reinforcing agents. MCM-41 particles are of interest for use as catalysts, adsorbents, and drug delivery systems for the development of optical devices, because of properties such as large internal surface areas, uniform frameworks and their easily controlled pore diameters. Recently MCM-41 has been used as an additive to improve polymer properties because it contains a large amount of internal hydroxyl groups, and its surface can be easily modified, and it has excellent thermal, chemical and mechanical stability [25-27]. The confinement of the polymer in the mesopores of the silica particles undoubtedly plays a significant role in the enhancement of the thermal, thermomechanical and mechanical properties of the polymer [28]. Ce:YAG is a yellow phosphor widely used in optical display and lighting applications, and it is regarded as the best phosphor applied in the white phosphor-based LED commercial market [29-31]. The presence of this phosphorescent filler showed significant improvement in the mechanical and thermal stability of polymers at very low loadings (0.1 to 5 wt.%) [32,33]. In this study, the use of MCM-41 and Ce:YAG particles to improve the thermal, mechanical, and thermomechanical properties of PMMA and PC has been investigated. We also studied the thermal degradation kinetics, and the usability of the phosphorescent composites in white light emitting diodes.

1.2 Literature review

1.2.1 Poly(methyl methacrylate) (PMMA)

PMMA, is an important member in the family of polyacrylic and methacrylic esters. It has several properties that allow it to be used in many applications, and its application has increased tremendously because of its beneficial physical and chemical properties, e.g., excellent transparency and good surface properties. Its optical clarity allows it to be used as a replacement for glass. Furthermore, its low toxicity and compatibility with human tissue, allows it to be used for bone cements, contact and intraocular lenses, screw fixation in bone, filler for bone cavities and skull defects. On the other hand, PMMA shows poor abrasion resistance and thermal stability, which limits its use in certain applications [34-36].

Over the past decades, the thermal degradation of PMMA was widely investigated, and a number of mechanisms have been proposed [37-42]. The degradation mechanism of PMMA depends on a number of factors that include the polymerization method and the polymer microstructure, including internal defects and type of chain end groups. Anionically polymerized PMMA shows only one degradation step at 360 °C, which is normally due to random chain scission. However, the degradation of PMMA polymerized with a free radical method proceeds in three steps due to the presence of chains with different structures. The first step occurs between 150 and 230 °C, and is attributed to the degradation initiated by chains containing head-to-head (H-H) linkages. The second step between 230 and 300 °C is associated with chains possessing unsaturated vinylidene ends, and the third step between 310 to 420 °C is attributed to chains undergoing degradation initiated by random chain scission. Anionically polymerized PMMA is more stable than free radical polymerized PMMA.

1.2.2 PMMA composites

1.2.2.1 Morphology

Only a few methods have been used to prepare PMMA-SiO_2 nanocomposites. One of these methods is *in situ* emulsion polymerization in the presence of an initiator [43-47]. Generally,

homogenous dispersions of silica in PMMA was obtained, even though there were some noticeable agglomerates at higher filler loadings. The dispersion of silica was attributed to the interaction at the silica-PMMA interface. In most of the studies, modified silica nanoparticles showed better interaction with the PMMA matrix which led to better transparency and stronger interaction at the interface. *In situ* radical polymerization prepared nanocomposites showed exceptional dispersion of silica in PMMA compared to those prepared through *in situ* emulsion polymerization [48]. In sol-gel prepared nanocomposites, the nano-scale SiO_2 particles were uniformly distributed in and covalently bonded to the PMMA matrix without macroscopic organic-inorganic phase separation. PMMA-SiO_2 nanocomposites prepared by solution mixing were also studied, with a good dispersion of the silica in the PMMA matrix at low contents, but small clusters were observed at higher silica contents. The dispersion was attributed to the size and shape of the nanoparticles which influenced the interfacial interaction. Sonication was found to be an effective way of ensuring the optimal dispersion of the particles in the polymer [49-51]. There were only a limited number of reports on the morphology of PMMA/mesoporous filler composites [53-55]. The preparation method and the amount of the particles played a significant role in the level of silica dispersion in the polymer matrix. Well dispersed silica particles were observed at low loadings, but at high loadings the dispersion was less uniform with large agglomerates. PMMA/mesoporous silica composites prepared by *in situ* batch polymerization gave rise to better dispersion compared to emulsion polymerization and melt mixing, because the batch polymerization resulted in an intimate nanoparticle mixture in which the polymer chains clung to the silica particles.

1.2.2.2 Thermal properties

A number of papers reported on the thermal properties of PMMA/mesoporous composites [52-56], and composites with other nanoparticles [57-60]. Different methods were used to prepare the PMMA/mesoporous silica composites, with silica having different framework pore structures. It was generally observed that the glass transition temperature of the polymer increased with an increase in silica content. This was attributed to the strong interfacial interactions between the polymer and the filler, which led to the adsorption of PMMA molecular chains onto the surface and inside the channels of the particle. The glass transition temperature

increased irrespective of the preparation method, and the nanocomposites prepared by *in situ* batch emulsion polymerization showed a larger increase due to the intimate initial mixing of the nanoparticles compared to physical mixing. It was observed that the silica with the largest pore volume gave rise to the highest glass transition temperature, and that about 13.4% of the PMMA can be confined in the pores of the silica at 5 wt.% loading [53]. The influence of the interphase region was sufficient to substantially restrict the segmental motions of the remaining unconfined polymer and increase the T_g by about 9 °C. A decrease in T_g was observed at higher filler loadings, and this was attributed to the presence of agglomerates which slightly increased the polymer mobility [54]. In the case of a polyhedral oligomeric silsesquioxane (POSS)/PMMA hybrid the decrease was attributed to the greater steric hindrance of POSS, which increased the free volume and decreased the reactivity of the MMA monomer leading to large fractions of low molecular weight components [61]. In a study where 6-palmitate ascorbic acid (6-PAA) was used as a coupling agent, the T_g of PMMA also decreased, and it was attributed to the plasticizing effect of TiO_2/6-PAA [62-63].

The presence of nanoparticles influences the thermal stability of the polymer in different ways, depending on factors such as the preparation method and the interaction between the two components. The effect of nanoparticles, including mesoporous silica, on the thermal stability of PMMA was reported in a number of papers [52-56,64-68]. Generally, it was observed that the addition of nanoparticles improved the thermal stability of PMMA, and the thermal stability of PMMA with mesoporous silica increased regardless of the pore size and framework structure of the mesoporous silica, and the preparation method used. This was attributed to the fact that the nanoparticles trap the generated free radicals or act as scavengers of radical species during degradation, and restrict the out-diffusion of volatile products. The stiffening of the polymer chains in the presence of nanoparticles was also responsible for the increase in degradation temperature [55]. The thermal stability of nanocomposites prepared by *in situ* polymerization decreased in the presence of the TiO_2 nanoparticles [69,70]. This was attributed to physisorbed water evaporating at lower temperatures. It is interesting that some authors [51,56,71,72] observed that the presence of silica had no effect on the thermal stability of PMMA.

1.2.2.3 Dynamic mechanical properties

Different authors investigated and reported on the thermo-mechanical and mechanical properties of PMMA with a number of fillers [52-56,72-76]. Generally, the addition of nanoparticles improved the storage and loss modulus of PMMA, and this behaviour was observed over the entire investigated temperature range. The increase in modulus was attributed to the rigid particles which increased the stiffness of the polymer, and to the particles that acted as reinforcing agents through their interaction with the polymer. A decrease in storage modulus of PMMA below the glass transition temperature was observed with the addition of and increase in the zirconia content from 1 to 5 wt.%, which was attributed to the nanoparticles causing more free space for molecular vibration [77]. In the rubbery state, the storage modulus of PMMA was independent of the ZrO_2 nanoparticles content, which was attributed to the weak interaction between the PMMA matrix and the ZrO_2 nanoparticles at high temperatures [76]. A few studies observed a decrease in T_g, as determined from the loss modulus curves, with filler addition. This was attributed to the presence of 2-hydroxyethyl methacrylate (HEMA) which acted as a plasticizer [78] and to a lack of interaction between the polymer and the filler [79-81].

1.2.2.4 Mechanical properties

The presence of nanoparticles generally increased the tensile modulus and tensile strength of PMMA, especially at low contents [82-83]. This was attributed to the reinforcing effect and good dispersion of the nanofillers in the polymer. The tensile strength and elastic modulus of PMMA increased significantly with the addition of mesoporous silica until 6%, due to the increase in the rigidity of the composite. At high filler loadings the mechanical properties decreased due to the presence of agglomerates which resulted in crazing and weakening of the adhesion between the filler and the matrix [52,54].

The addition of and increase in silica content from 0.5 to 1.5 wt.% [65] and graphite nanofibers (GNFs) from 1 to 15 wt.% [84] increased the impact strength of PMMA. This was attributed to the reinforcement sites formed along the polymer chains. The GNFs behaved as crack arrests rather than crack initiators, and it was suggested that there was fairly strong interfacial adhesion between the polymer and the filler. The impact properties of poly(styrene-

co-acrylonitrile)/PMMA(20/80) increased up to 1 wt. % zinc loading, and decreased at higher contents, which was attributed to the presence of aggregates that served as crack initiators [15]. Soygun *et al.* [85] also observed the same trend with lignin loading. However, some studies observed a decrease in impact strength with the addition of and increase in the contents of clay [86] and fly ash [87]. Hong *et al.* [88] studied the impact properties of PMMA in the presence of unmodified and γ-methacryloxy-propyl trimethoxy silane (KH570) modified silica. It increased with the addition of silica, but the composites with unmodified silica showed lower impact strength than the modified silica composites, and the unmodified samples were brittle and suffered from detrimental failure. This was attributed to the presence of aggregates that acted as cracking points.

1.2.3 Polycarbonate (PC)

PC, mainly known as bisphenol A polycarbonate, is a well-known engineering thermoplastic polymer with a high molecular weight and high impact strength over a wide temperature range. PC is amorphous and exhibits good transparency. It is a condensation polymer that forms a bulky stiff molecule which promotes rigidity, strength, creep resistance and a high heat deflection temperature. It has been widely used in a number of fields such as construction, electrical, automotive, aircraft, medical and packaging applications, and recently in car lights and laser optical data storage [89-92]. PC also has a high limiting oxygen index (LOI) and produces a large fraction of char upon combustion when subjected to thermogravimetric analysis. However, because of its high melt viscosity and poor resistance to abrasion and chemicals, it is not suitable for certain applications. Hard surface coatings are a common means of remedying the deficiencies of PC, whereas other approaches include addition of fillers or use of polymer blends.

1.2.4 PC composites

1.2.4.1 Morphology

One of the important parameters that control the level of polymer improvement in the presence of nanoparticles is the morphology of the final composites. A number of techniques which

include transmission electron microscopy (TEM), scanning electron microscopy (SEM) and atomic force microscopy (AFM) have been used to study the level of filler dispersion in PC. Blackwood *et al.* [93] and Imai *et al.* [94] studied the dispersion of TiO_2 and ZrO_2 particles in PC prepared by injection moulding and solution mixing. The particles were homogenously distributed throughout the polymer matrix along with minor agglomerates. Rouabah *et al.* [95] observed well dispersed TiO_2 particles in PC without agglomerates, even at higher filler loadings.

Some studies showed the presence of filler acting as a compatibilizer, while surface modification of the filler can reduce the sizes of nanoparticle agglomerates in a PC matrix. Vabahi *et al.* [96] studied the morphology of PC/POSS in the absence and presence of resorcinol bis(diphenyl phosphate) (RDP). The SEM images of the PC/POSS composites showed POSS aggregates in the 500-700 nm size range. This was attributed to the incompatibility between PC and POSS, and the formation of intermolecular hydrogen bonds between the POSS particles. In the presence of RDP the sizes of the aggregates decreased and a more homogenous dispersion was obtained, which was attributed to the presence of RDP located on the surfaces of the POSS particles. Feng *et al.* [97] prepared PC/SiO_2 composites with untreated and γ-glycidyloxypropyl trimethoxy silane (KH560) treated SiO_2 particles. They observed an obvious increase in the average size of the SiO_2 agglomerates from 85 nm at 1 wt.% to 200 nm at 5 wt.% loading. This was attributed to the stronger interaction between the nanoparticles at high loadings. In the presence of KH560 the average sizes of the agglomerates increased only slightly as a function of silica loading (from 85 nm at 1 wt.% to 100 nm at 5 wt.%). This was attributed to the decrease in surface energy of the silica particles.

1.2.4.2 Thermal properties

The addition of nanoparticles generally increased the thermal stability of PC and a number of factors were associated to this behaviour. Firstly, the immobilization of the polymer chains, free radicals and volatile degradation products, retards the onset of mass loss and releases the degradation products at higher temperatures [98,99]. Secondly, the nanoparticles act as barrier and hinder the transportation of volatile products so that they are released only at higher temperatures [100,101]. In the case of polymer mesoporous composites, the pore walls can act as

physical barriers, both to retard the movement of free radicals and prevent the transport of volatile products [52,53]. Nanoclays have to be organically modified to make them compatible with the polymer, but it has been established that the high processing temperature of PC causes degradation of the modifier through a Hoffmann elimination reaction, which generates reactive radicals that favour PC degradation at much lower temperatures [102-104]. A decrease in thermal stability with the addition of TiO_2, ZrO_2, and ZnO was also reported [94,90,105]. This behaviour was related to the catalytic effect of the nanoparticles, the state of nanoparticles dispersion within the polymer matrix, and the preparation conditions. The glass transition temperature of PC, observed from differential scanning calorimetry (DSC), generally increased with the addition of nanoparticles, and the authors attributed it to the confinement of polymer chains in the intra-gallery of the organoclays [102,104] and silica particles [107,108], which restricted the mobility of polymer chains.

1.2.4.3 Dynamic mechanical properties

Several groups investigated the dynamic mechanical properties of PC with MWCNT, ZrO_2, and clay nanoparticles [98,109,110]. Generally, the storage and loss modulus of PC increased with filler loading. This was attributed to the reinforcing effect of the nanofillers due to their high aspect ratios. The increase in modulus was also attributed to the formation of crystalline domains around the nanoparticles which effectively improved the interaction between the particles and the PC chains. Feng *et al.* [97] observed an increase in T_g at low silica contents, and a decrease at higher contents. This increase was attributed to the dispersed SiO_2 nanoparticles, which restricted the motions of polymer chains, while the decrease at higher filler loading was attributed to the increased free volume as a result of the disruption in the chain segment packing. The T_g of PC decreased with the addition of SiO_2 [111] and carbon nanotubes [105]. This was attributed to the higher mobility of the PC chains as a result of higher free volumes caused by the presence of non-adhering nanoparticles inside the polymer matrix.

1.2.4.4 Mechanical properties

The mechanical properties of PC nanocomposites have been well studied with tensile and impact testing [90,112-117]. The tensile modulus and tensile strength of PC generally increased after the addition of nanoparticles. This was attributed to the uniformly dispersed nanoparticles that increased the rigidity of PC, but at high filler loading the mechanical properties were reduced due to the presence of agglomerates. The elongation at break decreased with an increase in filler content, and this behaviour was attributed to the presence of agglomerates, cracks and voids formed around the filler particles which resulted in local detachment of the matrix from the particles [105,115,116]. However, the concentration corresponding to the decrease in elongation at break was dependent on the type of filler used. PC/carbon black composites showed an increase in elongation at break until 3 wt.% filler content, while that of PC/MWCNT composites increased up to 1.25 wt.% filler content [114].

The addition of, and increase in, TiO_2 [115], mica [116] and nanoclay [117] contents induced an almost linear decrease in the impact strength for both the notched and unnotched specimens. The authors attributed this behaviour to the decrease in ductility which promoted brittle fracture. The impact strength of a PC/poly(acrylonitrile-butadiene-styrene) (70/30) blend decreased by about 25% as the mica content in the blend increased from 0 to 30 phr. This was attributed to the reduction in polymer-filler interaction due to the presence of agglomerates which weakened the interfacial adhesion between the filler and polymer and became potential sites for crack growth [116]. Luyt *et al.* [111] studied the impact properties of PC reinforced with silica nanoparticles, and they observed the largest increase in impact strength at the lowest filler content, and a decrease as the content increased.

1.2.5 Polymer/phosphorescent filler composites

1.2.5.1 Morphology

So far there is a lack of research data on the effect of phosphorescent nanoparticles (PNP) on the properties of polymers. TEM, SEM and AFM analyses were used to study the dispersion of phosphorescent particles in different polymer matrices. *In situ* polymerization and solution

mixing methods were used to prepare the composites. Generally, homogenous dispersions of the nanoparticles were observed with a number of agglomerates at high loadings. AFM images showed that the sizes of the agglomerates increased with an increase in YAG:Tb^{3+} loading from 0.2 um at 0.01 wt.% to 0.4 um with 0.02 wt.% [32,118].

1.2.5.2 Thermal properties

There are a few studies on the thermal properties of polymer/PNP nanocomposites [32,120]. The thermal degradation of pure PMMA and PMMA/PNP prepared by solution casting showed two degradation steps. The first step observed in the temperature range 150 to 230 °C was associated with the depolymerisation initiated by the scission of weak head-to-head bonds, and the second step was observed above 300 °C and attributed to random chain scission. The presence of PNP increased the thermal stability of PMMA, and was attributed to the restriction of polymer chains and free radicals that took part in the degradation process. Generally, the T_g of PMMA observed from DSC increased with the addition of PNP, and it was associated with a decrease in molecular mobility of the polymer chains due to the adhesion of the polymer segments onto the surfaces of the particles [32,121,122]. PMMA/cobalt hexacyanoferrate (CoHCF) composites showed lower T_g values than PMMA/Ce:YAG composites at the same filler loading. This behaviour showed that the interaction between the Ce:YAG particles and the polymer chains, and the resultant immobilization of the polymer chains, was much stronger than that of PMMA/CoHCF [32].

1.2.5.3 Dynamic mechanical properties

The storage modulus, loss modulus and glass transition temperature of PMMA were found to increase with the addition of PNP. The PNP behaved as physical crosslinks and reduced the overall mobility of the polymer chains. However, at higher contents the modulus decreased, which was attributed to the presence of agglomerates. The composites prepared with modified PNP showed higher loss and storage moduli compared to the unmodified PNP composites [119,122].

1.2.6 Polymer/MCM-41 composites

1.2.6.1 Synthesis of MCM-41

The synthesis of MCM-41 requires a number of materials that include the silica precursor tetraethoxysilane (TEOS), the surfactant or template molecule cetyltrimthylammonium bromide (CTAB), hydrochloric acid and water. The formation of MCM-41 is illustrated in Figure 1.1. The surfactant is dissolved in HCL and the spherical micelles start to form when the silica precursor is added. The micelles elongate and arrange themselves into a hexagonal pattern, while the silica condenses on them to form the silica walls. The pore size can be tailored by using templates with variable chain length and through the addition of swelling organic compounds such as trimethylbenzene. Finally, the template is removed to obtain the porous structure. The template within the pores of MCM-41 can be removed by either calcination or washing. Calcination involves the burning out of the template under conditions that do not greatly affect the silicate structure. The process has the advantage of ensuring the removal of all carbonaceous material, but it can also cause significant shrinkage in the MCM-41 lattice parameter. Washing is done through boiling the MCM-41 in HCl/ethanol mixtures [123-126].

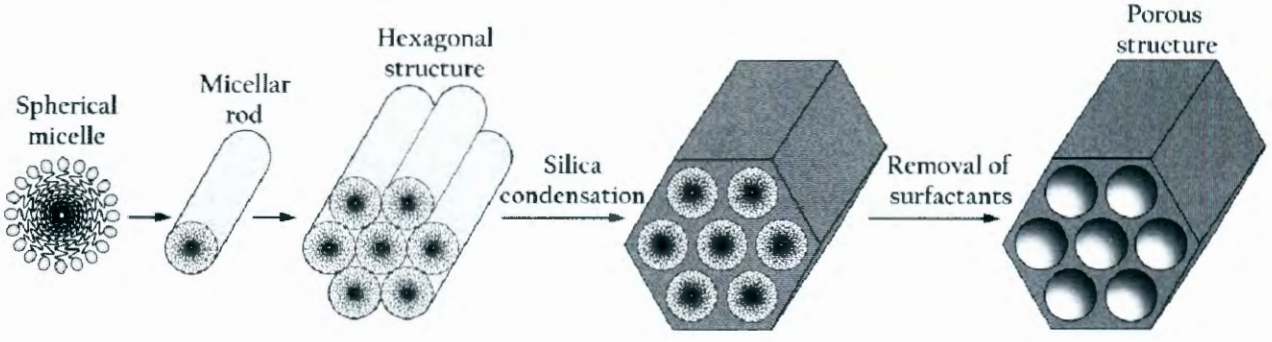

Figure 1.1 Illustration of the formation of MCM-41 [125]

1.2.6.2 Structure and morphology of MCM-41 and polymer/MCM-41 composites

The structure and morphology of MCM-41 and polymer/MCM-41 composites were studied using X-ray diffraction (XRD), transmission electron microscopy (TEM), and scanning electron microscopy (SEM). The polymer can be introduced inside the mesopores by melt compounding or *in situ* polymerization of organic monomers. One of the advantages of this method is that the microstructure of the interface between the matrix and the pore openings of the fillers can be easily tailored. The polymer in the nanosized pores, extending along the channels to the openings, will not only enhance the miscibility through entanglement and inter-diffusion between the matrix and the filler, but it will also supress the aggregation of the filler. They can also form a novel nanonetwork composite (Figure 1.2) [127-131].

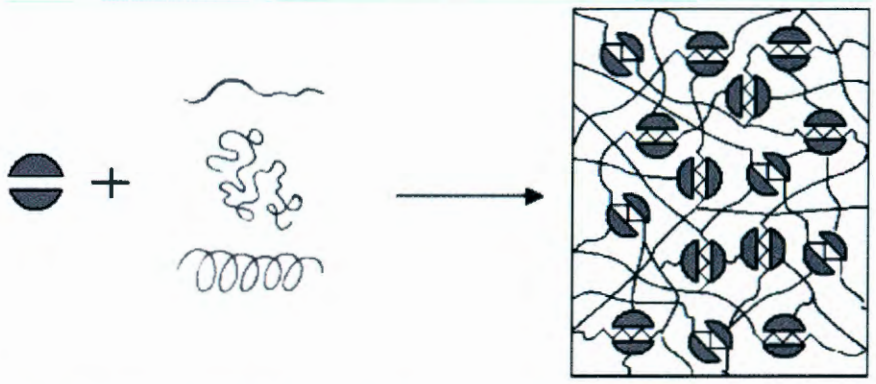

Figure 1.2 Model analogy novel nanonetwork composite [130]

MCM-41 exhibits an XRD pattern with one intense diffraction peak (100) and two additional small reflections (110) and (200) at low reflection angles, which suggests a highly ordered hexagonal pore structure. MCM-41, modified by silylation with chlorotrimethylsilane and oetyltrichlorosilane, showed a similar XRD pattern, which indicated that the basic framework ordering of the mesopores remained unchanged after surface silylation [131-135]. The XRD analysis of poly(acrylic acid)(PAA)/MCM-41 composites prepared by *in situ* polymerization [136] and PP/MCM-41 prepared by melt mixing [137,138] showed that one reflection with a lower intensity remained in the small angle 2θ region for the MCM-41 after composite preparation. This was attributed to the formation of polymer in the mesoporous channels of MCM-41, which reduced the scattering contrast between the pores and the wall of molecular sieves. XRD pattern of composites prepared with MCM-41 (with and without a

template) retained the characteristic diffraction peaks of MCM-41, which indicated that the hexagonal framework structure of the MCM-41 was retained during and after composite preparation.

SEM micrographs showed that MCM-41 is made up of tiny particle clusters, and TEM micrographs clearly showed the porous structure with regular hexagonal channels of MCM-41 particles [123,133,135,139]. It was generally found that MCM-41 particles were uniformly dispersed in polymer matrices, although large agglomerates where sometimes observed. However, modified MCM-41 particles were mostly dispersed without much agglomeration [140-142]. Wang *et al.* [135] studied the morphology of polydimethylsiloxane (PDMS)/MCM-41 composites with 50 wt.% of unmodified and chlorotrimethylsilane (M-MCM-41) or octyltrichlorosilane (O-MCM-41) modified MCM-41. The SEM images of membranes filled with unmodified MCM-41 showed many interfacial voids around the MCM-41 spheres. Comparatively, modified MCM-41 were uniformly dispersed in the PDMS membrane, which was attributed to the very hydrophobic silanized surface layer formed after silylation and the improved interfacial adhesion between MCM-41 particles and the polymer.

1.2.6.3 Mechanical and thermomechanical properties

The addition of MCM-41 increased the tensile strength and modulus of most of the investigated polymers, but the nature, concentration and dispersion of MCM-41, and the interfacial adhesion between the polymer and MCM-41 controlled the level of mechanical improvement [128,138,139,143-147]. Wang *et al.* [139] prepared PP/MCM-41 composites with MCM-41 with and without a template. They observed an increase in tensile strength at low MCM-41 contents, but higher strengths were obtained for composites prepared with MCM-41 (without template). The tensile strengths decreased with increasing MCM-41 (with template) contents, which was attributed to the fact that when the content of the MCM-41 (with template) increased, the template content in the interlayer increased which reduced the interfacial stress transfer efficiency. Wang *et al.* [139] observed an increase in tensile strength up to 15 wt.% loading. The same group observed an increase in tensile strength and modulus of natural rubber (NR) with increasing MCM-41 contents up to 5 wt.% loading, but a decrease at higher contents. This was

attributed to the presence of agglomerates and dispersion inhomogeneity due to poor MCM-41/NR miscibility.

The impact properties of polymers generally increased with the addition of MCM-41 [138,139,146,147]. Composites prepared with MCM-41 (with template) showed an increase in impact strength due to the improved interfacial interaction, which was the result of interdiffusion and entanglement between the polymer chains and the organic template mixture in the nanosized pores, and on the outer surface of the particles. The impact strength of composites with MCM-41 (without template) increased at lower filler contents, and decreased gradually with increase in filler content due to poor compatibility. In the case of a 80/20 w/w PP/polystyrene (PS) blend the impact strength increased with the addition of, and an increase in MCM-41 (with template) up to 1 wt.%, but decreased at higher loadings [147]. The increase in impact strength was attributed to the entanglement between the two polymers' chains and the template of the stiffer filler, and to the strong interfacial interaction which ensured stress transfer between the phases during fracture. The decrease in impact strength at higher loadings was attributed to the increase in the organic template, which had a low molecular weight providing a soft layer between the filler and matrix at higher nano-filler loadings.

The storage modulus of polymers increased with the addition of MCM-41 due to the increase in the stiffness of the composites [140,141,144], which was attributed to the higher stiffness and inherent reinforcement effect of the nanofiller [141]. Wang *et al.* [144] studied the storage modulus of natural rubber (NR) in the presence of MCM-41 and γ-methacryloxypropyltrimethoxysilane (KH570) modified MCM-41. The storage modulus of NR increased with the addition of MCM-41 and KH570 modified MCM-41, because the large specific areas and inherently high modulus of the filler enhanced the stiffness of the NR. The storage modulus of NR/KH570 modified MCM-41 nanocomposites was higher than that of the nanocomposites prepared with unmodified MCM-41, which was attributed to the improved dispersion of KH570 modified MCM-41 in the NR matrix and the good interfacial bonding between them.

1.2.6.4 Thermal analysis

The addition of MCM-41 (without template) increased the crystallinity, crystallization and melting temperature of PP, while the presence of MCM-41 (with template) decreased these properties. The increases were attributed to the fact that the MCM-41 (without template) nanoparticles acted as effective nucleating agents. Modification of MCM-41 decreased the glass transition temperature of the composites, which was attributed to the plasticizing effect caused by the trimethyl groups grafted on the silicate filler interface [137,148]. Khezri *et al.* [149] observed a decrease in the T_g of PS with an increase in MCM-41 loading, and ascribed it to the weak interaction between the polymer chains and OH-containing MCM-41 particles. The MCM-41 particles reduced the packing of the PS chains and increased the segmental mobility.

Generally the addition of MCM-41 increased the thermal stability of polymers [137,140,148,149], which was attributed to (i) the high thermal stability of the MCM-41 nanoparticles, and (ii) the physical interaction between the polymer chains and the surfaces of MCM-41 particles. PP composites prepared with MCM-41 (with template) had higher thermal stabilities than the MCM-41 (without template) composites, because the polymer and the template mixture enhanced the interaction through entanglement and interdiffusion, thus forming a network which enhanced the thermal stability. Cerrada *et al.* [141] observed a decrease in the thermal stability of HDPE with the addition of and increase in content of MCM-41, which was attributed to the catalytic effect of the filler.

1.3 Solid state NMR investigations of polymer-filler interactions

The addition of nanofillers in polymers improves the physical, mechanical and electrical properties of polymers. However, the level of reinforcement is controlled by the interaction between the polymer and the filler. Polymer-filler interactions are controlled by several parameters, depending not only on filler features, such as structure, morphology and surface activity, but also on the polymer characteristics, such as microstructure, conformation, molecular weight and polydispersity, and on the conditions of compounding. Various techniques, that include dynamic mechanical, thermal and sorption analysis, and spectroscopic techniques, have been used to study the exact nature of the interactions that may occur between the filler and the

polymer [150-151]. NMR can also be used to study the polymer-filler interactions, because it can investigate the changes at molecular level and provide detailed information about local segmental motions. A number of polymers, that include PMMA, PC, PP and epoxy were analysed *via* solid-state NMR, and it was showed that spin lattice relaxation in the laboratory frame (MHz) values are particularly sensitive to side chain motions, whereas spin lattice relaxations in the rotating frame are sensitive to molecular motions that occur in the kHz range. The cross polarization in a polymer system can be used to determine the extent of motional heterogeneity and phase separation in a polymer system [152-155].

The properties of a polymer blend depend on the miscibility and morphology of the components. High resolution NMR has also been used to study polymer blends, and was shown to be a valuable tool for the characterization of polymer-polymer miscibility and the forces that drive miscibility. Detailed information about the miscibility, intermolecular interaction, and morphology of polymer blends can be obtained through examining NMR parameters such as the chemical shift, line width, and relaxation parameters [156-158]. Asano *et al.* [156] studied the miscibility between PC and PMMA in PC/PMMA blends, and they observed a change in the ^{13}C spin-lattice relaxation time, which confirmed the presence of interactions between the methoxy group of PMMA and the phenyl group of PC. Zhang *et al.* [157] studied the miscibility and phase structure of amorphous/crystalline polymer blends of poly(vinyl phenol) (PVPh) and poly(ethylene glycol) (PEG). The ^{13}C CP/MAS spectra showed a downfield shift of the phenolic C-OH resonance, which was attributed to the intermolecular hydrogen-bonding interaction causing miscibility in the blend. When the blend was PVPh rich, it was completely miscible, and when it was PEG rich, it was partially miscible.

The use of NMR has been extended to polymer-filler nanocomposites in recent studies, due to the ability to study the interaction at the polymer-filler interface and the effect of the interaction on the mobility of the polymer chains. Zanotto *et al.* [32] and Saladino *et al.* [159] studied the ^{13}C cross-polarization magic-angle spinning nuclear magnetic resonance of a Ce:YAG-PMMA composite prepared by solution mixing and *in situ* polymerization respectively. The presence of the filler showed no modification in the chemical shift as such, and they concluded that the interaction between the polymer and filler occurred without the formation of chemical bonds. However, the spin-lattice relaxation time increased in the presence of the filler,

which was attributed to the increase in rigidity of the composites due to the immobilization of the chains as a result of filler-polymer interaction.

The interaction between the filler and the matrix has been studied by ^{13}C-CP-MAS-NMR spectroscopy and by acquiring spin-lattice relaxation times in the rotating frame ($T_{1\rho}$) [32]. It was generally found that the presence of filler did not induce any chemical modification in the polymer matrix and hence there were no new signals, changes in peak shapes or chemical shifts observed. The spin–lattice relaxation times in the rotating frame are sensitive to molecular motions that take place in the kHz range [159]. The $T_{1\rho}$ values of polymer increased with the addition of filler, which was attributed to the immobilization of the polymer chains as a result of filler-matrix interactions [32,161,162]. In a number of studies polymer composites were prepared by melt compounding, and a significant decrease in the crosspolarization time T_{CH} values of the polymer was observed with the addition of filler. This behaviour indicated an increase in the heteronuclear dipolar interactions between the carbons and the surrounding hydrogen nuclei. It was also evident that the presence of filler in the polymer made the polymer structure more rigid, because an increase in rigidity of a material favours the cross polarization mechanism to yield shorter T_{CH} values [163-166]. Saladino *et al.* [160], however, observed no change in the T_{CH} value of PMMA with the addition of Ce:YAG, which indicated that the filler did not alter the dipolar interactions.

1.4 Research objectives

The study focused on polymer composites based on glassy polymers (poly(methyl methacrylate) and polycarbonate) with mesoporous silica and yttrium aluminium garnet doped with cerium. The polymer composites were prepared with MCM-41 and Ce:YAG loadings between 0.1 and 5 wt.% using melt compounding. The samples were characterized using small angle X-ray scattering (SAXS), cross-polarization magic-angle spinning nuclear magnetic resonance spectroscopy (^{13}C {H} CP-MAS-NMR), transmission electron microscopy (TEM), thermogravimetric analysis (TGA), dynamic mechanical analysis (DMA), impact testing, and thermal degradation kinetics. The photo luminescence of the Ce:YAG composites was also investigated.

The first objective of the study was to investigate the effect of MCM-41 incorporation on the properties of poly(methyl methacrylate) and polycarbonate. There are three main questions that we wanted to address in this study.

- The morphology of a composite has a significant influence on the improvement of the polymer properties, and it is well known that MCM-41 has a porous structure with well-ordered channels and a hexagonal symmetry. The first question that we wanted to address was how the MCM-41 particles would be dispersed in the polymer matrix, and how did the filler content influence this dispersion. The second question was whether the particle morphology (porous structure) would play a role in the filler dispersion. Although the morphologies of composites of other polymers mixed with MCM-41 were investigated (section 1.2.6.2), there are no reports on the morphologies of PMMA/MCM-41 and PC/MCM-41 composites. There were also no reports on the influence of MCM-41 content on the morphologies of the composites, which was one of the focuses of our study.
- It has been established that the confinement of a polymer in the pores of mesoporous silica particles plays a significant role in the enhancement of the polymer properties. The second question we wanted to address was what influence the incorporation of MCM-41 has on the mechanical and dynamic mechanical properties, as well as thermal stability and degradation kinetics of the two polymers. One would expect to observe an improvement in impact strength, thermal stability, as well as loss and storage modulus, and an increase in the activation energy of degradation with the addition of MCM-41, because there were similar observations on other polymer/MCM-41 composites that were attributed to the interaction between the polymer and filler through entanglement and interdiffusion, and to the confinement of the polymer chains in the pores of MCM-41 [143,146,149]. It is known that the amount of filler and the interaction between the polymer and the filler play a significant role in the improvement of the polymer properties, so we also wanted to establish which MCM-41 content gave the optimum improvement in these properties.
- The composite morphology and resultant properties will be determined by polymer-filler and filler-filler interactions. The type of interaction is controlled by a number of factors that include particle size and shape, filler aspect ratio, filler content, surface tension and interfacial interaction. Part of our research was aimed at clarifying these interactions in our systems, and relating this information to the observed differences in properties. So far there

are no reports that address the interaction in polymer/mesoporous filler composites, but there are a number of studies that investigated the nature of the interaction in composites of polymers with other types of inorganic fillers (see section 1.3).

The second objective of this study was to investigate the effect of Ce:YAG incorporation on the properties of poly(methyl methacylate) and polycarbonate. The use of phosphorescent (Ce:YAG) particles as reinforcing agents in polymers has not been well studied, and in this study we wanted to address some unanswered questions. Previous research [32,159] focused on polymer/Ce:YAG composites prepared by solution mixing and *in situ* polymerization methods, and therefore we prepared our composites through melt mixing in order to get a full picture on the influence of the preparation method on the investigated properties. The mentioned studies also focused only on filler content, and we used different contents in order to establish the influence of filler content and the resultant morphology and polymer-filler interaction on the different thermal, mechanical and fluorescent properties. We planned our work to contribute to the lack of information by addressing the following questions.

- How will different contents of Ce:YAG particles disperse in the polymer matrix, and how will filler content influence the polymer-filler interaction?
- Low thermal stability is one of the drawbacks that limit the application of PMMA and PC. We wanted to establish what influence the presence and content of Ce:YAG has on the thermal stability and thermal degradation kinetics of PMMA and PC.
- How does the presence and content of Ce:YAG influence the impact strength of the polymers? There are no reports on the impact properties of polymer/phosphorescent filler composites, but the impact properties of PMMA and PC with other fillers have been studied (as discussed in sections 1.2.2.4 and 1.2.4.4). Generally, the addition of different fillers influence the impact strength of PC and PMMA in different ways, and therefore we decided to study the effect of Ce:YAG on the impact properties of PC and PMMA to add to the available knowledge in this field.
- Will these phosphorescent composites be usable for advanced applications in white light emitting diodes?

1.5 Thesis outline

Chapter 1 Introduction and literature review

Chapter 2 Materials and methods

Chapter 3 Morphology and properties of poly(methyl methacrylate) (PMMA) filled with mesoporous silica (MCM-41) prepared by melt compounding

Chapter 4 Morphology, mechanical and thermal properties of polycarbonate (PC) filled with mesoporous silica (MCM-41) prepared by melt compounding.

Chapter 5 Morphology, mechanical, thermal and luminescence properties of poly(methyl methacrylate) (PMMA) filled with yttrium aluminium garnet doped with cerium (Ce:YAG) prepared by melt compounding

Chapter 6 Morphology, mechanical, thermal and luminescence properties of polycarbonate (PC)/yttrium aluminium garnet doped with cerium (Ce:YAG) composites prepared by melt compounding

Chapter 7 Conclusions

1.6 References

1. N. Wang, Q. Fang. J. Zhang, E. Chen, X. Zhang. Incorporation of nano-sized mesoporous MCM-41 materials used as fillers in natural rubber composites. Materials Science and Engineering A 2011; 528:3321-3325.
   DOI: 10.1016/j.msea.2010.12.105
2. H. Zhang, C. Li, J. Guo, L. Zhang, J. Luo. In situ synthesis of poly(methyl methacylate)/SiO_2 hybrid nanocomposites via "grafting onto" strategy based on UV irradiation in the presence of iron aqueous solution. Journal of Nanomaterials 2011; 2012:1-9.
   DOI: 10.1155/2012/217412
3. L. Wang, L. Zhang, M. Tian. Effect of expanded graphite (EG) dispersion on the mechanical and tribological properties of nitrile rubber/EG composites. Wear 2012; 276-277:85-93.
   DOI: 10.1016/j.wear.2011.12.009

4. B. Chen, J.R.G. Evans. Impact and tensile energies of fracture in polymer-clay nanocomposites. Polymer 2008; 49:5113-5118.
DOI: 10.1016/j.polymer.2008.09.024

5. M. Abdalla. D. Dean, D. Adibempe, E. Nyairo, P. Robinson, G. Thompson. The effect of interfacial chemistry on molecular mobility and morphology of multiwalled carbon nanotubes epoxy nanocomposite. Polymer 2007; 48:5662-5670.
DOI: 10.1016/j.polymer.2007.06.073

6. D.B. Stojanovic, L. Brajovic, A. Orlovic, D. Dramlic, V. Radmilovic, P.S. Uskokovic, R. Aleksic. Transparent PMMA/ silica nanocomposites containing silica nanoparticles coating under supercritical conditions. Progress in Organic Coatings 2013; 79:626-631.
DOI: 10.1016/j.porgcoat.2012.12.002

7. Z. Guo, T. Pereira, O. Choi, Y. Wang, H.T. Hahn. Surface functionalized alumina nanoparticle filled polymeric nanocomposites with enhanced mechanical properties. Journal of Material Chemistry 2006; 16:2800-2808.
DOI: 10.1016/b603020c

8. C.Y. Chee, N.L. Song, L.C. Abdullah, T.S.Y. Choong, A. Ibrahim, T.R. Chantara. Characteristics of mechanical properties: Low-density polyethylene nanocomposite using nanoalumina particle as filler. Journal of Nanomaterials 2012; 2012:1-6.
DOI: 10.1155/2012/215978

9. N. Wang, C. Zhao, Z. Shai, Y. Shao, H. Li, N. Gao. Co-incorporation of MMT and MCM-41 nanomaterials used as fillers. Materials Science and Engineering B 2009; 157:44-47.
DOI: 10.1016/j.mseb.2008.12.007

10. H. Wang, P. Xu, S. Meng, W. Zhong, W. Du, Q. Du. Poly(methyl methacrylate)/silica/titania ternary nanocomposites with greatly improved thermal and ultraviolet-shielding properties. Polymer Degradation and Stability 2006; 91:1455-1461.
DOI: 10.1016/j.polymdegradstab.2005.10.008

11. B.A. Ibrahim, K.M. Kadum. Influence of polymer blending on mechanical and thermal properties. Modern Applied Science 2010; 4:157-161.
DOI: 10.5539/mas.v4n9p157

12. R.U. Arinze, A.N. Eboatu, N.H. Okeye, I.J. Dioha, P.U. Ofora, P.I. Udeozo, A. Ogbonna. Structure on the thermomechanical behaviour of PS:PMMA blends. Middle-East Journal of Science Research 2014; 21:1071-1074.
DOI: 10.5829/idosi.mejsr.2014.21.07.85146

13. A. Kausar. Study on physical properties of poly(methyl methacrylate)/poly(thiophene amide)-silica-titania-grafted multiwalled carbon nanotubes-based nanofiber composites. High Performance Polymers 2014; 26:961-969.
DOI: 10.1177/0954008314536213

14. N. Wang, J. Zhang, Q. Fang, D. Hui. Influence of mesoporous fillers with PP-g-MA on flammability and tensile behaviour of polypropylene composites. Composites: Part B 2013; 44:467-471.
DOI: 10.1016/j.compositesb.2012.04.006

15. S. Wacharawichanant, N. Thongbunyoung, P. Churdchoo, T. Sookjai. Effect of zinc oxide on the morphology and mechanical properties of poly(styrene-co-acrylonitrile)/poly(methyl methacrylate)/zinc oxide composites. Science Journal 2010; 1:21-26.

16. L.B. de Paiva, A.R. Morales, T.R. Guimaraes. Structural and optical properties of polypropylene-montmorillonite nanocomposites. Materials Science and Engineering A 2007; 447:261-265.
DOI: 10.1016/j.msea.2006.10.066

17. S. Ray, S.Y. Quek, A. Easteal, X.D. Chen. The potential use of polymer-clay nanocomposites in food packaging. International Journal of Food Engineering 2006; 2:1-11.
DOI: 10.2202/1556-3758.1149

18. A.B. Morgan, R.H. Harris Jr., T. Kashiwagi. L.J. Chyall, J.W. Gilman. Flammability of polystyrene layered silicate (clay) nanocomposites: Carbonaceous char formation. Fire and Materials 2002; 26:247-253.
DOI: 10.1002/fam.803

19. H. Zou, S. Wu, J. Shen. Polymer/silica nanocomposites: Preparation, characterization, properties and applications. Chemical Reviews 2008; 108:3893-3957.
DOI: 10.1021/cr068035q

20. M.M.A. Nikje, M.R. Khanmohammadi, A.B. Garmarudi, M. Haghshenas. Nanosilica reinforced epoxy floor coating composites: Preparation and thermophysical characterization. Current Chemistry Letters 2012; 1:13-20.
DOI:10.5267/j.ccl.2011.12.002

21. S. Chen, B. You, S. Zhou, L. Wu. Preparation and characterization of scratch and mar resistant waterborne epoxy/silica nanocomposites clearcoat. Journal of Applied Polymer Science 2009; 112:3634-3639.
DOI: 10.1002/APP.29865

22. E. Vasiliu, C.S. Wang, R.A. Vaia. Preparation of optically transparent films of poly(methyl methacrylate) (PMMA) and montmorillonite. Materials Research Society Symposium Proceedings 2002; 703:243-248.
DOI: 10.1557/PROC-703.V6.4

23. W. Brostow, M. Dutta, J. Ricardo de Souza, P. Rusek, A. Marco de Medeiros, E.N. Ito. Nanocomposites of poly(methyl methacrylate) (PMMA) and montmorillonites (MMT) Brazilian clay: A tribological study. eXPRESS Polymer Letters 2010; 4:570-575.
DOI: 10.3144/express polymlett.2010.17

24. D. Lomonaco, F.J.N. Maria, S.E. Mazzetto. Thermal evaluation of cashed nutshell liquid as new bioadditives for poly(methyl methacrylate). Journal of Thermal and Analytical Calorimetry 2013; 111:619-626.
DOI: 10.1007/s10973-012-2383-6

25. E. Caponetti, L. Pedone. M.L. Saladino, D.C. Martino, G. Nasillo. MCM-41-CdS nanocomposites materials. Preparation and characterization. Microporous and Mesoporous Materials 2010; 128:101-107.
DOI: 10.1016/j.micromeso.2009.08.010

26. E. Kraleva, M.L. Saladino. A. Spinella, G. Nasillo, E. Caponetti. $H_3PW_{12}O_{14}$ supported on mesoporous MCM-41 and AL-MCM-41 materials: Preparation and characterization. Journal of Material Science 2011; 46:7114-7120.
DOI: 10.1007/s10853-011-5505-9

27. K. Kherzi, H. Roghano-Mamaqani. Effect of MCM-41 nanoparticles on ARGET ATRP of styrene: Investigating thermal properties. Journal of Composite Materials 2015; 49:1525-1535.

DOI: 10.1177/0021998314535961

28. F.A. Zhang, D.K. Lee, T.J. Pinnavaia. PMMA/mesoporous silica nanocomposites: Effect of framework stricture and pore size on thermomechanical properties. Polymer Chemistry 2010; 1:107-113.
DOI: 10.1039/b9py00232d

29. H. Yang, L. Yuan, G. Zhu, A. Yu, H. Xu. Luminescent properties of YAG:Ce^{3+} phosphor powders prepared by hydrothermal-homogeneous precipitation method. Materials Letters 2009; 63:2271-2273.
DOI: 10.1016/j.matiet.2009.07.012

30. D.N. Chung, D.N. Hieu, T.T. Thao, V.V. Truong, N.N. Dinh. Synthesis and characterization of Ce-doped $Y_3Al_5O_{12}$ (YAG: Ce^{3+}) nanopowders used for solid-state lighting. Journal of Nanomaterials 2014; 2014:1-7.
DOI: 10.1155/2014/571920.

31. G. Xia, S. Zhong, J. Zhang, J. Xu. Structural and optical properties of YAG:Ce^{3+} phosphors by sol-gel combustion method. Journal of Crystal Growth 2005; 279:357-362.
DOI: 10.1016/j.jcrysgro.2005.01.072

32. A. Zanotto, A. Spinella, G. Nasillo, E. Caponetti, A.S. Luyt. Macro-micro relationship in nanostructured functional composites. eXPRESS Polymer Letters 2012; 6:410-416.
DOI: 10.3144/expresspolymlett.2012.43

33. D. Obradovic, N. Cosovic. Creating composite materials with polymeric matrix. International Journal of Composite Materials 2013; 3:25-31.
DOI: 10.5923/j.cmaterials.20130302.01

34. Y.C. Chen, X.L. Chen, R.L.H. Liu, H.J. Shu, M.D. Ger. Preparation of villus-like PMMA-silica hybrids via surface modification and wet grinding. Journal of Alloys and Compounds 2010; 507:302-308.
DOI: 10.1016/j.jallcom.2010.07.187

35. X. Huang, W.J. Brittain. Synthesis and characterization of PMMA nanocomposites by suspension and emulsion polymerization. Macromolecules 2001; 34:3255-3260.
DOI: 10.1021/ma001670s

36. X. Ma, B. Zhou, Y. Deng, Y. Sheng, C. Wang, Y. Pan, Z. Wang. Study on $CaCO_3$/PMMA nanocomposite microspheres by soapless emulsion polymerization. Colloids and Surface A: Physicochemical Engineering Aspects 2008; 312:190-194.
DOI: 10.1016/jcolsurfa.2007.06.058

37. P. Galka, J. Kowalonek, H. Kaczmarek. Thermogravimetric analysis of thermal stability of poly(methyl methacrylate) films modified with photoinitiators. Journal of Thermal Analysis and Calorimetry 2014; 115:1387-1394.
DOI: 10.1007/s10973-013-3466-z

38. C. Cao. Z. Tan, S. Sun, Z. Liu. H. Zhang. Enhancing the thermal stability of poly(methyl methacrylate) by removing the chains with weak links in a continuous polymerization. Polymer Degradation and Stability 2011; 96:2209-2214.
DOI: 10.1016/j.polymdegradstab.2011.09.005

39. B. Zhang, F.D. Blum. Thermogravimetric study of ultrathin PMMA films on silica: Effect of tacticity. Thermochimica Acta 2003; 396:211-217.
PII: S0040-6031(02)00518-X

40. B.J. Holland, J.N. Hay. The effect of polymerization condition on the kinetics and mechanism of thermal degradation of PMMA. Polymer Degradation and Stability 2002; 77:435-439.
PII: S0141-3910(02)00100-3

41. T. Tadano, R. Zhu, S. Suzuki, T. Hoshi, D. Sasaki, T. Hagiwara, T. Sawaguchi. Thermal degradation of transparent poly(methyl methacrylate)/silica nanoparticles hybrid films. Polymer Degradation and Stability 2014; 109:7-12.
DOI: 10.1016/j.polymdegradstab.2014.06.009

42. M. Ferriol, A. Gentilhomme, M. Coches, N. Oget, J.L. Mieloszynski. Thermal degradation of poly(methyl methacrylate) (PMMA): Modelling of DTG and TG curves. Polymer Degradation and Stability 2003: 79:271-281.
PII: S0141-3910(02)00291-4

43. J.L.H. Chau, C.C. Hsieh, Y.M. Lin, A.K. Li. Preparation of transparent silica-PMMA nanocomposites hard coatings. Progress in Organic Coatings 2008; 62:436-439.
DOI: 10.1016/j.porgcoat.2008.02.005

44. C. Barthet, A.J. Hickey, D.B. Cairns, S.P. Armes. Synthesis of novel polymer-silica colloidal nanocomposites via free-radical polymerization of vinyl monomers. Advanced Materials 1999; 11:408-410.
DOI: 10.1002/(SICI)1521-4095(199903)11:5<408::AID-ADMA408>3.0.CO;2-Y

45. X.L. Xie, Q.X. Liu, R.K.Y. Li, X.P. Zhou, Q.X. Zhang, Z.Z. Yu, Y.W. Mai. Rheological and mechanical properties of PVC/$CaCO_3$ nanocomposites prepared by *in situ* polymerization. Polymer 2004; 45:6665-6673.
DOI: DOI:10.1016/j.polymer.2004.07.045

46. T. Mizetani, K. Arai, M. Miyamoto, Y. Kimura. Preparation of spherical nanocomposites consisting of silica core and polyacrylate shell by emulsion polymerization. Journal of Applied Science 2006; 99:659-669.
DOI: 10.1002/app.22503

47. F. Yang, R. Yngard, A. Hernberg, G.L. Nelson. Thermal stability and flammability of polymer-silica nanocomposites prepared via extrusion. ACS Symposium Series 2005; 922:144-154.
DOI: 10.1021/bk-2006-0922.ch012

48. A.D. Brailsford. E.M. Logothetis. Selected aspects of gas sensing. Sensors and Actuators B: Chemical 1998; 52:195-203.
DOI: 10.1016/S0925-4005(98)00273-1

49. B. Zhang, F.D. Blum. Thermogravimetric study of ultrathin PMMA films on silica: Effect of tacticity. Thermochimica Acta 2003; 396:211-217.
DOI: 10.1016/s0040-6031(02)00518-X

50. R. Saito, S. Kobayashi, T. Shimo, H. Hayashi. Surface hardness of organic polymer-silica nanocomposites prepared with perhydropolysilazane. Proceedings of the 8th Polymer for Advanced Technologies International Symposium, Budapest, Hungary (2005).

51. Y. Kobayashi, Y.W.M. Sarata, H. Hamada, K. Yamada, M. Kotaki, K. Yoshinaga, H. Karakawa, H. Ito, K. Kamaza, T. Kikutani. Mechanical and thermal properties of micro- and nano-silica-filled PMMA micro injection moldings.16th International Conference on Composite Materials, Kyoto, Japan (2007).

52. M.T. Run, S.Z. Wu. D.Y. Zhang, G. Wu. A polymer/mesoporous molecular sieve composite: Preparation structure and properties. Materials Chemistry and Physics 2007; 105:341-347.
DOI: 10.1016/j.matchemphys.2007.04.070

53. F.A. Zhang, D.K. Lee, T.J. Pinnavaia. PMMA/mesoporous silica nanocomposites: Effect of framework structure and pore size on thermomechanical properties. Polymer Chemistry 2010; 1:107-113.
DOI: 10.1039/b9py00232d

54. L.D. Perez, L.F. Giraldo, W. Brostow, B.L. Lopez. Poly(methyl acrylate) plus mesoporous silica nanohybrids: Mechanical and thermophysical properties. e-Polymers 2007; 7:324-334.
DOI: 10.1515/epoly.2007.7.1.324

55. F.A. Zhang, D.K. Lee, T.J. Pinnavaia. PMMA-mesocellular foam silica nanocomposites prepared through batch emulsion polymerization and compression molding. Polymer 2009; 50:4768-4774.
DOI: 10.1016/j.polymer.2009.08.007

56. F.A. Zhang, C. Song, C.L. Yu. Effect of preparation methods on the property of PMMA/SBA-15 mesoporous silica composites. Journal of Polymer Research 2011; 18:1757-1764.
DOI: 10.1007/s10965-011-9582-x

57. S.R. Valandro, P.C. Lombardo, A.L. Poli, M.A. Horn, M.G. Neumann, C.C.S. Cavalheiro. Thermal properties of poly(methyl methacrylate)/organomodified montmorillonites nanocomposites obtained by in situ photopolymerization. Materials Research 2014; 17:265-270.
DOI: 10.1590/S1516-14392013005000173

58. K.I. Garcia-Chavez, C.A. Hernandez-Escobar, S.G. Flores-Gallardo, F. Soriano-Corral, E. Saucedo-Salazar, E.A. Zaragoza-Contreras. Morphology and thermal properties of clay/PMMA nanocomposites obtained by miniemulsion polymerization. Micron 2013; 49:21-27.
DOI: 10.1016/j.micron.2013.02.007

59. Y. Wang, J.Y. Guo. Melt compounding of PMMA/clay nanocomposites with styrene-maleic anhydride copolymers: Effect of copolymer types on the thermal, mechanical and dielectric properties. Polymer Composites 2010; 31:596-603.
DOI: 10.1002/pc.20832

60. J.M. Yeh, C.F. Hsieh, C.W. Yeh, M.J. Wu, H.C. Yang. Organic base-catalysed sol-gel route to prepare PMMA-silica hybrid materials. Polymer International 2007; 56:343-349.
DOI: 10.1002/pi.2143

61. X.M. Ma, B. Wang, M.X. Zhang, F.F. Min, J. He. Synthesis and thermal characterizations of PMMA nanocomposites functionalized by polyhedral oligomeric silsesquioxane. Phosphorus, Sulfur, and Silicon and Related elements 2013; 188:1819-1826.
DOI: 10.1080/10426507.2013.788001

62. E. Dzunuzovic, K. Jeremic, J.M. Nedeljkovic. In situ radical polymerization of methyl methacrylate in a solution of surface modified TiO_2 and nanoparticles. European Polymer Journal 2007; 43:3719-3729.
DOI: 10.1016/j.eurpolymj.2007.06.026

63. E. Dzunuzovic, M. Marinovic-Cincovic, J. Vukovic, K. Jeremic, J.M. Nedeljkovic. Thermal properties of PMMA/TiO_2 nanocomposites prepared by in-situ bulk polymerization. Polymer Composites 2009; 30:738-742.
DOI: 10.1002/pc.20606

64. N. Katsikis, F. Zahradnik, A. Helmoschrott, H. Munstedt, A. Vital. Thermal studies of poly(methyl methacrylate)/silica nano- and microcomposites as investigated by dynamic-mechanical experiments. Polymer Degradation and Stability 2007; 92:1966-1976.
DOI: 10.1016/j.polymdegradstab.2007.08.009

65. H.P. Fu, R.Y. Hong, Y.J. Zhang, H.Z. Li, B. Xu, Y. Zheng, D.G. Wei. Preparation and properties investigation of PMMA/silica composites derived from silicic acid. Polymers for Advanced Technologies 2009; 20:84-91.
DOI: 10.1002/pat.1226

66. X. Wang, L. Wu, J. Li. Synergistic flame retarded poly(methyl methacrylate) by nano-ZrO_2 and triphenylphosphine. Journal of Thermal Analysis and Calorimetry 2011; 103:741-746.

DOI: 10.1007/s10973-010-1050-z

67. N. Garcia, T. Corrales, J. Guzman, P. Tiemblo. Understanding the role of nanosilica particles surface in the thermal degradation of nanosilica-poly(methyl methacrylate) solution-blending nanocomposites: From low to high silica concentration. Polymer Degradation and Stability 2007; 92:635-643.
DOI: 10.1016/j.polymdegradstab.2007.01.006

68. H. Wang, S. Meng, P. Xu, W. Zhong, Q. Du. Effect of traces of inorganic content on thermal stability of poly(methyl methacrylate) nanocomposites. Polymer Engineering and Science 2007; 47:302-307.
DOI: 10.1002/pen.20708

69. T. Kashiwagi, A.B. Morgan, J.M. Antonucci, M.R.V. Landingham, R.H. Harris, W.H. Awad, J.R. Shields. Thermal and flammability properties of silica-poly(methylmethacrylate) nanocomposites. Journal of Applied Polymer Science 2003; 89:2072-2078.
DOI: 10.1002/app.12307

70. A. Laachachi, M. Ferriol, M. Cochez, D. Ruch, J.M.L. Cuesta. The catalytic role of oxide in the thermooxidative degradation of poly(methyl methacrylate)-TiO_2 nanocomposites. Polymer Degradation and Stability 2008; 93:1131-1137.
DOI: 10.1016/j.polymdegradstab.2008.03.006

71. Y.L. Liu, C.Y. Hsu, K.Y. Hsu. Poly(methyl methacrylate)-silica nanocomposites confirmed films from surface-functionalized silica nanoparticles. Polymer 2005; 46:1851-1856.
DOI: 10.1016/j.polymer.2005.01.009

72. J.M. Yeh, C.J. Weng, K.Y. Huang, C.C. Lin. Effect of baking treatment and materials composition on the properties of bulky PMMA-silica hybrid sol-gel materials with low volume shrinkage. Journal of Applied Polymer Science 2006; 101:1151-1159.
DOI: 10.1002/app.24211

73. P.S. Chimthamanipeta, S. Kobukata, H. Nakata, D.A. Shipp. Synthesis of poly(methyl methacrylate)-silica nanocomposites using methacrylate-functionalized silica nanoparticles and RAFT polymerization. Polymer 2008; 49:5636-5642.
DOI: 10.1016/j.polymer.2008.10.018

74. Y.H. Hu, C.Y. Chen, C.C. Wang. Viscoelastic properties and thermal degradation kinetics of silica/PMMA nanocomposites. Polymer Degradation and Stability 2004; 84:545-553.
DOI:10.1016/j.polymdegradstab.2004.02.001

75. N. Patra, M. Salerno, P.D. Cozzoli, A.C. Barone, L. Ceseracciu, F. Pignatelli, R. Carzino, L. Marini, A. Athanassiou. Thermal and mechanical characterization of PMMA nanocomposites filled with TiO_2nanorods. Composites: Part B 2012; 43:3114-3119.
DOI: 10.1016/j.compositesb.2012.04.028

76. A. Anzlovar, Z.C. Orel, M. Zigon. Mechanical properties of PMMA/ZnO nanocomposites. 15th European Conference on Composites Materials, Venice, Italy (2012).

77. T.E. Motaung, A.S. Luyt, M.L. Saladino, D.C. Martino, E. Caponetti. Morphology, mechanical properties and thermal degradation kinetics of PMMA-zirconia nanocomposites prepared by melt compounding. eXPRESS Polymer Letters 2012; 6:871-881.
DOI: 10.3144/expresspolymlett.2012.93

78. Y. Hu, G. Gu, S. Zhou, L. Wu. Preparation and properties of transparent PMMA/ZrO_2 nanocomposites using 2-hydroxylthyl methacrylate as a coupling agent. Polymer 2011; 52:122-129.
DOI: 10.1016/j.polymer.2010.11.020

79. B.J. Ash, L.S. Schadler, R.W. Siegel. Glass transition behavior of alumina/polymethylmethacylate nanocomposites. Materials Letters 2002; 55:83-87.
PII: S0167-577X(01)00626-7

80. B.J. Ash, R.W. Siegel. L.S. Schadler. Mechanical behavior of alumina/poly(methyl methacrylate) nanocomposites. Macromolecules 2004; 37:1358-1369.
DOI: 10.1021/ma0354400

81. B.J. Ash, D.F. Rogers, C.J. Wiegand, L.S. Schadler, R.W. Siegel. B.C. Benicewicz, T. Apple. Mechanical properties of Al_2O_3 polymethylmethacylate nanocomposites. Polymer Composites 2002; 23:1014-1025.
DOI: 10.1002/pc.10497

82. J. Jiao, L. Wang, P. Lv, P. Liu, Y. Cai. Low dielectric constant nano porous silica/PMMA nanocomposites with improved thermal and mechanical properties. Materials Letters 2013; 109:158-162.
DOI: 10.1016.j.matlet.2013.07.070

83. D. Singh, A. Kumar, K.N. Rai. Nanosil strengthening of PMMA composites panels. Journal of Thermoplastic Composite Materials 2011; 25:591-606.
DOI: 10.1177/0892705711412648

84. M.K. Seo, S.J. Park. Effect of graphite nanofibers on poly(methyl methacrylate) nanocomposites for bipolar plates. Bull Korean Chem Soc. 2009; 30:671-673

85. K. Soygun, S. Simsek, E, Yilmaz, G. Bolayir. Investigation of mechanical and structural properties of blend lignin-PMMA. Advances in Materials Science and Engineering. 2013; 2013:435260.
DOI: 10.1155/2013/435260

86. J.H. Park, S.C. Jana. The relationship between nano- and micro-structures and mechanical properties in PMMA-epoxy-nanoclay composites. Polymer 2003; 44:2091-2100.
DOI: 10.1016/S0032-3861(03)00075-2

87. M.B. Kulkarni, P.A. Mahanwar. Effect of methyl methacrylate-acrylonitrile-butadiene-styrene (MABS) on the mechanical and thermal properties of poly(methyl methacrylate) (PMMA)-fly ash cenospheres (FAC) filled composites. Journal of Minerals and Materials Characterization and Engineering 2012; 11:365-383.
DOI: 10.4236/jmmce.2012.114027

88. R.Y. Hong, H.P. Fu, Y.J. Zhang, L. Liu, J. Wang, H.Z. Li, Y. Zheng. Surface-modified silica nanoparticles for reinforcement of PMMA. Journal of Applied Polymer Science 2007; 105:2176-2184.
DOI: 10.1002/app.26164

89. R. Zong, Y. Hu, N. Liu, S. Wang, G. Liao. Evaluation of the thermal degradation of PC/ABS/montmorillonite nanocomposite. Polymers for Advanced Technologies 2005; 16:725-731.
DOI: 10.1002/pat.51

90. M.C. Gupta, S.G. Viswanath. Role of metal oxide in the thermal degradation of bisphenol A polycarbonate. Journal of Thermal Analysis 1996; 46:1671-1679.
DOI: 10.1021/ie9700167

91. H. Polli, L.A.M. Pontes, A.S. Araujo. Application of model-free kinetics to the study of thermal degradation of polycarbonate. Journal of Thermal Analysis and Calorimetry 2005; 79:383-387.
DOI: 10.1007/s10973-005-0070-6

92. B.N. Jang, C.A. Wilkie. A TGA/FTIR and mass spectra study on the thermal degradation of bisphenol A polycarbonate. Polymer Degradation and Stability 2004; 86:419-430.
DOI: 10.1016/j.polymdegradstab.2004.05.009

93. K.M. Blackwood, R.A. Pethrick, F.I. Simson, R.E. Day, C.L. Watson. Titanium dioxide induced failure in polycarbonate. Journal of Materials Science 1995; 30:4435-4445.
DOI: 10.1007/BF00361529

94. Y. Imai, A. Terahara, Y. Hakuta, K. Matsui, H. Hayashi, N, Ueno. Transparent (bisphenol A carbonate)-based nanocomposites with high refractive index nanoparticles. European Polymer Journal 2009; 45:630-638.
DOI: 10.1016/j.eurpolymj.2008.12.031

95. F. Rouabah, M. Fois, L, Ibos, A. Boudenne, D. Dadache. Mechanical and thermal properties of polycarbonate. II. Influence of titanium dioxide content and quenching on pigmented polycarbonate. Journal of Applied Polymer Science 2007; 106:2710-2717.
DOI: 10.1002/app.26807

96. H. Vahabi, O. Eterradossi, L. Ferry, C. Longuet, R. Sonnier, J.M. Lopez-Cuesta. Polycarbonate nanocomposites with improved fire behavior, physical and psychophysical transparency. European Polymer Journal 2013; 49:319-327.
DOI: 10.1016/j.eurpolymj.2012.10.031

97. Y. Feng, B. Wang, F. Wang, G. Zheng, K. Dai, C. Lui, J. Chen, C. Shen. Effect of modified silica on morphology, mechanical property, and thermostability of injection-molded polycarbonate/silica nanocomposites. Journal of Reinforced Plastics and Composites 2014; 33:911-922.
DOI: 10.1177/0731684413520188

98. S. Maiti, N.K. Shrivastava, S. Suin, B.B. Khatua. A strategy for achieving low percolation and high electrical conductivity in melt-blended polycarbonate (PC)/multiwalled carbon nanotubes (MWCNT) nanocomposites: Electrical and thermo-mechanical properties. eXPRESS Polymer Letters 2013; 7:505-518.
DOI: 10.3144/expresspolymlett.2013.47

99. A.S Luyt, M.D. Dramicanin, Z. Antic, V. Djokovic. Morphology, mechanical and thermal properties of composites of polypropylene and nanostructured wollastonite filler. Polymer Testing 2009; 28:348-356.
DOI: 10.1016/j.polymertesting.2009.01.010

100. X.Y. Yuan, L.L. Zou, C.C. Liao, J.W. Dai. Improved properties of chemically modified graphene/poly(methyl methacrylate) nanocomposites via a facile in-situ bulk polymerization. eXPRESS Polymer Letters 2012; 6:847-858.
DOI: 10.3144/expresspolymlett.2012.90

101. S.V. Krishna, G. Pugazhenthi. Influence of processing conditions on the properties of polystyrene (PS)/organomontmorillonite (OMMT) nanocomposites prepared via solvent blending method. International Journal of Polymeric Materials 2010; 60:144-162.
DOI: 10.1080/00914037.2010.504167

102. J. Feng, J. Hao, J. Du, R. Yang. Effect of organoclay on the flammability, thermal and mechanical properties of polycarbonate nanocomposites filled with a phosphate and organoclays. Polymer Degradation and Stability 2012; 97:108-117.
DOI: 10.1016/j.polymdegradstab.2011.09.019

103. K. Nevalainen, J. Vuorinen, V. Villman, R. Suihkonen, P. Jarvela. Characterization of twin-screw-extruder-compounded polycarbonate nanoclay composites. Polymer Engineering and Science 2009; 49:631-640.
DOI: 10.1002/pen.21086

104. S. Suin, N.K. Shrivastava, S. Maiti, B.B. Khatua. Phosphonium modified organoclay as potential nanofiller for the development of exfoliated and optically transparent polycarbonate/clay nanocomposites: Preparation and characterization. European Polymer Journal 2013; 49:49-60.
DOI: 10.1016/j.eurpolymj.2012.10.004

105. F.J. Carrion, J. Sanes, M.D. Bermudez. Influence of ZnO nanoparticles filler on the properties and wear resistance of polycarbonate. Wear 2007; 262:1504-1510.
DOI: 10.1016/j.wear.2007.01.016

106. S.H. Jin, D.K. Choi, D.S. Lee. Electrical and rheological properties of polycarbonate/multiwalled carbon nanotube nanocomposites. Colloids and Surfaces A: Physicochemical and Engineering Aspects 2008; 313-314:242-245.
DOI: 10.1016/j.colsurfa.2007.04.104

107. B.S. Rathore, M.S. Gaur, K.S. Singh. Investigation of optical and thermally stimulated properties of SiO_2 nanoparticles-filled polycarbonate. Journal of Applied Polymer Science 2012; 126:960-968.
DOI: 10.1002/app.37004

108. B.S. Rathore, M.S. Gaur, K.S. Singh. Investigation of thermally stimulated charge relaxation mechanism in SiO_2 filled polycarbonate nanocomposites. Journal of Thermal Analysis and Calorimetry 2012; 107:675-680.
DOI: 10.1007/s10973-011-1624-4

109. H.J. Hee, S.Y. Taek, S.K. Heon, K.W. Nylon, K. Byoung, K.S. Lyong, L.C. Hong. Morphology and dynamic mechanical properties of poly(acrylonitrile-butadiene-styrene)/polycarbonate/clay nanocomposites prepared by melt mixing. Instrumentation Science and Technology 2007; 14:519-532.
DOI: 10.1163/156855407781291290

110. T.E. Motaung, M.L. Saladino, A.S. Luyt, D.C. Martino. Influence of the modification, induced by zirconia nanoparticles, on the structure and properties of polycarbonate. European Polymer Journal 2013; 49:2022-2030.
DOI: 10.1016/j.eurpolymj.2013.04.019

111. A.S. Luyt, M. Messori, P. Fabbri, J.P. Mofokeng, B. Taurino, T. Zanasi, F. Pilati. Polycarbonate reinforced with silica nanocomposites. Polymer Bulletin 2011; 66:991-1004.
DOI: 10.1007/s00289-010-0408-5

112. M. Sanchez-Soto, D.A. Schiraldi, S. Illescas. Study of the morphology and properties of melt-mixed polycarbonate-POSS nanocomposites. European Polymer Journal 2009; 45:314-352.

DOI: 10.1016/j.eurpolymj.2008.10.026

113 M. Wegrzyn, B. Galindo, A. Benedito, E. Gimenaz. Effect of processing method on mechanical properties of PC/ABS-MWCNT nanocomposites. Macromolecular Symposia. 2012; 321-322:161-165.
DOI: 10.1002/masy.201251128

114. P. Potschke, M.H. Arnaldo, H.J. Radusch. Percolation behaviour and mechanical properties of polycarbonate composites filled with carbon black/carbon nanotube systems. Polymer 2012; 57:204-211.
DOI: 10.14314/polimery.2012.204

115. J. Vani, S.S. Mohanty, M.R. Parvaiz, S.K. Nayak. Influence of nanoclays and nano-TiO_2 on the mechanical and thermal properties of polycarbonate nanocomposites. Macromolecular Research 2011; 19:563-572.
DOI: 10.1007/s13233-011-0608-3

116. F. Asyadi, M. Jawaid, A. Hassan, M.U. Wahit. Mechanical properties of mica-filled polycarbonate/poly(acrylonitrile-butadiene-styrene) composites. Polymer-Plastics Technology and Engineering 2013; 52:727-736.
DOI: 10.1080/03602559.2012.762672

117. K. Nevalainen, J. Vuorinen, V. Villaman, R. Suihkonen, P. Jarvela, J. Sundelin, T. Lepisto. Characterization of twin-screw-extruder-compounded polycarbonate nanoclay composites. Polymer Engineering and Science 2009; 49:631-640.
DOI: 10.1002/pen.21086

118. J. Ryszkowska, E. Zawadzak, D. Hreniak, W. Strek, K. J. Kurzydlowski. Structure and properties of polyurethane/YAG:Tb^{3+} nanocomposites with luminescence properties. Polimery 2007; 52:340-344.

119. S.S Musbah, V. Radojevic, I. Radovic, P.S. Uskokovic, D.B. Stojanovic, M. Dramicanin, R. Aleksic. Preparation, characterization and mechanical properties of rare-earth-based nanocomposites. Journal of Mining and Metallurgy 2012; 48:309-318.
DOI: 10.2298/JMMB120508030M

120. M. Marinovic-Cincovic, Z. Antic, R. Krsmanovic, M. Mitric, M.D. Dramicanin. Thermal and luminesce properties of nano-Gd_2O_3: $Eu^{2+/}$ PMMA composite. Journal of Optoelectronics and Advanced Materials-Symposia 2009; 1:54-58.

121. L. Dacanin, S.R. Lukic, D.M. Petrovic, Z. Antic, R. Krsmanovic, M. Marinovic-Cincovic, M.D. Dramicanin. PMMA/Zn_2SiO_4: Eu^{3+} (Mn^{2+}) composites: Preparation, optical and thermal properties. Journal of Materials Engineering and Performance 2012; 21:1509-1513.
DOI: 10.1007/s11665-011-0049-3

122. Z. Antic, R. Krsmanovic, M. Marinovic-Cincivic. M.D. Dramicanin. Gd_2O_3:Eu^{3+}/PMMA composites: Thermal and luminescence properties. Acta Physica Polonica A 2010; 117:831-836.

123. J.S. Beck, J.C. Vartuli, W.J. Roth, M.E. Leonowicz, C.T. Kresge, K.D. Schimitt, C.T.W. Chu, D.H. Olson, E.W. Sheppard, S.B. McCullen, J.B. Higgins, J.L. Schlenker. A new family of mesoporous molecular sieves prepared with liquid crystal template. Journal of the American Chemical Society 1992; 114:10834.
DOI: 10.1021/ja00053a020

124. A. Corma, Q. Kan, M.T. Navarro, J.P. Pariente, F. Rey. Synthesis of MCM-41 with different pore diameters without addition of auxiliary organics. Chemistry of Materials 1997; 9:2123-2126.
DOI: 10.1021/cm970203v

125. A. Kierys, R. Zaleski, M. Grochowicz, J. Goworek. Thinning down of polymer matrix by entrapping silica nanoparticles. Colloid and Polymer Science 2011; 289:751-758.
DOI: 10.1007/s00396-011-2386-z

126. J.A. Araujo, F.T. Cruz, I.H. Cruz, D. Cardoso. Encapsulation of polymers in CTA-MCM-41 via microemulsion. Microporous and Mesoporous Materials 2013; 180:14-21.
DOI: 10.1016/j.micromeso.2013.05.010

127. N. Wang, H. Li, J. Zhang. Polymer-filled porous MCM-41: An effective means to design polymer-based nanocomposites. Materials Letters 2005; 59:2685-2688.
DOI: 10.1016/j.matlet.2005.04.020

128. N. Wang, Y. Shao, Z. Shi, J. Zhang. H. Li. Preparation and characterization of epoxy composites filled with functionalized nano-sized MCM-41 particles. Journal of Materials Science 2008; 43:3683-3688.
DOI: 10.1007/s10853-008-2591-4

129. N. Wang, Y. Shao, Z. Shi, J. Zhang, H. Li. Influence of MCM-41 particle on mechanical and morphological behavior of polypropylene. Materials Science and Engineering A 2008; 497:363-368.
DOI: 10.1016/j.msea.2008.07.019

130. N. Wang, Q, Fang, Y. Shao, J. Zhang. Microstructure and properties of polypropylene composites filled with co-incorporation of MCM-41 (with template) and OMMT nanoparticles prepared by melt-compounding. Materials Science and Engineering A 2009; 512:32-38.
DOI: 10.1016/j.msea.2009.01.027

131. M.L. Saladino, E. Kraleva, S. Todorova, A. Spinnella, G. Nasillo, E. Caponetti. Synthesis and characterization of mesoporous Mn-MCM-41 materials. Journal of Alloys and Compounds 2011; 509:8798-8803.
DOI: 10.1016/j.jallcom.2011.06.078

132. A. Sayari, Y. Yang. Highly ordered MCM-41 silica preparation in the presence of decyltrimethylammonium bromide. The Journal of Physical Chemistry B 2000; 104:4835-4839.
DOI: 10.1021/JP0001900

133. H.I. Melendez-Ortiz, A. Mercado-Silva, L.A. Garcia-Cerda, G. Castruita, Y.A. Perera-Mercado. Hydrothermal synthesis of mesoporous silica MCM-41 using commercial sodium silicate. Journal of the Mexican Chemical Society 2013; 57:73-79.

134. Y. Xia, R. Mokaya. A study of the behaviour of mesoporous silica in OH/CTABr/H2O system: Phase dependent stabilisation, dissolution or semi-pseudomorphoc transformation. Journal of Materials Chemistry 2003; 13:3112-3121.
DOI: 10.1039/b305404g

135. L. Wang, X. Han, J. Li, D. Zheng. Preparation of modified mesoporous MCM-41silica spheres and its application in pervaporation. Powder Technology 2012; 231:63-69.
DOI: 10.1016/j.powtec.2012.07.044

136. Z. Liu, Z. Dong, B. Han, J. Zhang, J. Zhang, Z. Hou, J. He, T. Jiang. Preparation of mesoporous MCM-41/poly(acrylic acid) composites using supercritical CO_2 as a solvent. Journal of Materials Chemistry 2003; 13:1373-1377.
DOI: 10.1039/b211818c

137 N. Wang, Q. Fang, E. Chen, J. Zhang, Y. Shao. Structure, crystallization behavior, and thermal stability of PP/MCM-41 nanocomposite. Polymer Engineering and Science 2009; 49:2459-2466.
DOI: 10.1002/pen.21497

138 N. Wang, C. Zhao, Z. Shi, Y. Shao, H. Li, N. Gao. Co-incorporation of MMT and MCM-41 nanomaterials used as fillers in PP composite. Materials Science and Engineering B 2009; 157:44-47.
DOI: 10.1016/j.mseb.2008.12.007

139. N. Wang, Q. Fang, E. Chen, J. Shaohang, Y. Shao. Preparation and characterization of polypropylene composites filled with different structured mesoporous particles. Journal of Composite Materials 2010; 44:2083-2093.
DOI: 10.1177/0021998309360934

140 M.A. Ver Meer, B. Narasimhan, B.H. Shanks, S.K. Mallapragada. Effect of mesoporosity on thermal and mechanical properties of polystyrene/silica composites. Applied Materials and Interfaces 2010; 2:41-47.
DOI: 10.1021/am900540x

141 M.L. Cerrada, E. Perez, J.P. Lourenco, J.M. Campos. M.R. Ribeiro. Sustainable polyethylene/MCM-41 nanocomposites by in-situ polymerization. Proceedings of the 12th International Conference on Mechanical and Technology of Composites Materials, Varna, Bulgaria (2009).

142 M.S. Cho, H.J. Choi, W.S. Ahn. Enhanced electrorheology of conducting polyaniline confined in MCM-41 channels. Langmuir 2004; 20:202-207.
DOI: 10.1021/Ia035051z

143. N. Wang, Z.X. Shi, J. Zhang, L. Wang. The influence of modification of mesoporous silica with polyethylene via in situ Ziegler-Natta polymerization on PE/MCM-41 nanocomposite. Journal of Composite Materials 2008; 42:1151-1157.
DOI: 10.1177/0021998308088568

144 N. Wang, Q. Fang, F. Zhang, E. Chen, X. Zhang. Incorporation of nano-sized mesoporous MCM-41 materials used as fillers in natural rubber composite. Materials Science and Engineering A 2011; 528:3321-3325.
DOI: 10.1016/j.msea.2010.12.105

145 L. Wang, X. Han, J. Li, D. Zheng, L. Qin. Modified MCM-41 silica spheres filled polydimethylsiloxane membrane for dimethylcarbonate/methanol separation via pervaporation. Journal of Applied Polymer Science 2013; 127:4662-4671.
DOI: 10.1002/app.38046

146 N. Wang, N. Gao, Q. Fang, E. Chen. Compatibilizing effect of mesoporous fillers on the mechanical properties and morphology of polypropylene and polystyrene blend. Materials and Design 2011; 32:1222-1228.
DOI: 10.1016/j.matdes.2010.10.012

147 N. Gao, N. Wang, Q. Fang, E. Chen, Y. Shao. Microstructure and mechanical properties of polypropylene/polystyrene blend filled with as-synthesized MCM-41 prepared by melt compounding. Journal of Materials Science 2010; 45:3052-3057.
DOI: 10.1007/s10853-010-4309-7

148 L.D. Perez, J.F. Lopez, V.H. Orozco, T. Kyu, B.L. Lopez. Effect of the chemical characteristics of mesoporous silica MCM-41 on morphology, thermal, and rheological properties of composites based on polystyrene. Journal of Applied Polymer Science 2009; 111:2229-2237.
DOI: 10.1002/app.29245

149. K. Khezri, H.R. Mamaqani. Activators generated by electron transfer for atom transfer radical polymerization of styrene in the presence of mesoporous silica nanoparticles. Materials Research Bulletin 2014; 59:241-248.
DOI: 10.1016/j.materresbull.2014.07.021

150. R. Mansencal, B. Haidar, A. Vidal, L. Delmotte, J.M. Chezeau. High-resolution solid-state NMR investigation of the filler-rubber interaction: 2. High-speed [H] magic-angle spinning NMR spectroscopy in carbon-black-filled polybutadiene. Polymer International 2001; 50:387-394.
DOI: 10.1002/pi.640

151. S. Olejniczak, S. Kazmierski, P.K. Pallathadka, M.J. Potrzebowski. A review on advances of high-resolution solid state NMR spectroscopy in structural studies of polymer/clay nanocomposites. Polimery 2007; 52:711-792.

152. T.M.F.F. Diniz, M.I.B. Tavares. A high-resolution solid-state NMR investigation of molecular mobility of poly(methyl methacrlate)/poly(vinyl pyrrolidone)/poly(ethylene oxide) ternary blends. 2006; 100:1492-1495.
DOI: 10.1002/app.23228

153. N.M. da Silva, M.I.B. Tavares. Mobility study of amorphous polymers by high-resolution NMR at solid-state. Polymer Bulletin 1995; 35:165-168.
DOI: 10.1007/BF00312909

154. O. Fricova, M. Uhrinova, V. Hronsky, M. Kovalakova, D. Olcak, I. Chodak, J. Spevacek. High-resolution solid-state NMR study of isotactic polypropylenes. eXPRESS Polymer Letters 2012; 6:204-212.
DOI: 10.3144/expresspolymlett.2013.23

155. D.G. Cory, W.M. Ritchey. Inversion recovery cross-polarization NMR in solid semicrystalline polymers. Macromolecules 1989; 22:1611-1615.
DOI: 10.1021/ma00194a018

156. A. Asano, K. Takegoshi, K. Hikichi. Inter-polymer interaction of polymer blend in solution as studied by NMR: Polycarbonate/poly(methyl methacrylate). Polymer Journal 1992; 24:473-477.
DOI: 10.1295/polymj.24.473

157. X. Zhang, K. Takegoshi, K. Hikichi. Composition dependence of the miscibility and phase structure of amorphous/crystalline polymer blends as studied by high-resolution solid-state ^{13}C NMR spectroscopy. Macromolecules 1992; 25:2336-2340.
DOI: 10.1021/ma00035a009

158. A. Asano, K. Takegoshi, K. Hikichi. Solid-state NMR study of miscibility and phase-separation of polymer-blends: Polycarbonate/poly methyl methacrylate. Polymer Journal 1992; 24:555-562.
DOI: 10.1295/polymj.24.555

159. S.L. Saladino, A. Zanotto, D.C. Martino, A. Spinella. G. Nasillo, E. Caponetti. Ce:YAG nanoparticles embedded in a PMMA matrix: Preparation and characterization. Langmuir 2010; 26:13442-13449.
DOI: 10.1021/1a9042809

160. M.L. Saladino, D.C. Martino, M.A. Floriano, D. Hreniak, L. Marciniak, W. Strek, E. Caponetti. Ce:$Y_3Al_5O_{12}$-poly(methyl methacrylate) composites for white-light emitting diodes. The Journal of Physical Chemistry 2014; 118:9107-9113.
DOI: 10.1016/jp412173g

161. T.E. Motaung, M.L. Saladino, A.S. Luyt, D.C. Martino. Influence of the modification, induced by zirconia nanoparticles, on the structure and properties of polycarbonate. European Polymer Journal 2013; 49:2022-2030.
DOI: 10.1016/j.europolymj.2013.04.019

162. T.E. Motaung, M.L. Saladino, A.S. Luyt, D.F.C. Martino. The effect of silica nanoparticles on the morphology, mechanical properties and thermal degradation kinetics of polycarbonate. Composites Science and Technology 2012; 73:34-39.
DOI: 10.1016/j.compscitech.2012.08.014

163. T.E. Motaung, A.S. Luyt, M.L. Saladino, E. Caponetti. Study of morphology, mechanical properties, and thermal degradation of polycarbonate-titania nanocomposites as function of titania crystalline phase and content. Polymer Composites 2013; 34:164-172.
DOI: 10.1002/pc.22389

164. T.E. Motaung, A.S. Luyt, F. Bondioli, M. Messori, M.L. Saladino, A. Spinella. G. Nasillo, E. Caponetti. PMMA-titania nanocomposites: Properties and thermal degradation behaviour. Polymer Degradation and Stability 2012; 97:1325-1333.
DOI: 10.1016/j.polymdegradstab.2012.05.022

165. T.E. Motaung, A.S. Luyt, M.L. Saladino. D.C. Martino, E. Caponetti. Morphology, mechanical properties and thermal degradation kinetics of PMMA-zirconia nanocomposites prepared by melt compounding. eXPRESS Polymer Letters 2012; 6:871-881.
DOI: 10.3144/expresspolymlett.2012.93

166. M.L. Saladino, T.E. Motaung, A.S. Luyt, A. Spinella, G. Nasillo, E. Caponetti. The effect of silica nanoparticles on the morphology, mechanical properties and thermal degradation kinetics of PMMA. Polymer Degradation and Stability 2012; 97:452-459.
DOI: 10.1016/j.polymdegradstab.2011.11.006

Chapter 2: Materials and Methods

2.1 Materials

2.1.1 Poly(methyl methacrylate) (PMMA)

Commercial grade PMMA (Altuglas® V920T), having a melt flow index (MFI) of 1g/10 min (230 °C/3.8 kg) and M_w = 110 000g mol^{-1} was obtained in pellet form from Bayer Materials Science in Italy.

2.1.2 Polycarbonate (PC)

Commercial grade bisphenol-A polycarbonate (Makrolon® 2407), produced and supplied in pellet form by Bayer Material Science, Germany and having a melt flow index of 20 g/10 min (300 °C/1.2 kg) and M_w = 26 576 g mol^{-1} was used.

2.1.3 Mesoporous silica (MCM-41)

MCM-41, having a surface area of ~1000 m^2g^{-1}, a pore size ranging from 2.1 to 2.7 nm, and a pore volume of 0.98 cm^3g^{-1} was supplied by Sigma Aldrich and used as received.

2.1.4 Yttrium aluminium garnet doped with cerium (Ce:YAG)

Yttrium aluminium garnet doped with cerium (Ce:YAG), with a density of 4.8 g cm^{-3}, was supplied as a yellow powder by Dogtai Tianyuan Fluorescent Materials, China and was used as received.

2.2 Methods

2.2.1 Preparation of polymer composites by melt compounding

PMMA and PC pellets, as well as MCM-41 and Ce:YAG particles, were dried in an oven at 80 °C for 12 hours before use. The composites with MCM-41 and Ce:YAG were prepared by mixing the respective polymers and fillers in a Brabender Plastograph 50 mL internal mixer at 200 °C and 50 rpm for 10 minutes. For the preparation of the composites, the polymer was first melted for 2 minutes at 200 °C, and different contents (0.1, 0.3, 0.5, 1, 2 and 5 wt.%) of the respective fillers were added into the molten polymer and mixed for a further 8 minutes. The samples were then melt pressed into 3 mm thick sheets at 200 °C for 5 minutes at 50 bar. Pure PMMA and PC, used as control samples, were taken through the same procedure.

2.3 Characterization

2.3.1 Small angle X-ray scattering (SAXS)

Small-angle X-ray scattering (SAXS) is a technique where the elastic scattering of X-rays by a sample, which has inhomogeneities in the nanometer range, is recorded at very low angles (typically 0.1-10°). A lot of information, which includes shapes and sizes of macromolecules, characteristic distances of partially ordered materials, and pore sizes, can be obtained from the angular distribution of the scattering intensity [1,2]. In this study, SAXS was used to investigate if the presence of the polymer had any influence on the pore structure of MCM-41.

SAXS measurements were performed by using a Bruker AXS Nanostar-U instrument, with a Cu rotating anode working at 40kV and 18mA. The X-ray beam was monochromatized at a wavelength λ of 1.54 Å (Cu K_α) using a couple of Göbel mirrors, and was collimated using a series of three pinholes with diameters of 500, 150 and 500 μm. Samples were directly mounted on the sample stage to avoid additional scattering of the holder. Data were collected at room temperature for 5000 sec by using a two-dimensional multiwire proportional counter detector placed at 24 cm from the sample, allowing the collection of data in the Q scattering vector (Q =

$4\pi\sin\theta/\lambda$) range of 0.02–0.78 $Å^{-1}$. The measurements were repeated on two samples of each composition to confirm homogeneity.

2.3.2 X-ray diffraction (XRD)

X-ray diffractometry is an important technique for determining the crystal structures of materials. The X-rays are directed onto the sample which is rotating with the detector. When the geometry of the incident beam of X-rays hitting the sample satisfies the Bragg equation, interference occurs and the peak intensity is recorded. A detector processes the X-ray signals and converts them into a count rate. Peaks appear where the X-ray beam is diffracted by the crystal lattice. The d-spacings between the lattices and their distribution in the crystalline structure is unique for each material, therefore the angular distribution of the diffraction peaks and their intensities (the diffraction pattern) serve as a fingerprint of that material. From the peak intensities on the diffraction patterns, that are directly proportional to average mass of the material, the concentration of the phases in the material can be obtained [3,4]. In this study X-ray diffraction was used to investigate if the presence of the polymer had any influence on the crystal structure of the filler (Ce:YAG).

The X-ray diffraction (XRD) patterns were recorded with a Philips diffractometer in the Bragg-Brentano geometry using a Ni filtered Cu K_α radiation (λ = 1.54056 Å) and a graphite monochromator in the diffraction beam. The X-ray generator worked at 40 kV and 30 mA, the instrument resolution (divergent and antiscatter slits of 0.5°) was determined using standards free from the effect of reduced crystallite size and lattice defects.

2.3.3 ^{13}C cross-polarization magic-angle spinning nuclear magnetic resonance spectroscopy (^{13}C {H} CP-MAS-NMR)

CP-MAS-NMR is a technique often used to perform experiments in solid-state NMR spectroscopy by spinning the sample, usually at a frequency of 1 to 100 kHz and a magic angle (θ_m) with respect to the direction of the magnetic field. The physical spinning of the sample is achieved *via* an air turbine mechanism. The nuclear spin causes a number of interactions that include dipolar, chemical shift anisotropy, and quadrupolar coupling. The

technique can give information about the structure of the polymer and the nature of the molecular motions. Relaxation measurements can be used to elucidate certain aspects of polymer microstructure and the properties that are affected by the molecular mobility. The relaxation times commonly studied include the spin-lattice relaxation time in the laboratory frame (MHz), which is particularly sensitive to side chain motions, and spin lattice relaxation in the rotating frame, which is sensitive to molecular motions that occur in the kHz range. The cross polarization in a polymer system can be used to determine the extent of motional heterogeneity and phase separation in a polymer system [5-7]. In this study CP-MAS-NMR was used to investigate the interaction between the polymer and the filler at molecular level.

^{13}C $\{^{1}H\}$ CP-MAS NMR spectra were obtained at room temperature by using a Bruker Avance II 400 MHz (9.4T) spectrometer operating at 100.63 MHz for the ^{13}C nucleus, with a MAS rate of 10 kHz, 400 scans, a contact time of 1.5 μs and a repetition delay of 2 s. The optimization of the Hartmann-Hahn condition was obtained using an adamantine sample. Each sample was placed in a 4 mm zirconia rotor with KEL-F caps using silica as filler to avoid inhomogeneities inside the rotor.

The proton spin–lattice relaxation time in the rotating frame $T_{1\rho}(H)$ was indirectly determined with a variable spin lock (VSL) pulse sequence by the carbon nucleus observation using a 90°–τ–spin-lock pulse sequence prior to cross-polarization. The data acquisition was performed by ^{1}H decoupling with a delay time, τ, ranging from 0.1 to 7.5 ms and a contact time of 1.5 ms.

The ^{13}C spin–lattice relaxation time in the rotating frame $T_{1\rho}(C)$ was determined, with the variable spin lock (VSL) pulse sequence, applying the spin-lock pulse after the cross-polarization on the carbon channel. The data acquisition was performed by 1H decoupling with a spin lock pulse length, τ, ranging from 0.4 to 30 ms and a contact time of 1.5 ms.

2.3.4 Transmission electron microscopy (TEM)

Transmission electron microscopy can provide microstructural, crystallographic, compositional and electronic information from micrometre to sub-nanometre sized regions of thin samples. During the analysis a beam of electrons is transmitted through an ultra-thin specimen and interacts with the specimen as it passes through it. An image appears on a screen, and can be

magnified from 100 to approximately 500 000 times [8-9]. In this study, TEM was used to study the dispersion of MCM-41 and Ce:YAG particles in the polymer matrices.

TEM micrographs were acquired using a JEM-2100 (JEOL, Japan) electron microscope operating at 200 kV accelerating voltage. The MCM-41 powder was dispersed in isopropanol and a drop of this suspension was put on a carbon coated nickel grid holey. For the observation of the composites, 100 nm thick slices were prepared by using a Leica EM UC6 ultra-microtome, and were put onto a 3 mm Cu grid "lacey carbon" for analysis.

2.3.5 Dynamic mechanical analysis (DMA)

Polymers are viscoelastic materials, which in limiting cases can behave as either elastic solids or viscous liquids. Viscoelasticity describes the time-dependent mechanical properties of these materials. DMA is used to study both molecular relaxation processes in polymers, and to determine the inherent mechanical or flow properties as a function of time or temperature. Dynamic mechanical analysis involves imposing a small cyclic strain on a sample and measuring the resultant stress response, or equivalently imposing a cyclic stress on a sample and measuring the resultant strain response. DMA is used to study the elastic modulus (storage modulus, E') which measures the recoverable strain energy in a deformed specimen, the viscous modulus (loss modulus, E") which measures the energy lost due to energy dissipation, and the damping coefficient (tan δ) which is the ratio of loss modulus to storage modulus, as a function of time, temperature or frequency [10,11].

DMA of the polymers and composites were done using a Perkin Elmer Diamond DMA from Waltham, Massachusetts, U.S.A. The conditions for the analyses were as follows:

Frequency	1 Hz
Amplitude	20 μm
Temperature range	40 to 160 °C
Temperature programme mode	Ramp
Measurement mode	Bending (dual cantilever)
Heating rate	5 °C min^{-1}
Preloading force	0.02 N

Sample length	50 mm
Sample width	10.0-10.9 mm
Sample thickness	3.0-3.4 mm

2.3.6 Impact testing

Impact testing is used to study the toughness of a material. The toughness of a material is its ability to absorb energy during plastic deformation. Brittle materials have low toughness as a result of the small amount of plastic deformation that they can endure. Two methods can be used to study the impact strength, the Charpy and Izod impact tests. Both methods involve striking a standard specimen with a controlled weight pendulum travelling at a set speed. When the pendulum impacts the specimen, the specimen will absorb energy until it yields and the energy that is needed to break the sample is measured in kJ m^{-2}. During the Charpy test the sample is placed horizontally and the hammer strikes the sample on the opposite side of the notch, and unnotched specimens can also be tested. During the Izod test the sample is placed vertically and clamped at one end just below the notch, or the centre of the sample if it is unnotched. The hammer hits the sample either on the notched side which is the most common way, or on the opposite side (reverse notched test). A notch serves as a crack initiation point, and both the notch depth and radius have an effect on the impact behaviour of materials [12,13]. In this study the Charpy testing method was used to study the impact strength of PC, PMMA and their composites.

A Ceast Impactor II was used to investigate the impact properties of the composites. The samples were rectangular in shape with a width of 10 mm, a thickness of 3 mm and length of 80 mm, and were V-notched (3 mm deep) edgewise. The pendulum hammer was situated at an angle of 150° from the release spot and the samples were tested at room temperature. Five samples of each composition were tested and the average values were calculated.

2.3.7 Thermogravimetric analysis (TGA)

Thermogravimetric analysis is a technique where the mass of a polymer is measured as a function of temperature or time while the sample is subjected to a controlled temperature

programme in a controlled atmosphere. The heart of the thermogravimetric analyser is the thermobalance, which is capable of measuring the sample mass as a function of temperature or time. A gas, such as nitrogen, argon or helium flowing through the balance creates an inert atmosphere. The instrument cannot identify the evolved products, unless it is coupled to another analytical tool such as a mass spectrometer (MS) or a Fourier-transform infrared spectrometer (FTIR) [10]. TGA is mostly used to study the decomposition behaviour, thermal stability and ash content of polymer nanocomposites. It can also be used to study the degradation kinetics of materials.

TGA analysis was performed in a Perkin Elmer STA6000 simultaneous thermal analyzer. Samples with masses ranging between 20 and 25 mg were heated from 30 to 650 °C at a heating rate of 10 °C min^{-1} under nitrogen at a constant flow rate of 20 mL min^{-1}. The degradation kinetic analysis was performed using the Ozawa-Flynn-Wall (OFW) method with samples heated from 30 to 600 °C at different heating rates (3,5,7, and 9 °C min^{-1}). The Ozawa-Flynn-Wall method is an isoconversional linear method which involves the measurement of the temperature, corresponding to a fixed value of the degree of conversion (α), for samples heated at different rates. The (OFW) method is based on equation (2.1):

$$\ln \beta = c - 1.052\frac{E_a}{RT} \qquad (2.1)$$

where β is the heating rate in K min^{-1}, c is a constant, E_a is the activation energy in kJ mol^{-1}, R is the universal gas constant, and T is the temperature in K. A plot of ln β against 1/T is obtained from the TGA curves analysed at different heating rates, and it should be a straight line. The activation energies of degradation can be evaluated from the slopes of the curves.

2.3.8 Luminescence spectroscopy

Luminescence is defined as the phenomenon in which the electronic state of a substance is excited by some kind of external energy, and the excitation energy is given off in the form of light. Materials exhibiting this phenomenon are known as luminescent materials or phosphors. Depending on how the phosphor is excited, several types of luminescence can be distinguished,

amongst them is photoluminescence (PL). Photoluminescence is a non-contact, non-destructive method of probing the electron structure of materials. In essence, when light is incident on a sample, photons are absorbed and electronic excitations are created. Eventually the excitations relax and the electrons return to the ground state. Excess energy is released when the electrons return to their equilibrium states. Photoluminescence spectra are recorded by measuring the intensity of emitted radiation as a function of either the excitation wavelength or the emission wavelength [14-15]. In this study photoluminescence spectroscopy was used to study the optical properties of the polymer and the polymer/Ce:YAG composites. The composites were also combined with a blue LED in order to investigate the effect of the amount of Ce:YAG on the resulting emitted light in view of possible application in white LED manufacture.

The emission and excitation spectra were measured using a Fluoromax 4 HORIBA JobinYvon spectrofluorometer. Samples were placed at an angle of 45° and excited by a xenon (Xe) source operating at 150 W. The polymer/Ce:YAG composites were excited with a wavelength of 450 nm for emission measurement and 550 nm for excitation measurement. The emission spectra of the polymer/Ce:YAG composites combined with a blue LED (InGaN, Quantum Light technology, Voltage 3.2V, Current 350 mA) were measured using an Ocean USB2000+ spectrometer operating in the wavelength range 200-1100 nm. The chromaticity coordinates were calculated from the emission spectra following the standard Commission Internationale de I' Eclairage (CIE) 15:2004.

2.4 References

1. G. Cao, Y. Wang. Nanostructures and Nanomaterials. Synthesis, Properties and Applications. World Scientific, Singapore (2011).
   ISBN: 9814324558
2. C.D. Putnam, M. Hammel, G.L. Hura, J.A. Tainer. X-ray solution scattering (SAXS) combined with crystallography and computation: Defining accurate macromolecular structures, conformations and assemblies in solution. Quarterly Reviews of Biophysics 2007; 40:191-285.
   DOI: 10.1017/S033583507004635

3. Y. Leng. Materials Characterization: Introduction to Microscopic and Spectroscopic Methods. John Wiley & Sons, Singapore (2008).
ISBN: 978-0-470-82298-2 (HB)
4. I.L. Hosier, A.S. Vaughan, G.R. Mitchell, J. Siripitayananon, F.J. Davis. Polymer characterization. In: F.J. Davis (Ed). The Practical Approach in Chemistry Series: Polymer Chemistry. Oxford University Press, New York (2004).
5. V.I. Bakhmutov. Solid-state NMR in Materials Science. Principles and Applications. CRC Press, New York (2012).
ISBN: 978-1-4398-6963-5
6. R. Mansencal, B. Haidar, A. Vidal, L. Delmotte, J.M. Chezeau. High-resolution solid-state NMR investigation of the filler-rubber interaction: 2 High-speed [^{1}H] magic-angle spinning NMR spectroscopy in carbon-black-filled polybutadiene. Polymer International 2001; 50:387-394.
DOI: 10.1002/pi.640
7. T.M.F.F. Diniz, M.I.B. Tavares. A high-resolution solid-solid NMR investigation of molecular mobility of poly(methyl methacrylate)/poly(vinyl pyrrolidone)/poly(ethylene oxide) ternary blends. Journal of Applied Polymer Science 2006; 100:1492-1495.
DOI: 10.1002/app.23228
8. S.L. Flegler, J.W. Heckman Jr, K.L. Klomparens. Scanning and Transmission Electron Microscopy. An Introduction. W.H. Freeman and Company, New York (1993).
ISBN 0-7167-7047-4
9. M.R. Lee. Transmission electron microscopy (TEM) of earth and planetary materials: A review. Mineralogical Magazine 2010; 74:1-27.
DOI: 10.1180/minmag.2010.074.1.1
10. J.D. Menczel, R.B. Prime. Thermal Analysis of Polymers. Fundamentals and Applications. Wiley, New Jersey (2009).
ISBN: 978-0-471-76917-0
11. G. Sui, S. Jana, A. Salehi-Khojin, S. Neema, W.H. Zhong, H. Chen, Q. Huo. Preparation and properties of natural sand particles reinforced epoxy composites. Macromolecular Materials and Engineering 2007; 292:467-473.
DOI: 10.1002/mame.200600479

12. R. Brown. Handbook of Polymer Testing. Short-Term Mechanical Tests. Rapra Polymer Testing Series, United Kingdom (2002).
ISBN: 1-85957-324-X
13. I.M. Ward, J. Sweeney. An Introduction to The Mechanical Properties of Solid Polymers, 2nd Edition. Wiley, England (2005).
ISBN: 9780470020371
14. R. Sharma. Optical Characterization of Mn doped ZnS Nanoparticles. Synthesis, Photoluminescence and Absorption Spectra. LAP Lambert Academic Publishing, Saarbrucken (2011)
ISBN: 978-3-8454-2479-8
15. S. Tiwari, J.V. Yakhmi. Recent advances in luminescence nanomaterials for solid state lightning applications. Defect and Diffusion Forum 2015; 361:15-68
DOI: 10.4028/www.scientific.net/DDF.361.15

Chapter 3: Morphology and properties of poly(methyl methacrylate) (PMMA) filled with mesoporous silica (MCM-41) prepared by melt compounding

3.1 Small angle X-ray scattering (SAXS)

The scattering intensities of MCM-41, PMMA and the PMMA/MCM-41 composites after background and thickness corrections are reported as function of the scattering vector Qin Figure 3.1. The SAXS peaks are indicative of the repeating distances in the sample, and the porous MCM41 shows an intense (100) peak at 0.15 $Å^{-1}$, and two low-intensity reflections ((110) at 0.26 $Å^{-1}$ and (200) at 0.32 $Å^{-1}$) that are characteristic of hexagonal structures [1]. SAXS measurements carried out on different portions of the samples looked the same, which confirmed the homogeneity of the samples.

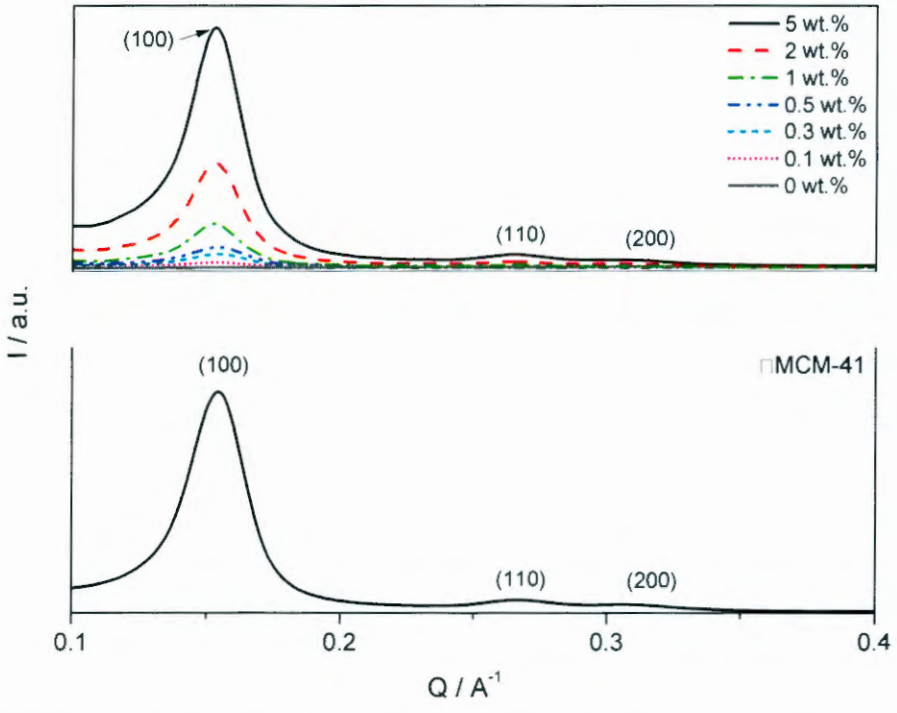

Figure 3.1 SAXS intensities vs. scattering vector Q of MCM-41, PMMA and PMMA/MCM-41 composites

The SAXS pattern of the pure PMMA does not show any peak in the investigated scattering intensity *I(Q)* range because it is an amorphous polymer. The SAXS patterns of the PMMA/MCM-41 composites show the three characteristic peaks of MCM-41, which indicates that it maintained its hexagonal lattice symmetry after composite formation. The intensity of the MCM-41 peak at 0.15 $Å^{-1}$ increased with an increase in MCM-41 content as a result of more MCM-41 content in the sample (Figure 3.2). The straight line drawn through the points show that there is direct relation between the amount of MCM-41 added into the polymer and the intensity of the peak at 0.15 $Å^{-1}$, which is to be expected for polymer samples containing evenly dispersed filler particles.

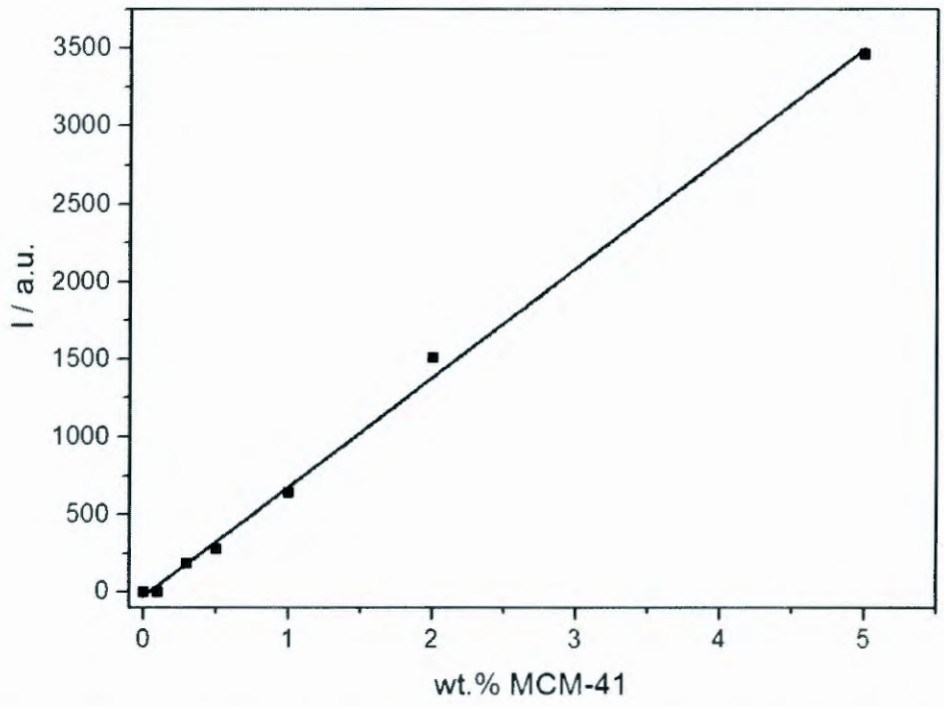

Figure 3.2 Effect of MCM-41 content on the intensity of the MCM-41 peak at 0.15 $Å^{-1}$

Araujo *et al.* [2] prepared polymer/mesoporous composites by *in situ* polymerization in the presence of a precursor, and observed a shift in the (100) peak to smaller angles, indicating that the interplanar distance (d_{100}) and the distance between the centers of two adjacent pores in the hexagonal structure (a_0) increased in the presence of the polymer. This was attributed to the presence of part of the polymer chains in the MCM-41 channels. We therefore decided to also calculate these parameters to investigate whether melt mixing could cause any change in the

MCM-41 porous structure. The interplanar distance in the (100) direction, d_{100}, was calculated using Equation 3.1. [3]

$$d_{100} = 2\pi/Q \qquad (3.1)$$

where Q is the scattering vector at the (100) peak. The unit cell parameter a_0, which indicates the distance between the centre of two adjacent pores in the hexagonal structure, was calculated using Equation 3.2. [4]

$$a_0 = 2d_{100}/\sqrt{3} \qquad (3.2)$$

Where d_{100} is the interplanar distance in the (100) direction. Figure 3.3 schematically shows the relationship between the MCM-41 hexagonal structure and the calculated parameters. The interplanar distance in the (100) direction was calculated as 4.1 nm and the unit cell parameter as 4.8 nm for MCM-41. Other studies foundd_{100} values in the range of 3.1-3.4 nm and a_0 values in the range of 3.6-3.9 nm [5,6]. The confinement of the polymer chains in the mesopores of the silica particles should play a significant role in enhancing the physical properties of the polymer [7], so we investigated the probability of the polymer chains entering the pores of MCM-41 by calculating the radius of gyration of the polymer chains using Equation 3.3 [8]

$$R_g^2 = \frac{nl^2}{6} \qquad (3.3)$$

in which n represents the number of monomer units constituting a polymer chain, and l represents the length of a repeating monomer unit. The weight-average molecular weight and polydispersity index of the commercial polymer we used in this research was previously determined to be respectively 110 000 g mol^{-1} and 2.15 [9], and we used these values to calculate the number-average molecular weight using Equation 3.4 [3].

$$PDI = \frac{\overline{M}_w}{\overline{M}_n} \qquad (3.4)$$

where PDI is the polydispersity index, $\overline{M}_w$ is the weight-average molecular weight, and $\overline{M}_n$ is the number-average molecular weight. This gives a number-average molecular weight of 51 162 g mol^{-1}. We used these values in our calculation of the radius of gyration, and obtained values of 1.42 and 2.09 nm. On average these values are of the same order as the pore sizes calculated above, and we can confidently assume that it must have been possible for the polymer chains to at least partially penetrate the MCM-41 pores during composite preparation. Figure 3.1 clearly shows that there was no shift in the position of the (100) peak in the presence of the polymer after introducing the nano-filler, and therefore the d_{100} and a_0 values remained constant. Even though the polymer chains penetrated the pores (at least partially) during the preparation process, they obviously did not change the dimensions of the hexagonal pore structure, which was expected due to the preparation method. In the work reported by Araujo *et al.* [2] the pore structure was probably built around the polymer chains formed during the *in situ* polymerization.

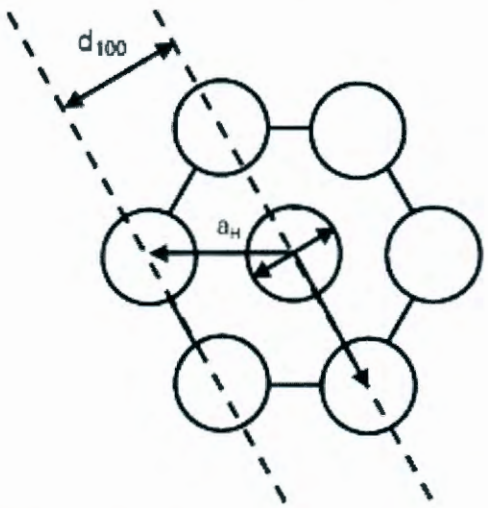

Figure 3.3 Schematic diagram of the relationship between the interplanar distance (d_{100}) and the hexagonal parameter (a_H) [2]

3.2 Transmission electron microscopy (TEM)

The TEM images of the MCM-41 powder are shown in Figure 3.4. Well-ordered channels with a hexagonal symmetry typical of the mesoporous structure are observed, and Figure 3.4(b) clearly shows the pore structure of MCM-41. Figure 3.5 shows the TEM images of the PMMA/MCM-41 composites with different MCM-41 contents. Figure 3.5(a) shows small MCM-41

agglomerates well dispersed in the polymer matrix. Because of this, the composite maintained its transparency up to 0.5 wt.% MCM-41 (Figure 3.6). The high magnification image (Figure 3.5(b)) clearly shows the agglomerated MCM-41 particle in the polymer matrix. Figure 3.5(c,d) shows well dispersed, but highly agglomerated, filler particles, which is the reason for the clear loss in transparency observed in Figure 3.6.

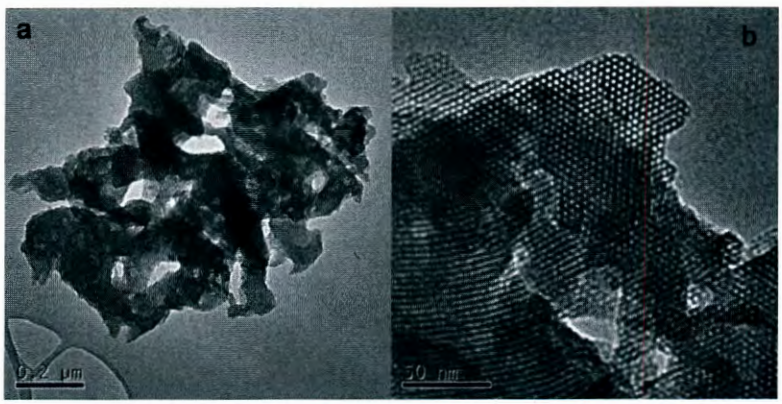

Figure 3.4 TEM micrographs of MCM-41 powder at different magnifications

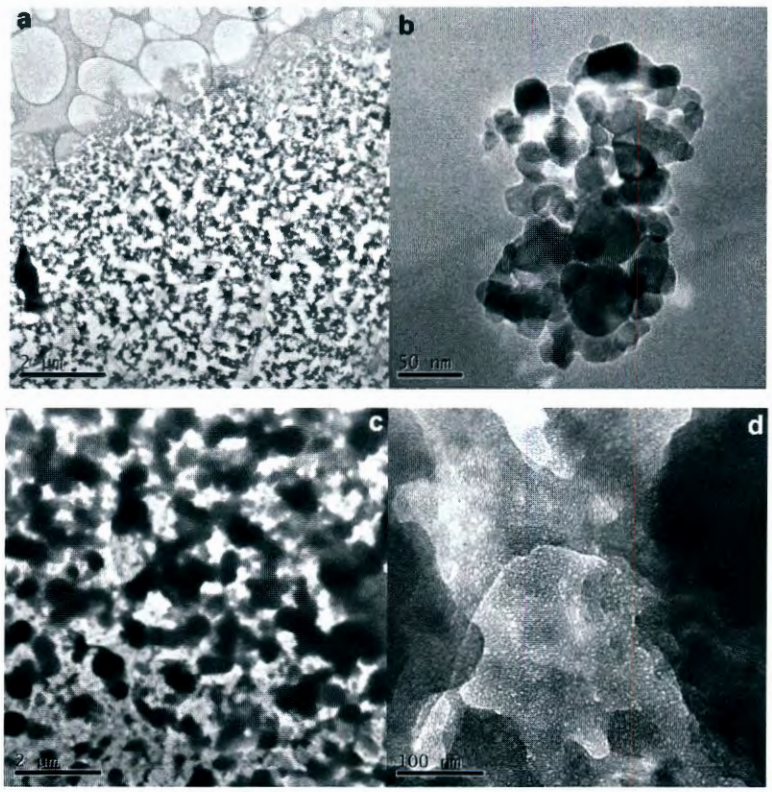

Figure 3.5 TEM micrographs of PMMA/MCM-41 composites with 0.5 wt.% MCM-41 (a,b) and with 5 wt.% MCM-41 (c,d)

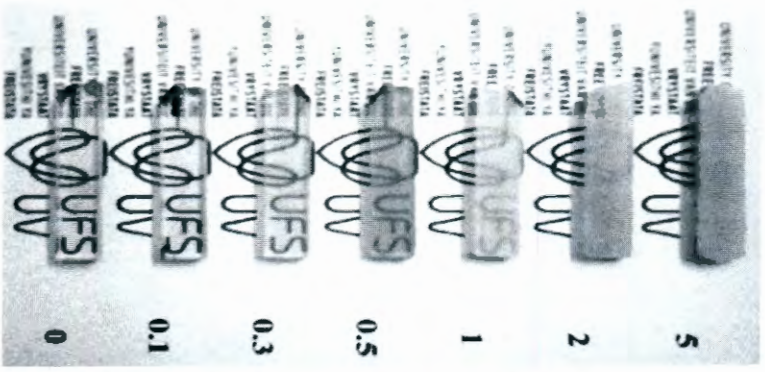

Figure 3.6 Picture of PMMA and the PMMA/MCM-41 composites to illustrate their transparency

3.3 ^{13}C cross-polarization magic-angle spinning nuclear magnetic resonance (^{13}C $\{^{1}H\}$ CP-MAS-NMR) spectroscopy

The ^{13}C $\{^{1}H\}$ CP MAS NMR measurements were performed to understand possible changes caused by the presence of MCM-41 in the polymer, and to attempt a correlation between the macroscopic, microscopic and molecular properties. Figure 3.7 shows the NMR spectra and the assignment of the ^{13}C chemical shifts of the polymer. All the spectra show five resonances at 177.9, 55.4, 52.3, 45.2 and 16.6 ppm due to respectively the carbonyl carbon, methoxyl group, and quaternary carbon of the polymer chain, and the methylene and methyl groups. The presence of MCM-41 had no effect on the chemical shift, shape and intensity of the PMMA spectra for the investigated samples. This shows that there were no chemical interactions and that only physical interactions occurred between the polymer matrix and MCM-41 particles.

A spin-lattice relaxation process is stimulated by time dependent perturbations on the nuclei such as dipole-dipole coupling. The time dependence arises from molecular motions and the measurements of the relaxation times are used to study molecular motions of polymer chains [10]. The proton and carbon spin lattice relaxation times in the rotating frame, $T_{1\rho}(H)$ and $T_{1\rho}(C)$, were determined through solid-state NMR measurements in order to detect dynamic changes in the polymer induced by the presence of the MCM-41. The $T_{1\rho}$ is sensitive to molecular motions in the kHz region and it is inversely proportional to the spectral density of motion. These motions reflect the dynamic behaviour of a polymer chain in a range of a few nanometers. However, for natural-abundance experiments the spin diffusion is less effective in the $T_{1\rho}(C)$

averaging, and this parameter is therefore a good probe for local mobility [11-13]. The relaxation time values for some of the investigated samples are reported in Table 3.1. The presence of MCM-41 did not have a significant effect on the $T_{1\rho}(H)$ values, but the relaxation time for the carbonyl carbon peak (peak 5) increased compared to that of the neat polymer. A longer relaxation time can be ascribed to a local stiffness of the polymer (within a few nanometers length) as a result of the presence of the filler.

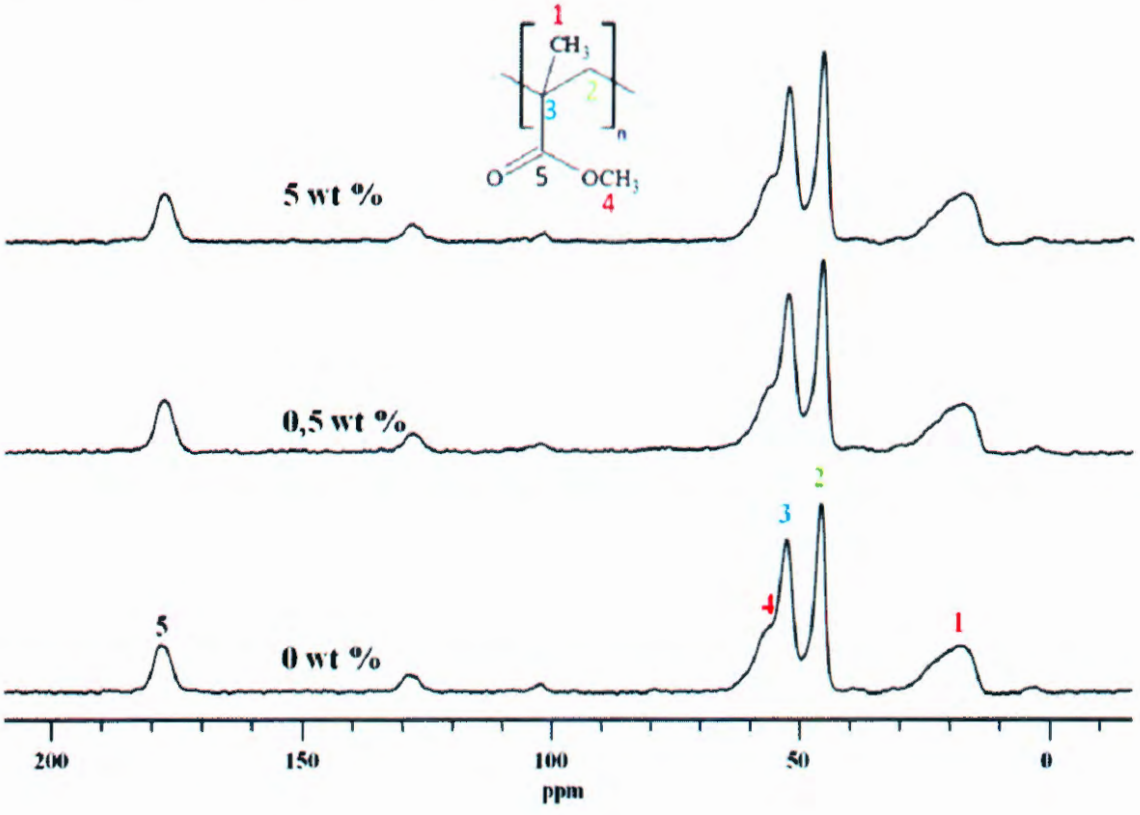

Figure 3.7 ^{13}C (^{1}H) CP-MAS NMR spectra of PMMA and PMMA/MCM-41 composites with 0.5 wt.% and 5 wt.% MCM-41

The $T_{1\rho}(C)$ values of PMMA located in the quaternary carbon (3) and methoxyl (4) groups decreased with the addition of 0.5 wt.% MCM-41, but the $T_{1\rho}(C)$ values for the methylene (2) and carbonyl carbon (5) peaksincreased in the presence of MCM-41. This observation implies that the main chain motions, in particular those of the carbonyl carbon and methylene, were hindered by the presence of MCM-41. This can be attributed to intermolecular interactions involving various parts of the polymer chain, and in particular the local motions of the carbonyl

carbon, being hindered by the presence of mesoporous silica, probably because of specific interactions such as hydrogen bonding. The MCM-41 particles naturally have silanol groups (Si-OH) on their surfaces that are capable of forming hydrogen bonding interactions with the carbonyl groups on the PMMA chains (Figure 3.8) [14-16]. Different behaviour was observed for the composite containing 5 wt.% MCM-41. In this case there was a decrease in the $T_{1\rho}(C)$ values, which can be attributed to a lack of polymer-filler interaction due to the presence of a large number of agglomerates because of more favourable filler-filler interactions. This behaviour could also be the result of larger free volumes caused by the presence of non-adhering MCM-41 agglomerates, which increased the mobility of the polymer chains resulting in shorter relaxation times [17].

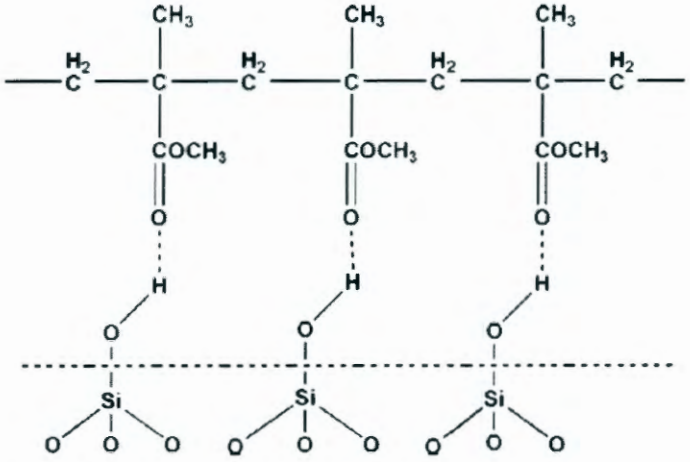

Figure 3.8 Hydrogen bonding between the ester carbonyl groups in PMMA and the silanol groups in MCM-41 [16]

Table 3.1 Relaxation time values for all the peaks in the ^{13}C spectra of PMMA and PMMA/MCM-41 composites with 0.5 and 5 wt% MCM-41 content

Signal / ppm	$T_{1\rho}$ (H) / ms			$T_{1\rho}$ (C) / ms		
	0%	0.5%	5%	0%	0.5%	5%
177.9	14.9 ± 0.2	17.5 ±0.2	13.8 ± 0.2	30.1± 0.3	53.3 ± 0.4	48.0 ± 0.2
55.4	-	44.5 ± 0.3	-	41.0 ± 0.2	20.4 ± 0.3	23.2 ± 0.2
52.3	23.0 ± 0.2	21.0 ± 0.2	21.7 ± 0.3	62.6 ± 0.4	37.9 ± 0.2	36.4 ± 0.3
45.2	19.4 ± 0.1	18.2 ± 0.2	12.0 ± 0.2	65.3 ± 0.2	81.5 ± 0.2	26.3 ± 0.3
16.6	19.4 ± 0.2	9.6 ± 0.2	19.7 ± 0.3	17.0 ± 0.1	19.6 ± 0.3	15.9 ± 0.2

3.4 Dynamic mechanical analysis (DMA)

The storage modulus curves of PMMA and the PMMA/MCM-41 composites are shown as function of temperature in Figure 3.9, and the E' values at 80 and 140 °C are reported in Table 3.2. The storage modulus of the samples increased slightly below the glass transition, with the introduction of the MCM-41 partieles, because the polymer chains are already frozen in and fairly immobile at this temperature. However, the amount of MCM-41 particles had little influence on the value of E', and no particular trend was observed (Table 3.2). This is probably because the hard, brittle polymer and the MCM-41 particles have very similar stiffness values in this temperature range. Contrary to our own results, Saladino *et al.* [18] observed a decrease in storage modulus values for the PMMA samples in the presence of non-porous silica nanoparticles, and they attributed this to the nanoparticles having a plasticizing effect on the PMMA. Above the glass transition there was a much more significant increase in storage modulus in the presence of and with an increase in MCM-41 loading, which can be attributed to (at least part of) the polymer chains penetrated into the pores of the MCM-41 particles, which restricted the mobility of these chains and increased the stiffness of the polymer. The rigid MCM-41 particles also contributed to this increase in modulus, because the physical properties of a composite normally lie somewhere between those of the polymer and the filler, depending on the interaction between these two components. Saladino *et al.* [18], however, observed that the composites containing 1 and 2 wt.% of silica had lower storage modulus values compared to those of the pure PMMA, and an increase was only observed at 5 wt.% of silica loading. The presence of MCM-41 clearly had a more significant effect on the storage modulus of PMMA than the normal, non-porous silica used by Saladino *et al.* This is probably the result of the porous structure of MCM-41, where the pores can be penetrated by the polymer chains, that are immobilized as a result. The use of smaller, non-porous particles could be the reason for the plasticizing effect at low contents, with more effective immobilization of the polymer chains only taking place at higher silica content (5 wt.%).

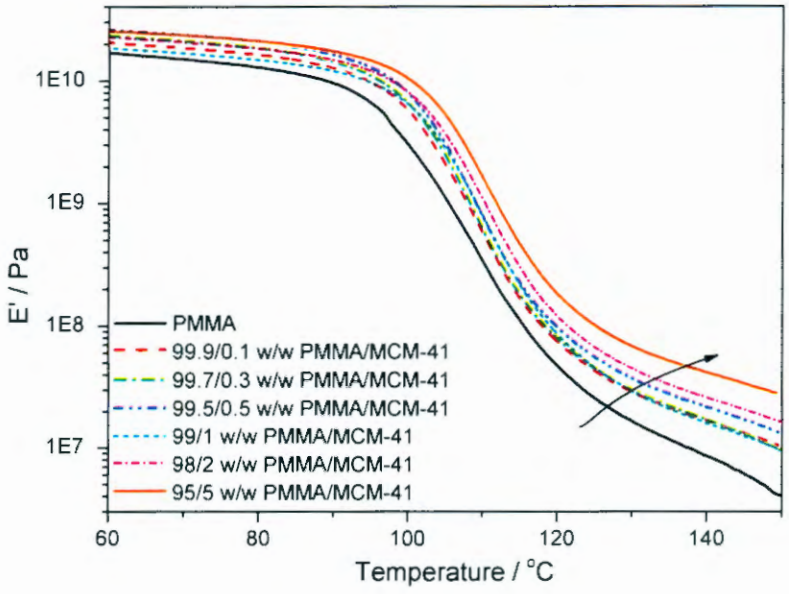

Figure 3.9 Storage modulus curves of PMMA and the PMMA/MCM-41 composites

Table 3.2 DMA results of PMMA and the PMMA/MCM-41 composites

Sample	10^{-10} E' / Pa at 80 °C	10^{-7} E' / Pa at 140 °C	T_g / °C from E"	T_g / °C from tan δ
PMMA	1.3	0.8	95.3	115.7
99.9/0.1 w/w PMMA/MCM-41	1.6	1.7	98.3	115.9
99.7/0.3 w/w PMMA/MCM-41	1.8	1.6	99.4	114.7
99.5/0.5 w/w PMMA/MCM-41	2.0	2.1	99.2	115.2
99/1 w/w PMMA/MCM-41	1.5	1.2	100.2	116.5
95/2 w/w PMMA/MCM-41	1.7	2.5	100.5	116.3
98/5 w/w PMMA/MCM-41	1.9	3.9	102.8	116.8

The loss modulus curves as function of temperature of PMMA and the composites are shown in Figure 3.10, the tan δ curves in Figure 3.11. The glass transition temperature (T_g) values taken from the peak maxima in the E" and tan δ curves are summarised in Table 3.2. The loss modulus also increased with increasing filler content, as was observed and discussed for the storage modulus. There was an observable increase in T_g from both the loss modulus and tan δ

curves (Table 3.2), which was due to the immobilization of the polymer chains trapped in the filler pores. Normally the E" curves give more acceptable glass transition values, because it represents the initial drop in E' from the glassy state into the transition, while the tan δ corresponds more closely to the transition midpoint or inflection point of the decreasing log E' curve [19]. The presence of MCM-41 decreased the transition peak intensities of PMMA (Figures 3.11), which can be attributed to the enhancement in the stiffness of the PMMA/MCM-41 composites. It is known that the extent of damping is directly related to the mobility of polymer chains, and this confirms the immobilization of the PMMA chains because of the good adhesion between the polymer chains and the porous MCM-41, where part of polymer chains were trapped in the pores of the filler [20-22]. The maximum value of tan δ ($(\tan \delta)_{max}$) is also related to the number of polymeric chains that undergo a glass transition, so a decrease in the fraction of the polymer in the sample (because of the presence of the filler), will also contribute to a reduction in $(\tan \delta)_{max}$ [23,24].

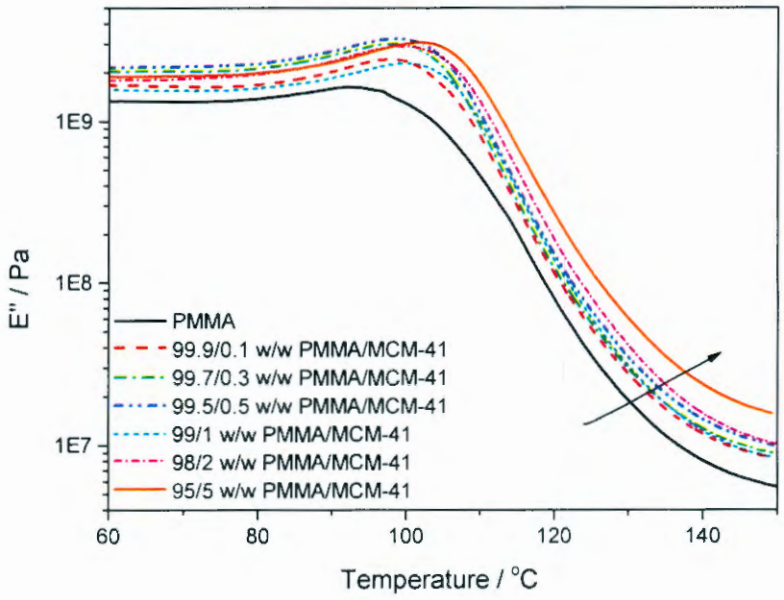

Figure 3.10 Loss modulus curves of PMMA and the PMMA/MCM-41 composites

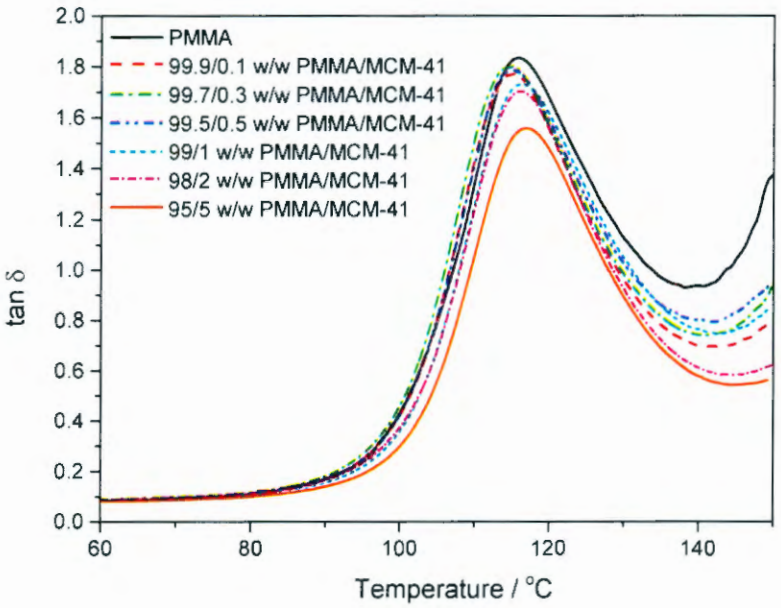

Figure 3.11 Tan δ curves of PMMA and the PMMA/MCM-41 composites

3.5 Impact testing

The addition of filler into a polymer matrix can result into two different types of interactions: (i) polymer-filler and (ii) filler-filler interaction. These interactions significantly affect the flow behaviour and mechanical performance of the composites, and are controlled by a number of factors that include particle size and shape, filler aspect ratio, and filler content [24,25].

The impact properties of PMMA and its composites are reported in Figure 3.12. The impact strength of PMMA increased with an increase in the filler content up to approximately 1.0 wt.% filler. This is due to the homogenously dispersed MCM-41 particles and small agglomerates, and fairly strong polymer-filler interaction at lower filler contents. The presence of polymer chains in the pores also provided good stress transfer between the polymer and the filler, which increased the toughness of the polymer so that more energy was needed to break the composite material. However, at higher filler contents (>1 wt.%) the impact strength decreased due to the presence of more and larger MCM-41 agglomerates (Figure 3.4(c,d)), and also weaker interactions between the polymer and filler at higher filler loading (see discussion of NMR

results). The agglomerates acted as stress concentration points for the formation of crazes, that easily developed into cracks because the crazes did not effectively terminate at other filler agglomerates, and the applied stress was therefore not effectively transferred between the polymer and the filler. In this case less energy was needed to break the sample.

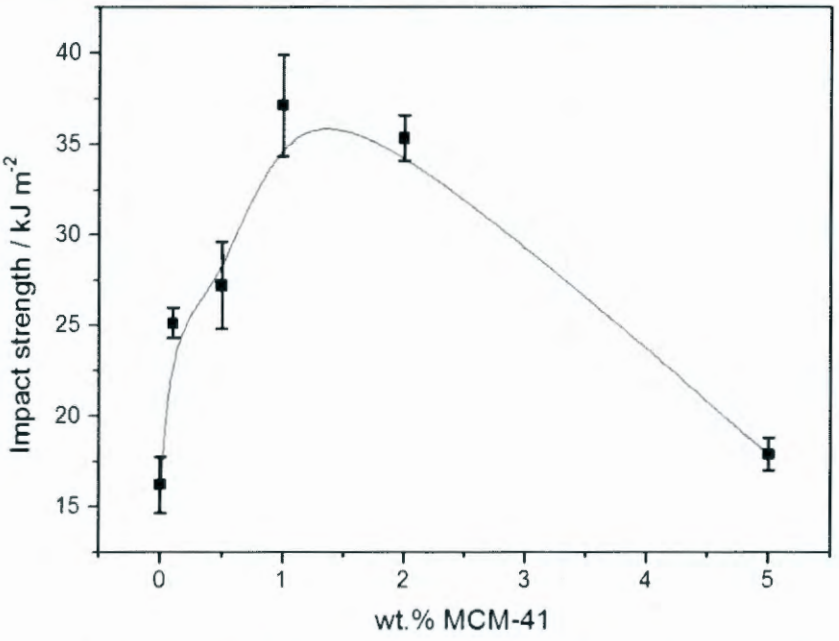

Figure 3.12 Impact properties of PMMA and PMMA/MCM-41 composites (line added to lead the eye)

3.6 Thermogravimetric analysis (TGA)

The TGA results for PMMA and the PMMA/MCM-41 composites with different MCM-41 loadings are presented in Figure 3.13 and Table 3.3. The thermal degradation of PMMA has been widely investigated, and a number of mechanisms have been proposed [14,26,27]. The degradation mechanism of PMMA depends on a number of factors that include the polymerization method and the polymer microstructure, including internal defects and type of chain end groups. The degradation of PMMA polymerized with a free radical method proceeds in three steps due to the presence of chains with different structures. The first step occurs between 150 and 230 °C, and is attributed to degradation initiated by chains containing head-to-head (H-H) linkages. The second step between 230 and 300 °C is associated with chains possessing unsaturated vinylidene ends, and the third step between 310 to 420 °C is attributed to

chains undergoing degradation initiated by random chain scission. Anionically polymerized PMMA shows only one degradation step around 360 °C, which is attributed to random chain scission. Figure 3.13 shows that all the TGA curves have one degradation step around 330 °C, which indicates that the PMMA used in this study was probably prepared through anionic polymerization.

The mass loss temperatures of PMMA increased with the addition of and increase in MCM-41 loading (Table 3.3). The increase is probably due to the presence of polymer chains in the MCM-41 pores, which restricted the polymer and free radical chain mobility, as was mentioned in the discussion of the DMA results. These pores could also have trapped the volatile degradation products, delaying their transport out of the polymer, so that they were only released at higher temperatures. It is therefore possible that the higher mass loss temperatures are not necessarily an indication of increased thermal stability in this case [28]. The amounts of residue observed at 450 °C are summarized in Table 3.3. The values correlate reasonably well with the amount of MCM-41 initially mixed into the sample, although they are generally somewhat higher. It is possible that some of the polymer chains that were trapped inside the pores of the filler got charred inside the pores, which contributed to the amount of residue. This was confirmed through analysis of the TGA results published by Saladino *et al.* [18] on PMMA/silica composites. The % residue from their results correlated well with the amount of silica initially mixed into their samples, confirming that only silica was left after decomposition of their samples.

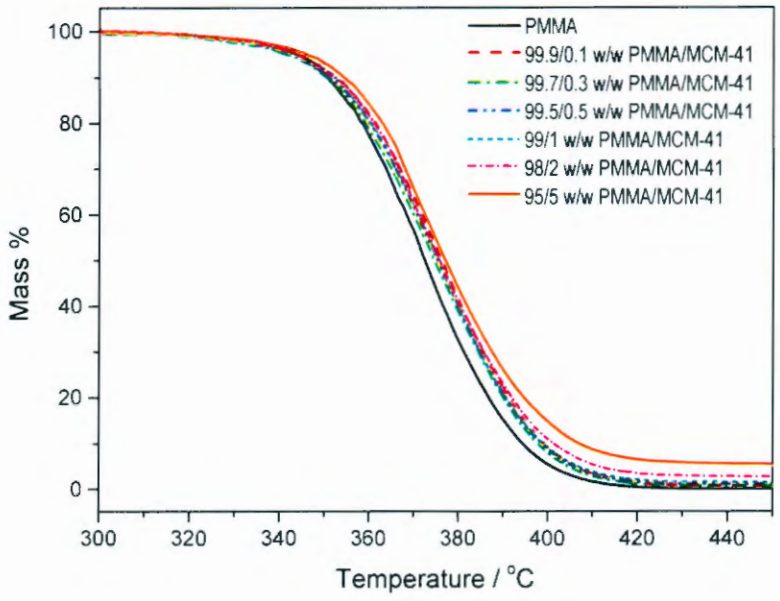

Figure 3.13 TGA curves of PMMA and the PMMA/MCM-41 composites

Table 3.3 TGA results for PMMA and the PMMA/MCM-41 composites

Samples	T_{40} / °C	T_{max} / °C	% Residue
PMMA	368.5	372.7	-
99.9/0.1 w/w PMMA/MCM-41	371.9	376.0	0.3
99.7/0.3 w/w PMMA/MCM-41	369.8	374.5	0.4
99.5/0.5 w/w PMMA/MCM-41	371.1	375.3	0.7
99/1 w/w PMMA/MCM-41	370.8	375.5	1.4
95/2 w/w PMMA/MCM-41	370.8	375.8	2.4
98/5 w/w PMMA/MCM-41	372.4	377.9	5.2

3.7 Thermal degradation kinetics

Kinetic analysis is of value for understanding the mechanism of the thermal processes in polymers and composites. Isoconversional graphs of ln β *versus* 1/T, shown in Figures 3.14 to 3.16, were plotted from the TGA curves obtained at heating rates of 3, 5, 7 and 9 °C min^{-1}, of PMMA and the PMMA/MCM-41 composites with 0.5 and 5 wt.% MCM-41 content. The

activation energy of degradation (E_a) values were calculated from the slopes of the isoconversional plots according to Equation 2.1. The relationship between the activation energies and the extent of mass loss is illustrated in Figure 3.17. The activation energy of degradation for PMMA continuously increases with an increase in extent of mass loss. This means that the degradation mechanism of PMMA changed during the degradation process, and it probably involved multiple steps, because of the dependence of E_a on the extent of degradation [19,29]. Gao *et al.* [30] attributed it to the change in reaction order which may have been brought about by a change in degradation mechanism from a first order unzipping reaction to a higher order chain scission reaction. However, for the composites there is an initial increase, but the E_a values seem to flatten off at higher extents of mass loss. The fast initial increase in E_a is probably due to the trapping by the filler of the volatile degradation products formed during the initial stages of degradation, and which are released as the degradation proceeds, giving rise to an apparent levelling off of the activation energy of degradation at higher extents of mass loss. There was probably no change in the degradation mechanism, but rather an immobilization of the free radical chains and trapping of the volatile degradation products by the porous filler. Contrary to our observation, Saladino *et al.* [18] observed a decrease in E_a at low extent of mass loss, followed by an increase at higher extents of mass loss. They attributed this behaviour to the catalytic effect of the silica particles during the initial stages of degradation, but immobilization of the free radical chains and trapping of the volatile degradation products as the degradation proceeds.

The composites show much higher activation energies that can be attributed to the well dispersed MCM-41 which probably trapped the free radical chains and volatile degradation products, resulting in more energy required to initiate and propagate the degradation of the polymer, as monitored through its mass loss. The E_a values of the composites are very similar, this suggests that the amount of MCM-41 does not have a significant effect on the E_a values.

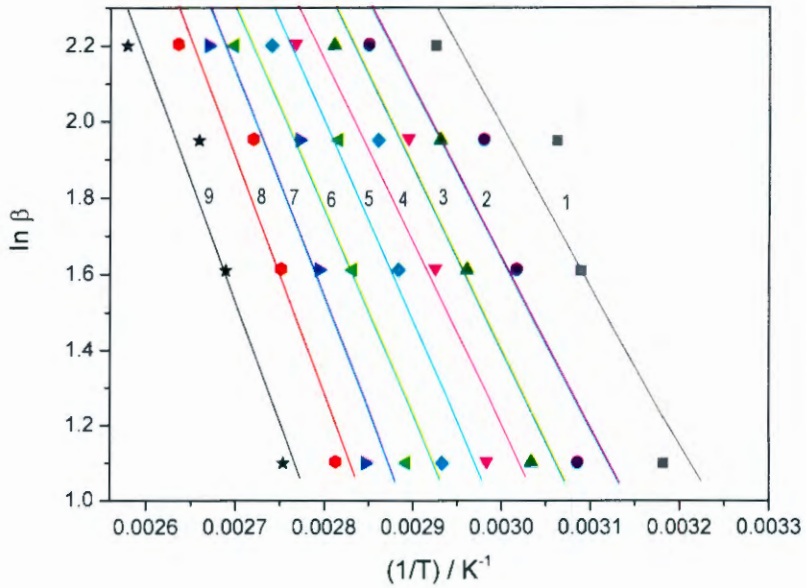

Figure 3.14 Ozawa–Flynn-Wall plots for PMMA for the following degrees of conversion: 1) α = 0.1, 2) α = 0.2, 3) α = 0.3, 4) α = 0.4, 5) α = 0.5, 6) α = 0.6, 7) α = 0.7, 8) α = 0.8, 9) α = 0.9

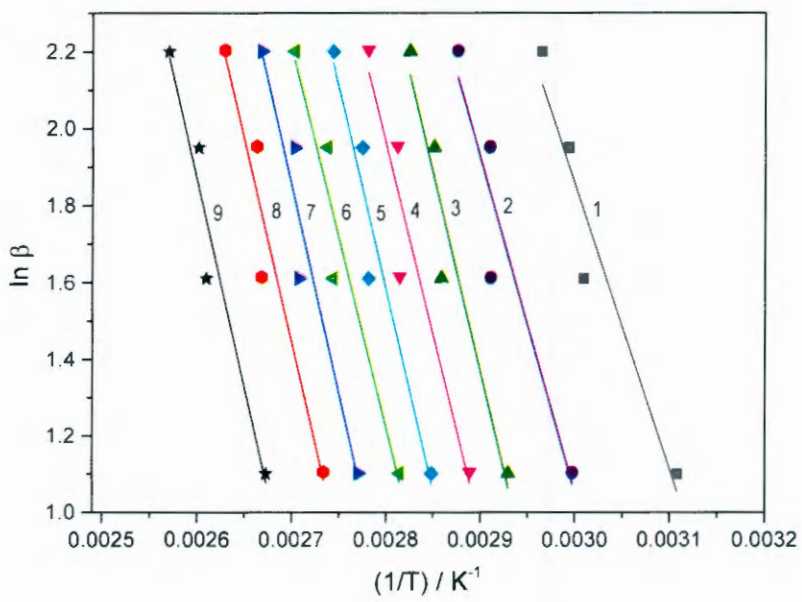

Figure 3.15 Ozawa–Flynn-Wall plots for PMMA/MCM-41 (0.5 wt.%) for the following degrees of conversion: 1) α = 0.1, 2) α = 0.2, 3) α = 0.3, 4) α = 0.4, 5) α = 0.5, 6) α = 0.6, 7) α = 0.7, 8) α = 0.8, 9) α = 0.9

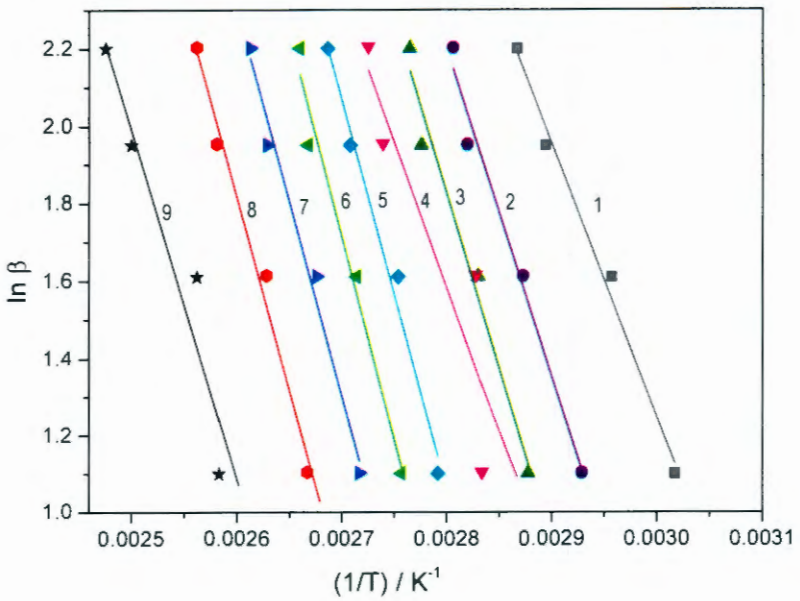

Figure 3.16 Ozawa–Flynn-Wall plots for PMMA/MCM-41 (5 wt.%) for the following degrees of conversion: 1) α = 0.1, 2) α = 0.2, 3) α = 0.3, 4) α = 0.4, 5) α = 0.5, 6) α = 0.6, 7) α = 0.7, 8) α = 0.8, 9) α = 0.9

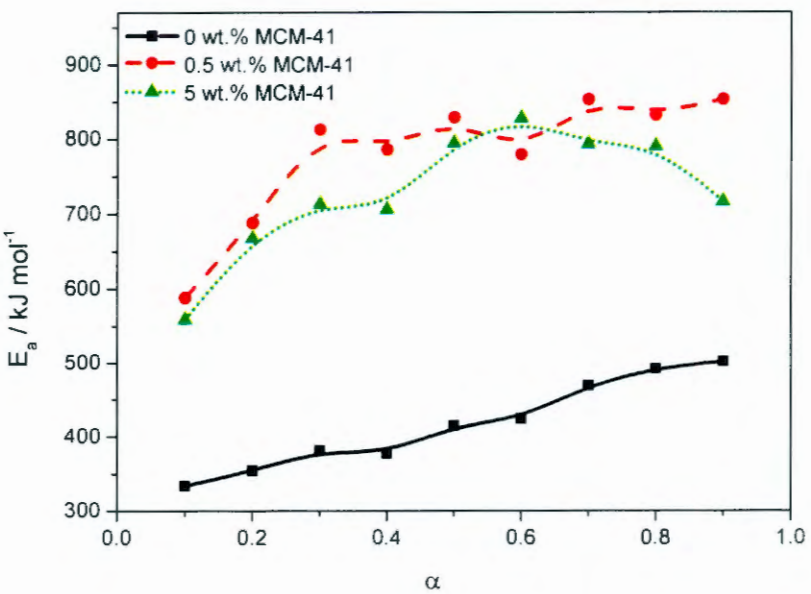

Figure 3.17 Activation energy vs. extent of degradation for PMMA and PMMA/MCM-41 composites with 0.5 and 5 wt.%

3.8 Conclusions

The purpose of the work reported in this chapter was to investigate the influence of the presence of different amounts of mesoporous silica (MCM-41) on the mechanical and thermomechanical properties, as well as thermal degradation behaviour of PMMA. The PMMA/MCM-41 composites maintained their transparency until 0.5 wt.% MCM-41 loading, while higher filler contents resulted in a loss of transparency due to nanoparticle agglomeration at these filler levels. The confinement of the polymer chains in the mesopores of the silica particles played a significant role in enhancing the properties of the PMMA. Part of the polymer chains were trapped in the pores of MCM-41 without altering the hexagonal structure or pore size of MCM-41, but the presence of polymer chains in the pores and its interaction with the particles had a significant influence on the mechanical and thermo-mechanical properties. The storage modulus, loss modulus and glass transition temperature of PMMA increased with the addition of, and increase in, MCM-41 content as a result of the interaction of the polymer chains with the porous filler which restricted the mobility of the polymer chains and increased the stiffness of the composites. This interaction was confirmed through ^{13}C cross-polarization magic-angle spinning nuclear magnetic resonance (^{13}C $\{^{1}H\}$ CP-MAS-NMR) spectroscopy analysis.

The impact strength of PMMA increased for the samples containing up to 1 wt.% MCM-41, and decreased at higher loadings, but did not reach values below that of the pure polymer. The lower impact strength was due to the presence of filler agglomerates that served as defect points for the initiation of crazes and cracks. The addition of MCM-41 seemed to increase the thermal stability of PMMA, but this apparent increase in thermal stability was most probably due to delayed mass loss because of the trapping of volatile degradation products in the pores of MCM-41.

3.9 References

1. L. Wang, X. Han, J. Li, D. Zheng. Preparation of modified mesoporous MCM-41 silica spheres and its application in pervaporation. Powder Technology 2012; 231:63-69. DOI: 10.1016/j.powtec.2012.07.044

2. J.A. Araujo, F.T. Cruz, I.H. Cruz, D. Cardoso. Encapsulation of polmers in CTA-MCM-41 via microemulsion. Microporous and Mesoporous Materials 2013; 180:14-21.
DOI: 10.1016/j.micromeso.2013.05.010
3. R.J. Young, P.A. Lovell. Introduction To Polymers. Third edition. CRC Press Taylor & Francis Group: Boca Raton (2011).
ISBN: 978-0-8493-3929-5
4. A.M. Mendonza, J. Warzywoda, A. Sacco. Jr. Investigation of structural order and morphology of MCM-41 mesoporous silica using an experimental design methodology. Journal of Porous Materials 2006; 13:37-47.
DOI: 10.1007/s10934-006-5488-0
5. P. Horcajada, A. Ramila, J. Perez-Pariente, M. Vallet-Regi. Influence of pore size of MCM-41 matrices on drug delivery rate. Microporous and Mesoporous Materials 2004; 68:105-109.
DOI: 10.1016/j.micromeso.2003.12.012
6. K.S Hui, C.Y.H. Chao. Synthesis of MCM-41 from coal fly ash by a green approach: Influence of synthesis pH. Journal of Hazardous Materials 2006; B137:1135-1148.
DOI: 10.1016/j.jhazmat.2006.03.050
7. F.A. Zhang, D.K. Lee, T.J. Pinnavaia. PMMA/mesoporous silica nanocomposites: Effect of framework structure and pore size on thermomechanical properties. Polymer Chemistry 2010; 1:107-113.
DOI: 10.1039/b9py00232d
8. Y. Gnanou, M. Fontanille. Organic and Physical Chemistry of Polymers. John Wiley & Sons: New Jersey (2008).
ISBN: 978-0-471-72543-5
9. X. Li, G.B. McKenna, G. Miquelard-Garnier, A. Guinault, C. Sollogoub, G. Regnier, A. Rozanski. Forced assembly by multilayer coextrusion to create oriented graphene reinforced polymer nanocomposites. Polymer 2013; 55:248-257.
DOI: 10.1016/j.polymer.2013.11.025
10. R.N. Ibbett. NMR Spectroscopy of Polymers. Blackie Academic & Professional: London (1993).
ISBN: 0-7514-0005-X

11. K. Hatada T. Kitayama. NMR Spectroscopy of Polymers. Springer: New York (2004). ISBN: 3-540-40220-9

12. R. Avolio, G. Gentile, M. Avella, D. Capitani, M.E. Errico. Synthesis and characterization of poly(methylmethacrylate)/silica nanocomposites: Study of the interphase by solid-state NMR and structure/properties relationships. Journal of Polymer Science Part A: Polymer Chemistry 2010; 48:5618-5629. DOI: 10.1002/pola.24377

13. A. Zanotto, A. Spinella, G. Nasillo, E. Caponetti, A.S. Luyt. Macro-micro relationship in nanostructured functional composites. eXPRESS Polymer Letters 2012; 6:410-416. DOI: 10.3144/expresspolymlett.2012.43

14. B. Zhang, F.D. Blum. Thermogravimetric study of ultrathin PMMA films on silica; Effect of tacticity. Thermochimica Acta 2003; 396:211-217. DOI: 10.1016/S0040-6031(02)00515-X

15. P. Rittigstein, J.M. Torkelson. Polymer-nanoparticles interfacial interactions in polymer nanocomposites: Confinement effects on glass transition temperature and suppression of physical aging. Journal of Polymer Science: Part B: Polymer Physics 2006; 44:2935-2943. DOI: 10.1002/polb.20925

16. N. Wang, N. Gao, S. Jiang, Q. Fang, E. Chen. Effect of different structure MCM-41 fillers with PP-g-MA on mechanical and crystallization performances of polypropylene. Composites: Part B 2011; 42:1571-1577. DOI: 10.1016/j.compositesb.2011.04.012

17. A.S. Luyt, M. Messori, P. Fabbri, J.P. Mofokeng, B. Taurino, T. Zanasi, F. Pilati. Polycarbonate reinforced with silica nanocomposites. Polymer Bulletin 2011; 66:991-1004. DOI: 10.1007/s00289-010-0408-5

18. M.L. Saladino, T.E. Motaung, A.S. Luyt, A. Spinella, G. Nasillo, E. Caponetti. The effect of silica nanoparticles on the morphology, mechanical properties and thermal degradation kinetics of PMMA. Polymer Degradation and Stability 2012; 97:452-459. DOI: 10.1016/j.polymdegradstab.2011.11.006

19. J.D. Menczel. R.B. Prime. Thermal Analysis of Polymers. Fundamentals and Applications. Wiley: New Jersey (2009).

ISBN: 978-0-471-76917-0

20. L.A. Pothan, Z. Oommen, S. Thomas. Dynamic mechanical analysis of banana fiber reinforced polyester composites. Composites Science and Technology 2003; 63:283-293. PII: S0266-3538(02)00254-3

21. D. Romanzini, A. Lavoratti, H.L. Ornaghi Jr, S.C. Amico, A.J. Zattera. Influence of fiber content on the mechanical and dynamic mechanical properties of glass/ramie polymer composites. Materials and Design 2013; 47:9-15. DOI: 10.1016/j.matdes.2012.12.029

22. L.E. Nielsen, R.F. Landel. Mechanical Properties of Polymers and Composites. Marcel Dekker, Inc.: New York (1994). ISBN: 0 8247 8964 4

23. L.D. Perez, L.F. Giraldo, W. Brostow, B.L. Lopez. Poly(methyl acrylate) plus mesoporous silica nanohybrids: Mechanical and thermophysical properties. e-Polymers 2007; 7:324-334. DOI: 10.1515/epoly.2007.7.1.324

24. N. Wang, L. Mi, Y. Wu, X. Wang, Q. Fang. Enhanced flame retardancy of natural rubber composite with addition of microencapsulated ammonium polyphosphate and MCM-41 fillers. Fire Safety Journal 2013; 62:281-288. DOI: 10.1016/j.firesaf.2013.09.008

25. H.X. Huang, J.J. Zhang. Effects of filler-filler and polymer–filler interactions on rheological and mechanical properties of HDPE-wood composites. Journal of Applied Polymer Science 2009; 111:2806-2812. DOI: 10.1002/app.29336

26. S. Majoni, S. Su, J. Hossenlopp. The effect of boron-containing layered hydroxyl salt (LHS) on the thermal stability and degradation kinetics of poly(methy methacrylate). Polymer Degradation and Stability 2010; 95:1593-1604. DOI: 10.1016/j.polymdegradstab.2010.05.033

27. C. Cao. Z. Tan, S. Sun, Z. Liu. H. Zhang. Enhancing the thermal stability of poly(methyl methacrylate) by removing the chains with weak links in a continuous polymerization. Polymer Degradation and Stability 2011; 96:2209-2214. DOI: 10.1016/j.polymdegradstab.2011.09.005

28. A.S. Luyt. Using thermogravimetric analysis to determine polymer thermal stability: Relevance of changes in onset temperature of mass loss. eXPRESS Polymer Letters 2015; 9:756.
DOI: 10.3144/expresspolymlett.2015.70

29. B.J. Holland, J.N. Hay. The value and limitations of non-isothermal kinetics in the study of polymer degradation. Thermochimica Acta 2002; 388:253-273.
PII: S0040-6031(02)00034-5

30. Z. Gao, T. Kaneko, D. Hou, M. Nakada. Kinetics of thermal degradation of poly(methyl methacylate) studied with the assistance of the fractional conversion at the maximum reaction rate. Polymer Degradation and Stability 2004; 84:399-403.
DOI: 10.1016/j.polymdegradstab.2003.11.015

Chapter 4: Morphology, mechanical and thermal properties of polycarbonate (PC) filled with mesoporous silica (MCM-41) prepared by melt compounding.

4.1 Small angle X-ray scattering (SAXS)

The SAXS pattern of PC and the PC/MCM-41 composites after background and thickness corrections are reported as a function of the scattering vector Qin Figure 4.1. The pattern of MCM-41 has already been reported in Chapter 3, and it showed a high-intensity peak at 0.15 $Å^{-1}$ (100) and two low-intensity reflections ((110) at 0.26 $Å^{-1}$ and (200) at 0.32 $Å^{-1}$) that are characteristic of hexagonal structures. SAXS measurements, carried out on different portions of the samples, gave the same results which confirmed the homogeneity of the samples.

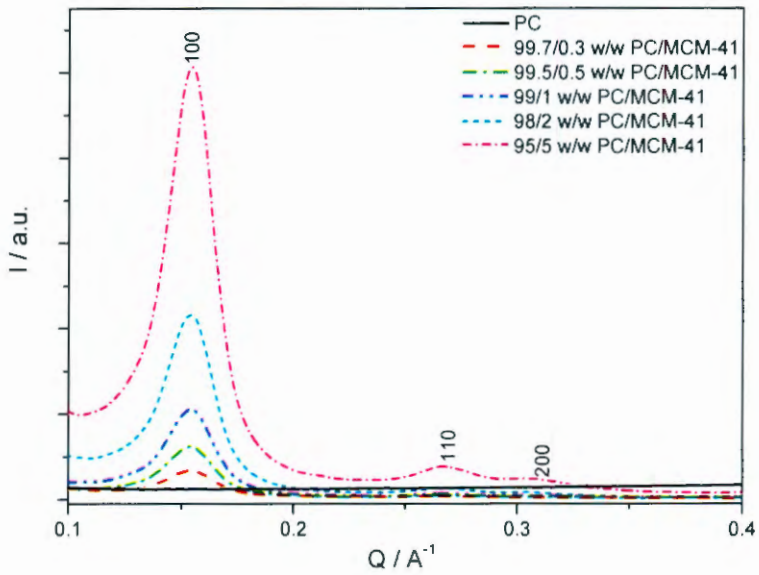

Figure 4.1 SAXS intensities vs. scattering vector Q of MCM-41 and PC/MCM-41 composites.

The SAXS pattern of the pure PC does not show any peak in the investigated scattering intensity *I(Q)* range because it is an amorphous polymer, while the PC/MCM-41 composites

show the three characteristic peaks of MCM-41, indicating that the MCM-41 maintained its hexagonal lattice symmetry after composite formation. The intensity of the MCM-41 peak at 0.15 $Å^{-1}$ increased with an increase in MCM-41 content as a result of more MCM-41 in the sample (Figure 4.2).

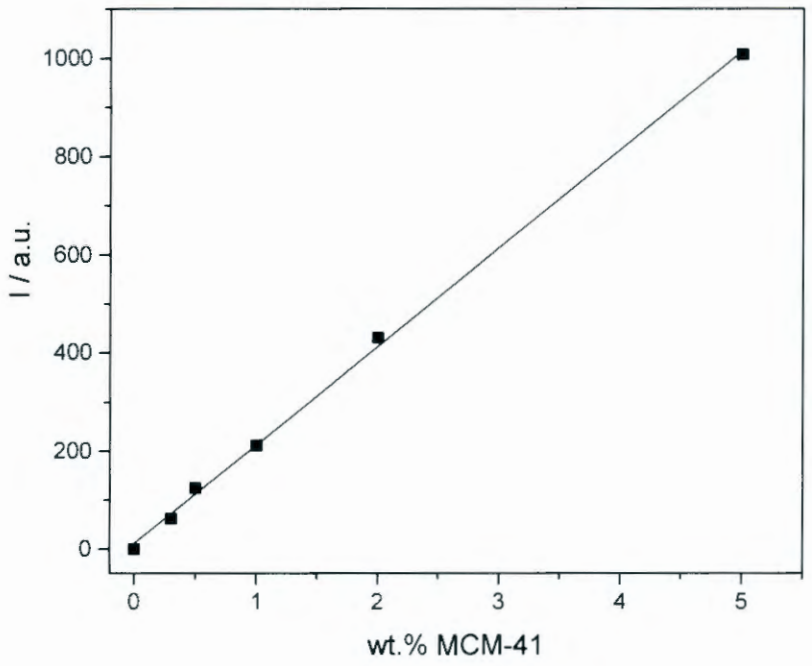

Figure 4.2 Relationship between the intensity of the MCM-41 peak at 0.15 $Å^{-1}$ and the MCM-41 content in the composite samples

During the preparation process of polymer/mesoporous composites, there is a possibility that the polymer chains might be trapped or penetrate the pores of the mesoporous silica [1,2], thus altering the interplanar distance (d_{100}) and the distance between the centers of the two adjacent pores in the hexagonal structure (a_0), which should give rise to (100) peak shifts to smaller angles. Araujo *et al.* [2] prepared polymer/mesoporous composites by *in situ* polymerization in the presence of a precursor, and observed a shift in the (100) peak to smaller angles. This was attributed to the presence of part of the polymer chains in the MCM-41 channels. In this chapter we also decided to calculate the interplanar distance (d_{100}) and the distance between the centers of two adjacent pores in the hexagonal structure (a_0) and confirm

whether melt mixing could cause any change in the MCM-41 porous structure. The interplanar distance in the (100) direction, d_{100}, was calculated using Equation 4.1 [3].

$$d_{100} = 2\pi/Q \tag{4.1}$$

where Q is the scattering vector at the (100) peak. The unit cell parameter a_0, which indicates the distance between the centre of two adjacent pores in the hexagonal structure, was calculated using Equation 4.2 [4].

$$a_0 = 2d_{100}/\sqrt{3} \tag{4.2}$$

Where d_{100} is the interplanar distance in the (100) direction. The interplanar distance and the unit cell parameter (100) direction for MCM-41 have already been calculated in Chapter 3 as 4.1 nm and 4.8 nm respectively. The confinement of the polymer chains in the mesoporous silica might restrict the mobility of the polymer chains, which may enhance the properties of the composites, so we also decided to investigate the probability of the polymer chains entering the pores of MCM-41 by calculating the radius of gyration of the polymer chains using Equation 4.3 [5].

$$R_g^2 = \frac{nl^2}{6} \tag{4.3}$$

in which n represents the number of monomer units constituting a polymer chain, and l represents the length of a repeating monomer unit. The weight-average molecular weight and polydispersity index of the commercial polymer we used in this research was previously obtained as 57 404 g mol^{-1} and 2.16 [6], and we used these values to calculate the number-average molecular weight using Equation 4.4 [3].

$$PDI = \frac{\overline{M}_w}{\overline{M}_n} \tag{4.4}$$

where PDI is the polydispersity index, $\overline{M}_w$ is the weight-average molecular weight, and $\overline{M}_n$ is the number-average molecular weight. This gives a number-average molecular weight of 26 576 g mol^{-1}. We used these values in our calculation of the radius of gyration, and obtained values of

0.65 and 0.94 nm. These values are smaller than the pore sizes of MCM-41 calculated above, so it is possible that the polymer chains can at least partially penetrate the MCM-41 pores during preparation. Figure 4.1 clearly shows that there was no shift in the position of the (100) peak in the presence of the polymer after introducing the nano-filler, and therefore the d_{100} and a_0 values remained constant. Even though the polymer chains penetrated the pores (at least partially) during the preparation process, they obviously did not change the dimensions of the hexagonal pore structure, which was expected due to the preparation method. In the work reported by Araujo *et al.* [2] the pore structure was probably built around the polymer chains formed during the *in situ* polymerization.

4.2 Transmission electron microscopy (TEM)

Figure 4.3 shows the TEM images of MCM-41 powder at different magnifications. Well-ordered channels with a hexagonal symmetry typical of the mesoporous structure are observed, and Figure 4.3(b) clearly shows the pore structure of the MCM-41 particles. TEM images of the PC/MCM-41 composites loaded with 0.5 and 5 wt.% are shown in Figure 4.4. Figure 4.4(a) clearly shows the agglomerated MCM-41 particle in the polymer matrix, and the small MCM-41 agglomerates are well dispersed in polymer matrix (Figure 4.4(b)). This composite is less transparent than the composites containing lower MCM-41 contents (Figure 4.5), indicating that these composites probably had smaller agglomerates or even individual nanoparticles dispersed in the PC matrix. Figure 4.4(c,d) shows poorly dispersed and highly agglomerated MCM-41 particles, which is the reason for the clear loss in transparancy observed in Figure 4.5.

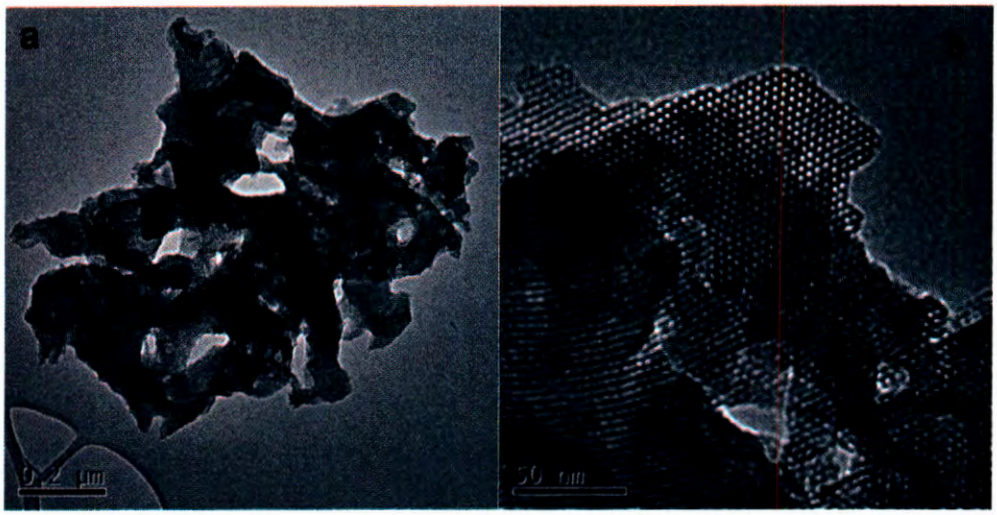

Figure 4.3 TEM micrographs of the MCM-41 powder at different magnifications

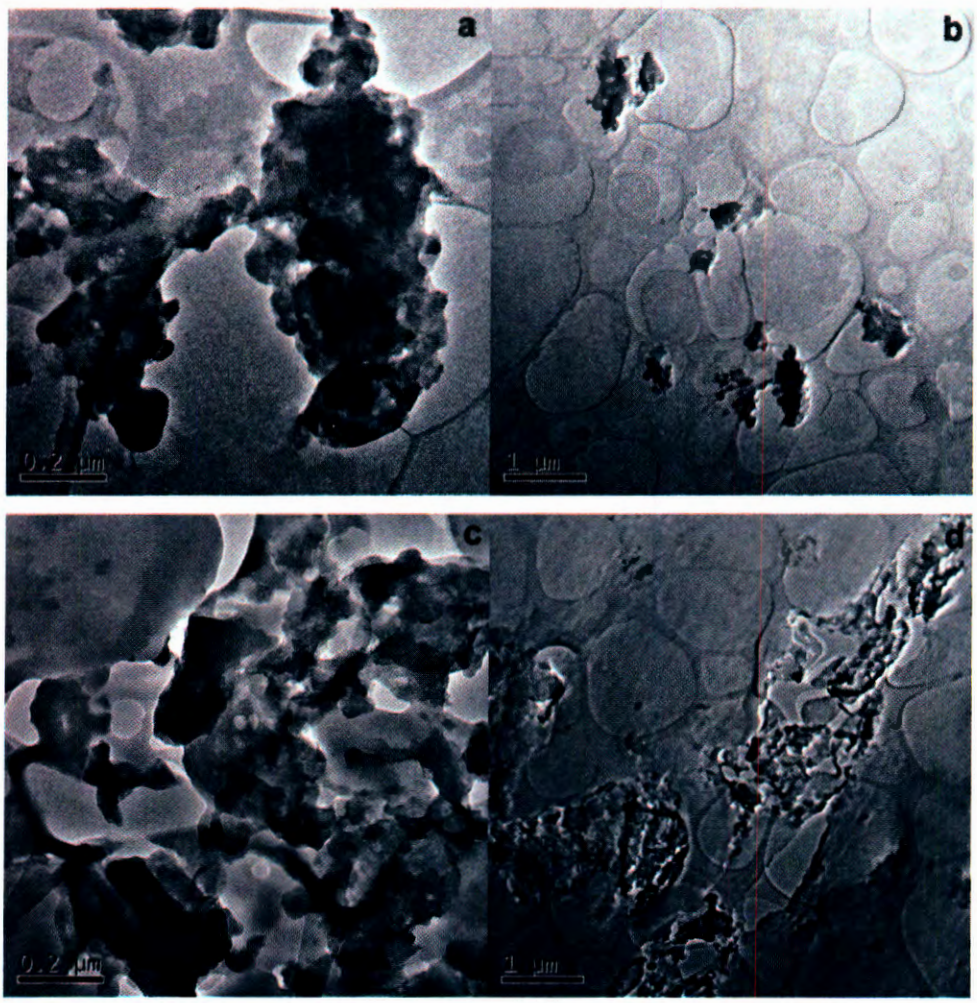

Figure 4.4 TEM micrographs of the PC/MCM-41 composites with 0.5 wt.% (a,b) and 5 wt.% (c,d) loading at different magnifications

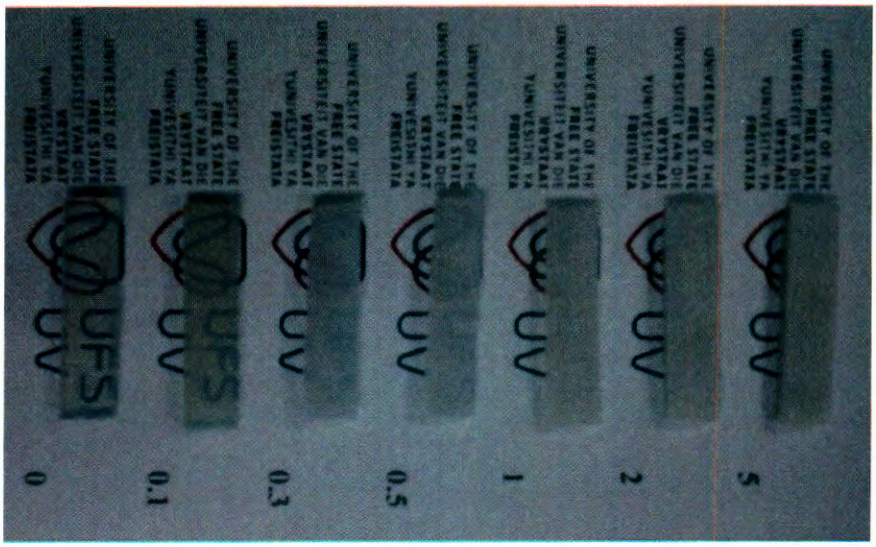

Figure 4.5 Picture of PC and the PC/MCM-41 composites to illustrate their transparency

4.3 ^{13}C cross-polarization magic-angle spinning nuclear magnetic resonance (^{13}C {^{1}H} CP-MAS-NMR) spectroscopy

The ^{13}C {^{1}H} CP MAS NMR spectra of PC and the PC/MCM-41 composites loaded with 0.5 and 5 wt.% MCM-41 are reported in Figure 4.6 to show the assignment of the ^{13}C chemical shifts of the polymer. All the spectra show five resonances, peak 1 at 149 ppm is related to the quaternary carbons of the aromatic rings and to the carbonyl carbon, peak 2 at 127 ppm to the aromatic carbon in meta to the oxygen, peak 3 at 120 ppm to the aromatic carbon in ortho to the oxygen, peak 4 at 42 ppm to the quaternary carbon bonded to the methyl groups, and peak 5 at 31 ppm to the methyl carbons. The presence of MCM-41 does not induce any modification in the chemical shift and in the signal shape, indicating that only physical interaction is possible between PC and MCM-41 particles.

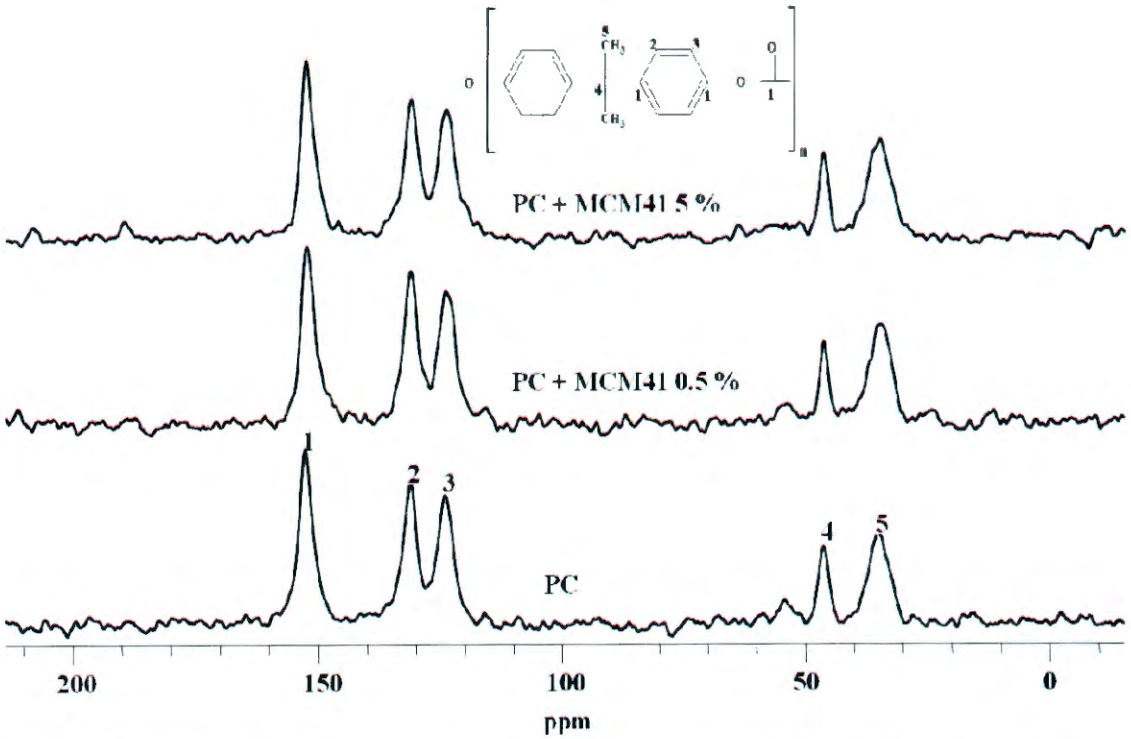

Figure 4.6 ^{13}C {^{1}H} CP-MAS NMR spectra of PC and the PC/MCM-41 composites

The proton and carbon spin lattice relaxation times in the rotating frame, $T_{1\rho}(H)$ and $T_{1\rho}(C)$, were determined through solid-state NMR measurements in order to detect dynamic changes in the polymer induced by the presence of the MCM-41. The $T_{1\rho}$ is sensitive to molecular motions in the kHz region and it is inversely proportional to the spectral density of motion. The $T_{1\rho}(H)$ and $T_{1\rho}(C)$ values for pure PC and the PC/MCM-41 composites loaded with 0.5 and 5 wt.% MCM-41 obtained from each peak in the ^{13}C spectra are reported in Table 4.1. The presence of MCM-41 at 0.5 and 5 wt.% loading did not significantly affect the $T_{1\rho}(H)$ values, but the relaxation time for the carbonyl carbon peak (peak 1) increased at 5 wt.% loading. This is evidence that the interaction between the MCM-41 and the polymer matrix was principally localized in this nuclear environment. However, the $T_{1\rho}(C)$ values are affected by the presence of MCM-41. The carbon 1 value for PC decreased after the addition of 0.5 wt.% MCM-41, but at the higher filler loading it increased, not only for carbon 1 but also for carbons 3 and 4. These increases can be attributed to the hindering of the mobility of the polymer chains. The carbonyl carbon are particularly hindered by the presence of MCM-41 particles because of a specific interaction which is probably hydrogen bonding with the Si–OH groups on MCM-41 [7,8].

Table 4.1 Relaxation time values for all the peaks in the ^{13}C spectra of PC and the PC/MCM-41 composites loaded with 0.5 and 5 wt.% of MCM-41

		$T_{1\rho}H$ (ms)			$T_{1\rho}C$ (ms)		
Carbon	**ppm**	**0 wt.%**	**0.5 wt.%**	**5 wt.%**	**0 wt.%**	**0.5 wt.%**	**5 wt.%**
1	149	4.9 ± 0.2	4.9 ± 0.2	6.0 ± 0.2	95.3 ± 0.3	38.8 ± 0.4	102.9 ± 0.2
2	127.5	4.9 ± 0.2	5.2 ± 0.2	5.4 ± 0.3	10.9 ± 0.2	11.1 ± 0.2	10.6 ± 0.2
3	120	4.4 ± 0.2	5.6 ± 0.2	4.4 ± 0.2	11.2 ± 0.2	10.9 ± 0.2	29.1 ± 0.2
4	42	3.9 ± 0.2	4.2 ± 0.2	4.5 ± 0.3	28.4 ± 0.3	31.6 ± 0.2	55.6 ± 0.2
5	31	6.6 ± 0.3	4.9 ± 0.2	5.9 ± 0.2	30.5 ± 0.2	23.2 ± 0.2	20.5 ± 0.2

4.4 Dynamic mechanical analysis (DMA)

Figure 4.7 shows the storage modulus curves of PC and the PC/MCM-41 composites as a function of temperature, and the E' values at 100 and 170 °C are reported in Table 4.2. Below the glass transition temperature the storage modulus of PC decreases with the addition of MCM-41, but the amount of filler had no significant effect and there was no clear trend. Above the glass transition there was a much more significant increase in storage modulus in the presence of and with an increase in MCM-41 loading, which can be attributed to (at least part of) the polymer chains which penetrated into the pores of the MCM-41 particles, restricted the mobility of the polymer chains, and increased the stiffness of the polymer. Motaung *et al.* [9] prepared PC composites with non-porous silica and they observed a decrease in storage modulus of PC at low contents (1 and 2 wt.%) over the whole investigated temperature range, which they attributed to a plasticizing effect of the silica particles. An increase in storage modulus was only observed at 5 wt.% silica content, and they concluded that effective immobilization of the polymer chains only takes place at higher silica contents. Biswal *et al.* [8] attributed the lower storage modulus of PC over the whole investigated temperature range, with the addition of $nSiO_2$ at 3 wt.%, to a reduction in the hard phase formation. Apparently the interfacial interaction between the –OH groups on the $nSiO_2$ surface and the C=O groups in the bulk polymer disrupted the stoichiometry ratio so that the hard phase domains were limited. The presence of both porous and non-porous silica particles seems to have the same influence on the E' below the glass transition temperature, but the presence of MCM-41 clearly had a more significant effect on the storage modulus of PC

above the glass transition temperature compared to the normal, non-porous silica used by Motaung *et al.* and Biswal *et al.* This can only be attributed to the porous structure of MCM-41, where the pores can be penetrated by the polymer chains, leading to their immobilization.

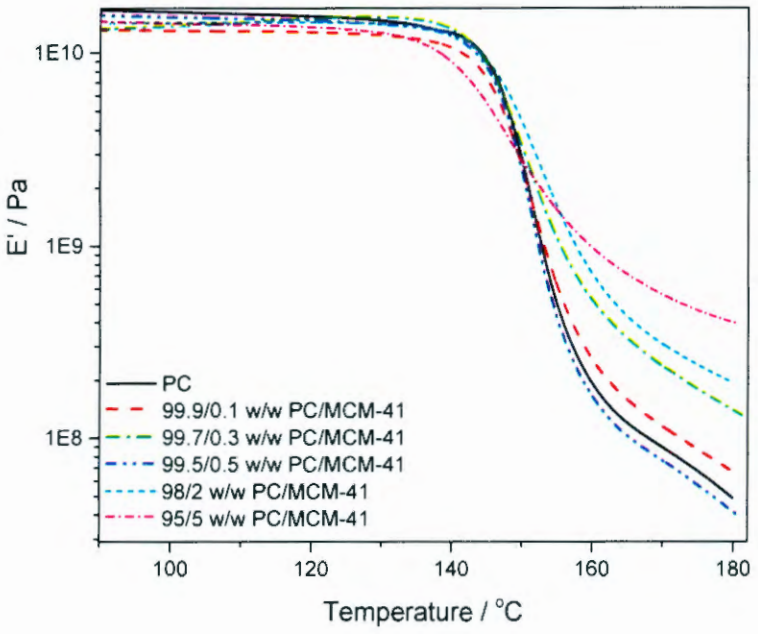

Figure 4.7 Storage modulus curves of PC and the PC/MCM-41 composites

The loss modulus and tan δ curves of PC and the PC/MCM-41 composites as a function of temperature are shown in Figure 4.8 and Figure 4.9 respectively, and the glass transition temperatures taken from the E" and tan δ curves are reported in Table 4.2. The loss modulus followed the same pattern as the storage modulus. The addition of MCM-41 until 2 wt.% did not have a significant influence on the glass transition temperature of PC, but at 5 wt.% loading the glass transition temperature observably decreased. This can be attributed to the agglomerates observed in the TEM images, which probably reduced the effectiveness of the filler particles to immobilize the polymer. Feng *et al.* [10] observed an increase in the T_g of PC at low silica contents (1 wt.%) and a decrease at higher contents (3 and 5 wt.%). The increase was attributed to the dispersed SiO_2 nanoparticles, which restricted the motions of the polymer chains, while the decrease at higher filler loadings was attributed to the increased free volume as a result of the disruption in the chain segment packing.

Table 4.2 DMA results of PC and PC/MCM-41 composites

Sample	10^{-10} E' / Pa at 100 °C	10^{-8} E' / Pa at 170 °C	T_g / °C from E" curves	T_g / °C from tan δ curves
PC	1.6	0.9	147.1	154.1
99.9/0.1 w/w PC/MCM-41	1.3	1.1	147.0	154.2
99.7/0.3 w/w PC/MCM-41	1.4	2.3	146.5	153.7
99.5/0.5 w/w PC/MCM-41	1.5	0.7	147.1	154.0
98/2 w/w PC/MCM-41	1.4	3.1	147.6	156.0
95/5 w/w PC/MCM-41	1.4	5.5	144.2	152.3

The maximum value of tan δ ($(\tan \delta)_{max}$) of PC significantly decreased after the addition of MCM-41, and with increasing filler content. This is normally attributed to the good adhesion between the polymer and the filler, because composites with a weak filler-polymer interface tends to dissipate more energy than composites with good interfacial bonding [11,12]. Polymer composites with good interfacial bonding allows less energy to be dissipated due to the restriction of the polymer chain mobility. However, weak interfacial bonding reduces the effectiveness of filler particles to immobilize polymer chains and more energy should therefore be dissipated. The decrease in the fraction of the polymer in the sample (because of the presence of the filler) also reduces the number of the mobile chains during the glass transition, thus contributing to the reduction in $(\tan \delta)_{max}$. However, the filler contents are relatively low so that this factor will have a minor contribution. The decrease in the $(\tan \delta)_{max}$ of PC with the addition of MCM-41 can therefore be attributed to the reinforcing effect of MCM-41, which is the result of the penetration of the polymer chains into the MCM-41 pores and the hydrogen bonding interaction between the polymer and filler, and to a lesser extent to the reduction in the amount of polymer in the sample. Wang *et al.* [13] also observed a decrease in the intensity of the tan δ peak of natural rubber (NR) with the addition of MCM-41. They attributed it to the reinforcing tendency of the nano filler on the matrix due to the physical and chemical adsorption of the NR molecules on the filler surface.

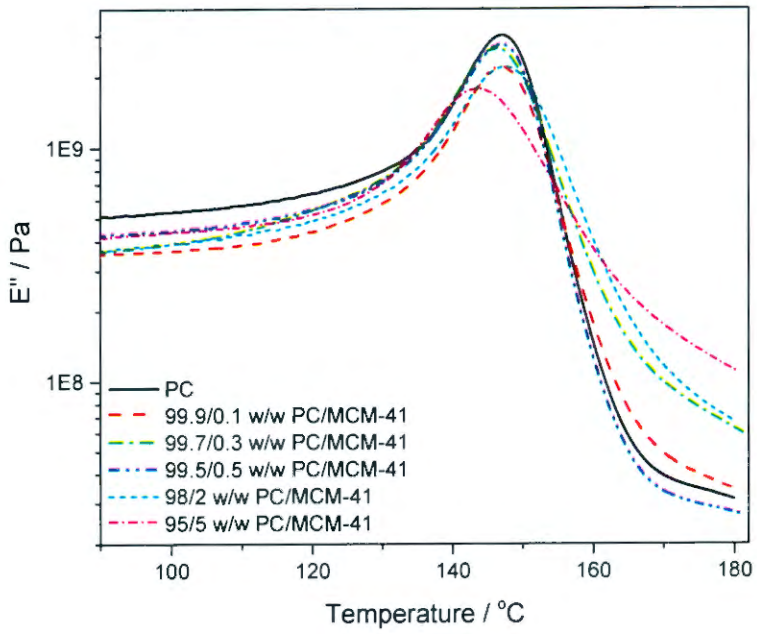

Figure 4.8 Loss modulus curves of PC and the PC/MCM-41composites

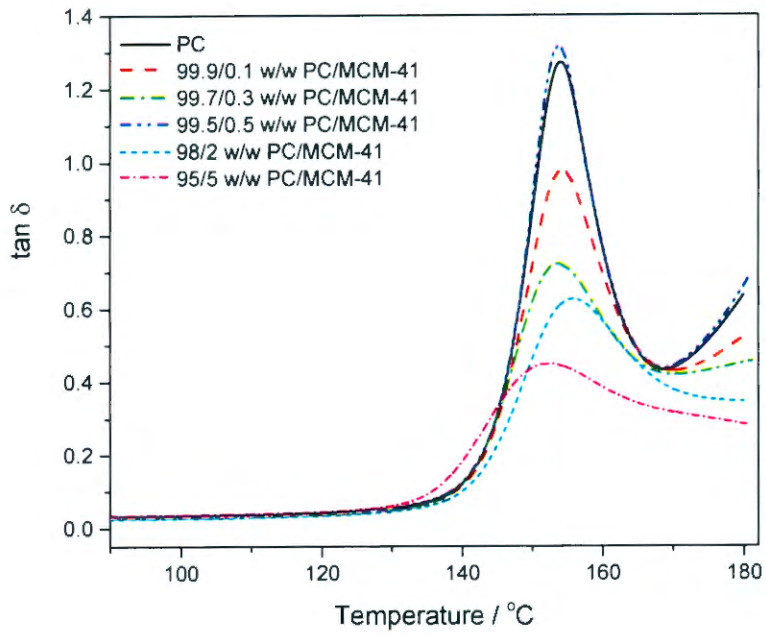

Figure 4.9 Tan δ curves of PC and the PC/MCM-41 composites

4.5 Thermogravimetric analysis (TGA)

The TGA curves of PC and the PC/MCM-41 composites are shown in Figure 4.10. The degradation process of both PC and its composites occur in one step in the temperature range of 360 to 520 °C. The thermal stability of the polymer nanocomposites has been found to depend on a number of factors that include nanoparticle loading and dispersion. In the case of epoxy resin/TiO_2 nanocomposites, at low filler loading the nanoparticles were uniformly dispersed and formed a barrier to heat due to their ceramic nature. When the content of the nanoparticles was increased, the particles tended to form agglomerates, that were non-uniformly distributed and less effective in blocking the heat [13,14].

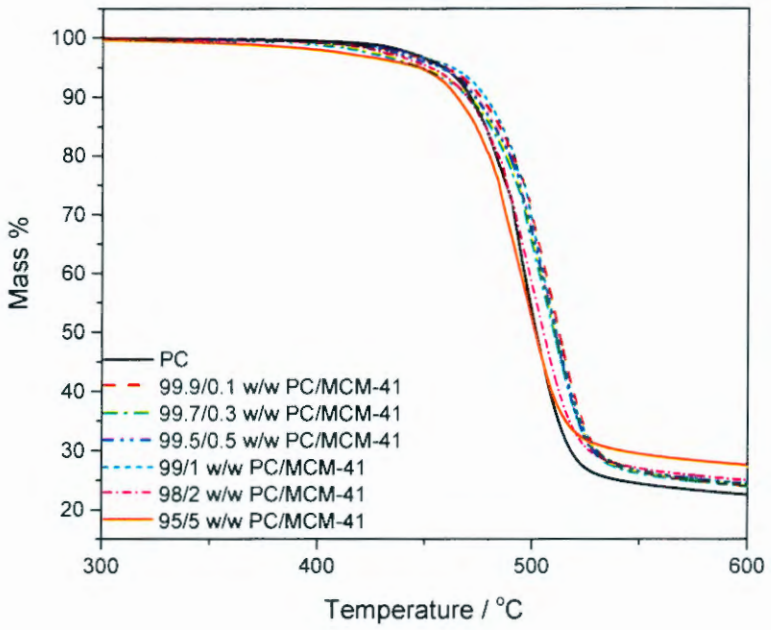

Figure 4.10 TGA curves of PC and PC/MCM-41 composites

The addition of MCM-41 up to 1 wt.% increased the thermal stability of PC (Table 4.3). The increase in thermal stability can be attributed to the presence of part of the polymer chains in the porous filler. The pores would act as physical barrier which would trap the volatile degradation products and delay their diffusion out of the polymer, so that they were only released at higher temperatures. Mingtao *et al.* [15] also observed an increase in thermal stability of poly(ethylene terephthalate) in the presence of mesoporous molecular sieves. They related the

increase to the presence of polymer chains in the mesoporous channels, making them less prone to oxidation due to the protection of the inorganic pore-wall. It is, however, also possible that the polymer chains and free radical chains were immobilized through their interaction with the small and well dispersed filler particles, which would delay the propagation of the degradation reaction, or that the diffusion of the volatile degradation products was delayed because of similar interactions. The sample with 5 wt.% MCM-41, on the other hand, shows a decrease in mass loss temperature to values approximately the same as that of pure PC. This can be attributed to the agglomerates observed in the TEM images, which reduced the effectiveness of the filler particles to immobilize the polymer and free radical chains, and the volatile degradation products. The decrease in glass transition temperature was also observed on the on the DMA results. Motaung *et al.* [9] studied the same system, but used non-porous silica particles at 1,2 and 5 wt.% loadings. They observed an insignificant increase in thermal stability with the addition of 1 and 2 wt.% silica, while a decrease in the thermal stability was observed for the sample containing 5 wt.% silica. They attributed the decrease to the catalytic effect of the silica particles. Carrion *et al.* [16] also observed lower decomposition temperatures for polycarbonate heated in the presences ZnO nanoparticles, and they only attributed it to the presence of large aggregated nanoparticles.

Table 4.3 TGA results for PC and the PC/MCM-41 composites

Sample	T_{30} / °C	T_{max} / °C	% Residue
PC	491.6	496.3	22.2
99.9/0.1 w/w PC/MCM-41	499.2	510.2	23.8
99.7/0.3 w/w PC/MCM-41	496.7	508.4	23.8
99.5/0.5 w/w PC/MCM-41	497.7	509.4	24.2
99/1 w/w PC/MCM-41	500.3	508.1	24.5
98/2 w/w PC/MCM-41	491.9	502.6	24.9
95/5 w/w PC/MCM-41	487.4	497.6	27.3

The amounts of residue observed at 600 °C for the investigated samples are summarized in Table 4.3. PC left about 22% residue, while the composites left more residue. The differences between the residues left by the composites and that left by neat PC are observably higher than

the amounts of MCM-41 initially mixed into the samples, but only for filler loadings up to 1%. This is probably the result of a fairly uneven dispersion of the filler particles at these low contents. Motaung *et al.*, on their PC/silica composites, found that the % residue correlated well with the amount of silica initially mixed into the samples, taking into account the amount of residue left by the neat polymer [9].

4.6 Thermal degradation kinetics

A number of papers reported different and sometimes contradictory results concerning the effect of the nanoparticles on the thermal stability of PC. There are papers suggesting that nanoparticles have no obvious effect on the thermal stability [10], some suggested a small to large enhancement [17-19], and others suggested a decrease in the thermal stability [9,16]. In order to get a better understanding of the degradation process and the effect of the MCM-41 loading on the thermal stability of PC, the minimum amount of energy that is required to initiate and propagate the degradation process was determined. The activation energy (E_a) for mass loss was determined from the slope of the isoconversional plots of ln β versus 1/T (Figures 4.11 to 4.13) taken at a heating rate of 3, 5, 7 and 9 °C $min^{-1}$for the degradation of PC and the composites filled with 0.5 and 5 wt.% MCM-41. The relationship between the activation energy and the extent of mass loss is shown in Figure 4.14. The activation energy of mass loss for PC and the PC/MCM-41 composites increased with increase in the extent of mass loss, which means that the degradation process involved multiple steps [20].

The activation energies of the sample containing 0.5 wt.% were higher than those of pure PC, which can be attributed to more energy required for mass loss to occur. As already discussed, this may result from an increase in thermal stability through immobilization of the polymer and free radical chains by the MCM-41 particles, or through delaying of the diffusion of volatile degradation products out of the molten sample. However, the sample containing 5 wt.% shows lower activation energy values than pure PC, which can be attributed to a catalytic effect of the larger MCM-41 agglomerates on the PC degradation. Araujo *et al.* [21] and Motaung *et al.* [9] gave the same explanation for similar observations.

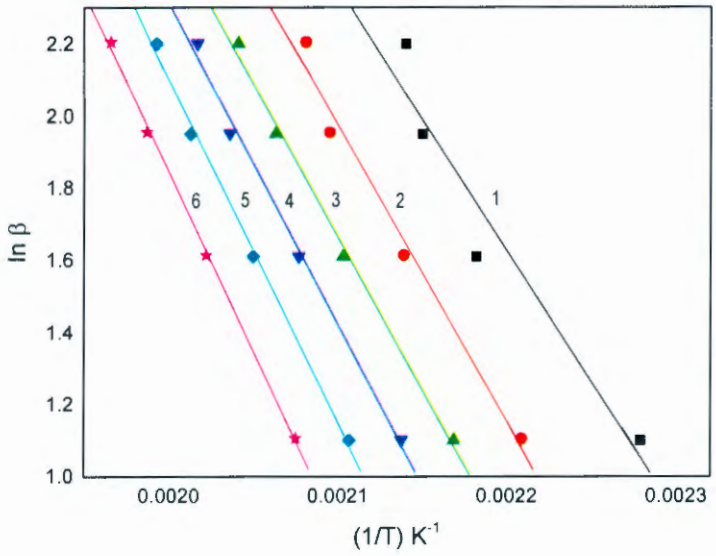

Figure 4.11 Ozawa–Flynn-Wall plots derived from the PC mass loss curves for the following degrees of conversion: 1) α = 0.1; 2) α = 0.2; 3) α = 0.3; 4) α = 0.4; 5) α = 0.5; 6) α = 0.6

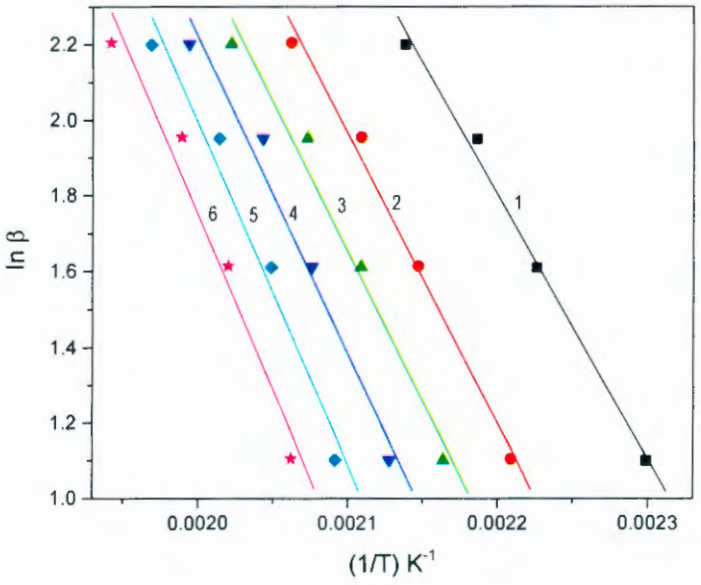

Figure 4.12 Ozawa–Flynn-Wall plots derived from the 99.5/0.5 w/w PC/MCM-41 mass loss curves for the following degrees of conversion: 1) α = 0.1; 2) α = 0.2; 3) α = 0.3; 4) α = 0.4; 5) α = 0.5; 6) α = 0.6

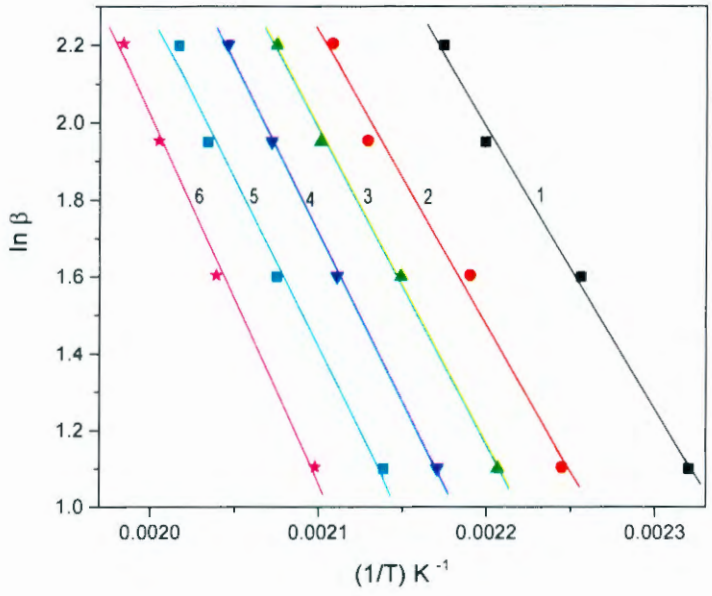

Figure 4.13 Ozawa–Flynn-Wall plots derived from the 95/5 w/w PC/MCM-41 mass loss curves for the following degrees of conversion: 1) α = 0.1; 2) α = 0.2; 3) α = 0.3; 4) α = 0.4; 5) α = 0.5; 6) α = 0.6

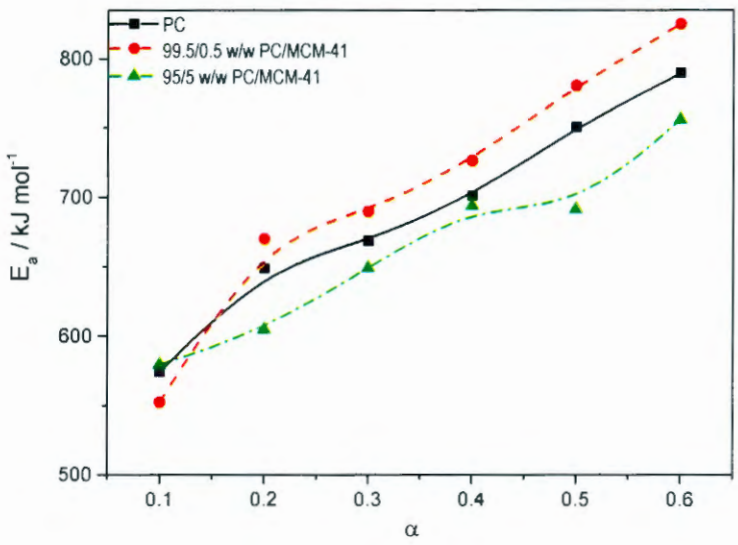

Figure 4.14 Activation energy vs. extent of mass loss for PC and the PC/MCM-41composites with 0.5 and 5 wt.% MCM-41

4.7 Conclusions

The purpose of the work reported in this chapter was to investigate the influence of mesoporous silica (MCM-41) in the range of 0.1 to 5 wt.% on the thermo-mechanical properties, as well as the thermal stability and thermal degradation kinetics behaviour of PC. The composites maintained their transparency at low MCM-41 loadings, while higher filler contents resulted in a total loss of transparency due to the presence of agglomerates. Part of the polymer chains were trapped in the pores of the MCM-41 without altering its hexagonal structure or pore size, but the presence of polymer chains in the pores and their interaction with the particles had an influence on the thermo-mechanical properties and thermal stability of the PC. The storage and loss modulus decreased with the addition of MCM-41 below the glass transition temperature, but this decrease was independent of the content. However, the moduli of the samples increased with increasing filler content above the glass transition temperature, due to the interaction of the polymer chains with the filler and the present of part of polymer chains in the pores, which restricted the mobility of the polymer chains and increased the stiffness of the composites. This interaction between the PC and MCM-41 was confirmed through $^{13}C\{^{1}H\}$CP-MAS-NMR spectroscopic analysis. The addition of MCM-41 up to 1 wt.% increased the thermal stability of PC, which was probably due to a delayed mass loss because of the trapping of the volatile degradation products in the pores of MCM-41. However, the thermal stability decreased at 5 wt.% due to the agglomerated MCM-41, which reduced the effectiveness of the filler particles to immobilize the free radical chains and volatile degradation products.

4.8 References

1. L. Wang, X. Han, J. Li, D. Zheng. Preparation of modified mesoporous MCM-41 silica spheres and its application in pervaporation. Powder Technology 2012; 231:63-69. DOI: 10.1016/j.powtec.2012.07.044
2. J.A. Araujo, F.T. Cruz, I.H. Cruz, D. Cardoso. Encapsulation of polmers in CTA-MCM-41 via microemulsion. Microporous and Mesoporous Materials 2013; 180:14-21. DOI: 10.1016/j.micromeso.2013.05.010

3. R.J. Young, P.A. Lovell. Introduction To Polymers. Third edition. CRC Press Taylor & Francis Group: Boca Raton (2011).
ISBN: 978-0-8493-3929-5
4. A.M. Mendonza, J. Warzywoda, A. Sacco. Jr. Investigation of structural order and morphology of MCM-41 mesoporous silica using an experimental design methodology. Journal of Porous Materials 2006; 13:37-47.
DOI: 10.1007/s10934-006-5488-0
5. K.S Hui, C.Y.H. Chao. Synthesis of MCM-41 from coal fly ash by a green approach: Influence of synthesis pH. Journal of Hazardous Materials 2006; B137:1135-1148.
DOI: 10.1016/j.jhazmat.2006.03.050
6. E. Rouabah, M. Fois, L. Ibos, A. Boudenne, D. Dadache, N. Haddaoui, P. Ausset. Mechanical and thermal properties of polycarbonate. II. Influence of titanium dioxide content and quenching on pigmented polycarbonate. Journal of Applied Polymer Science 2007; 106:2710-2717.
DOI: 10.1002/app.26807
7. A.S. Luyt, M. Messori, P. Fabbri, J.P. Mofokeng, R. Taurino, T. Zanasi, F. Pilati. Polycarbonate reinforced with silica nanoparticles. Polymer Bulletin 2011; 66:991-1004.
DOI: 10.1007/s00289-010-0408-5
8. M. Biswal, S. Mohanty, S.K. Nayak, P.S. Kumar. Effect of functionalized nanosilica on the mechanical, dynamic-mechanical, and morphological performance of polycarbonate/nanosilica nanocomposites. Polymer Engineering and Science 2013; 53:1287-1296.
DOI: 10.1002/pen.23288
9. T.E. Motaung, M.L. Saladino, A.S. Luyt, D.F.C. Martino. The effect of silica nanoparticles on the morphology, mechanical properties and thermal degradation kinetics of polycarbonate. Composites Science and Technology 2012; 73:34-39.
DOI: 10.1016/j.compscitech.2012.08.014
10. Y. Feng, B. Wang, F. Wang, G, Zheng, K. Dai, C. Liu, J. Chen, C. Shen. Effects of modified silica on morphology, mechanical property, and thermostability of injection-molded polycarbonate/silica nanocomposites. Journal of Reinforced Plastics & Composites 2014; 33:911-922.

DOI: 10.1177/0731684413520188

11. L.A. Pathon, Z. Oommen, S. Thomas. Dynamic mechanical analysis of banana fiber reinforced polyester composites. Composites Science and Technology 2003; 63:283-293.
PII: S0266-3538(02)00254-3

12. D. Romanzini, A. Lavoratti, H.L. Ornaghi Jr, S.C. Amico, A.J. Zattera. Influence of fiber content on the mechanical and dynamic mechanical properties of glass/ramie polymer composites. Materials and Design 2013; 47:9-15.
DOI: 10.1016/j.matdes.2012.12.029

13. N. Wang, Q. Fang, J. Zhang, E. Chen, X. Zhang. Incorporation of nano-sized mesoporous MCM-41 material used as fillers in natural rubber composite. Materials Science and Engineering A. 2011; 528:3321-3325
DOI: 10.1016/j.msea.2010.12.105

14. D. Bikiaris. Can nanoparticles really enhance thermal stability of polymers? Part II: An overview on thermal decomposition of polycondensation polymers. Thermochimica Acta 2011; 523:25-54.
DOI: 10.1016/j.tca.2011.06.012

15. R. Mingtao, Z. Dayu, W. Sizhu, W. Gang. Thermal decomposition of poly(ethylene terephthalate)/mesoporous molecular sieve composites. Frontiers of Chemical Engineering in China 2007; 1:50-54.
DOI: 10.1007/s11705-007-0010-z

16. F.J. Carrion, J. Sanes, M.D. Bermudez. Influence of ZnO nanoparticles filler on the properties and wear resistance of polycarbonate. Wear 20017; 262:1504-1510.
DOI: 10.1016/j.wear.2007.01.016

17. Y. Feng, B. Wang, F. Wang, G, Zheng, K. Dai, C. Liu, J. Chen, C. Shen. Effects of modified silica on morphology, mechanical property, and thermostability of injection-molded polycarbonate/silica nanocomposites. Journal of Reinforced Plastics & Composites 2014; 33:911-922.
DOI: 10.1177/0731684413520188

18. S. Suin, N.K. Shrivastsva. S. Maiti, B.B. Khatua. Phosphonium modified organoclay as potential nanofiller for the development of exfoliated and optically transparent

polycarbonate/clay nanocomposites: Preparation and characterization. European Polymer Journal 2013; 49:49-60.
DOI: 10.1016/j.eurpolymj.2012.10.004

19. S. Maiti, N.K. Shrivastava, S. Suin, B.B. Khatua. A strategy for achieving low percolation and high electrical conductivity in melt-blended polycarbonate (PC)/multiwall carbon nanotube (MWCNT) nanoparticles: Electrical and thermo-mechanical properties. eXPRESS Polymer Letters 2013; 7:505-518.
DOI: 103144/expresspolymlett.2013.47

20. J.D. Menczel, R.B. Prime. Thermal Analysis of Polymers. Fundamentals and Applications. Wiley, New Jersey (2009).
ISBN: 978-0-471-76917-0

21. S.A. Araujo, A.S. Araujo, N.S. Fernandes, V.J. Fernandes Jr, M. Ionashiro. Effect of the catalyst MCM-41 on the kinetics of the thermal decomposition of poly(ethylene terephthalate). Journal of Thermal Analysis and Calorimetry 2010; 99:465-469.
DOI: 10.1007/s10973-009-0490-9

Chapter 5: Morphology, mechanical, thermal and luminescence properties of poly(methyl methacrylate) (PMMA) filled with yttrium aluminium garnet doped with cerium (Ce:YAG) prepared by melt compounding

5.1 X-ray diffraction

Yttrium-alumina systems are made up of three phases that are stable at room temperature. They are the yttrium aluminium garnet (YAG), yttrium aluminium perovskite (YAP), and yttrium aluminium monoclinic (YAM) phases. Pure yttrium aluminium garnet is processed at a high temperature in order to eliminate intermediate phases, because it is the only phase favourable for the luminescent properties of phosphors. Figure 5.1 shows a single YAG phase with sharp peaks related to its crystalline structure; the same diffraction pattern for Ce:YAG was also observed in other studies [1-5]. The X-ray pattern for PMMA shows a broad diffraction band around 14°, together with two broad bands with lower intensities around 30 and 42°, typical of an amorphous material [6,7]. The composites loaded with 0.1 and 0.3 wt.% Ce:YAG show similar diffraction patterns as the neat PMMA due to the small amount of filler. A small diffraction peak at 33°, which is the angle for the most intense Ce:YAG peak, appears in the pattern of the sample loaded with 0.5 wt.% Ce:YAG, while all the peaks related to the garnet phase are observed for sample loaded with 1, 2 and 5 wt.% Ce:YAG. The positions of the garnet phase peaks in the composite samples did not shift with respect to those of the powder, confirming that no structural modification occurred when the filler was embedded in the polymer.

5.2 Transmission electron microscopy (TEM)

Figure 5.2 shows the TEM images of the PMMA/Ce:YAG composites filled with different Ce:YAG contents. The TEM image of the PMMA/Ce:YAG composite containing 0.5 wt.% Ce:YAG (Figure 5.2(a)) shows isolated Ce:YAG clusters in the polymer matrix, due to the very small amount of filler in the composite which was also not detected in the XRD for the samples containing less than 1 wt.% filler. This composite is also less transparent than those containing

smaller amounts of filler (Figure 5.3). Figure 5.2(b) shows smaller and better dispersed Ce:YAG clusters, but the clusters are still fairly big, which is probably the reason for the clear loss in transparancy observed in Figure 5.3. The difference in viscosity of the sample during mixing can be responsible for the difference in the size and distribution of the particles when comparing the composites that contain respectively 0.5 and 5% Ce:YAG. Increasing the amount of filler in the sample increases the viscosity of the sample during mixing, and this will increase the torque [8]. High torque during mixing should contribute to breaking up the Ce:YAG clusters into smaller particles that are better dispersed in the polymer matrix.

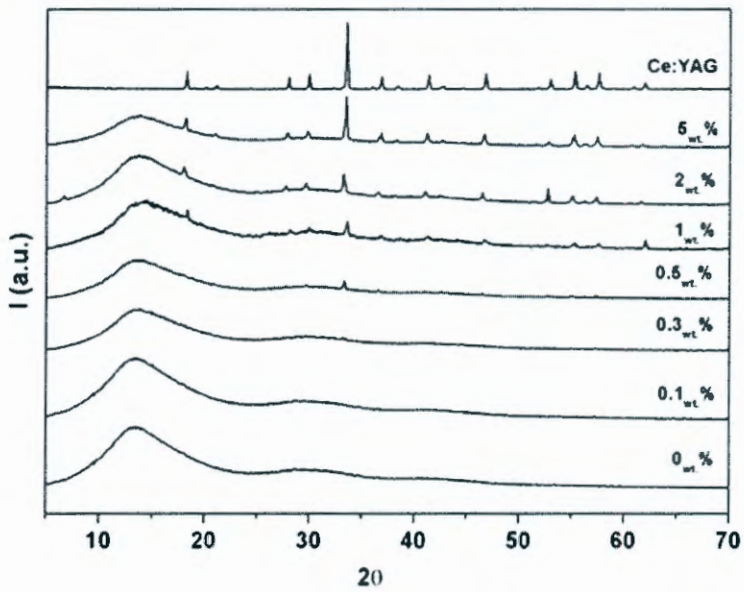

Figure 5.1 XRD patterns of Ce:YAG, PMMA and the PMMA/Ce:YAG composites

5.3 ^{13}C cross-polarization magic-angle spinning nuclear magnetic resonance (^{13}C {^{1}H} CP-MAS-NMR) spectroscopy

To gain insight into the organization of the polymer molecules in contact with the nanoparticle surface, ^{13}C {^{1}H} CP-MAS NMR experiments were performed. All the NMR spectra in Figure 5.4 show five resonances at 177.9, 55.4, 52.3, 45.2 and 16.6 ppm due to respectively the carbonyl carbon, methoxyl group, quaternary carbon of the polymer chain, and the methylene and methyl groups. In the presence of the filler, there are no new signals, changes in peak shapes or chemical shifts, indicating that the presence of filler did not induce any chemical modifications. All the interactions between the polymer and filler were therefore physical.

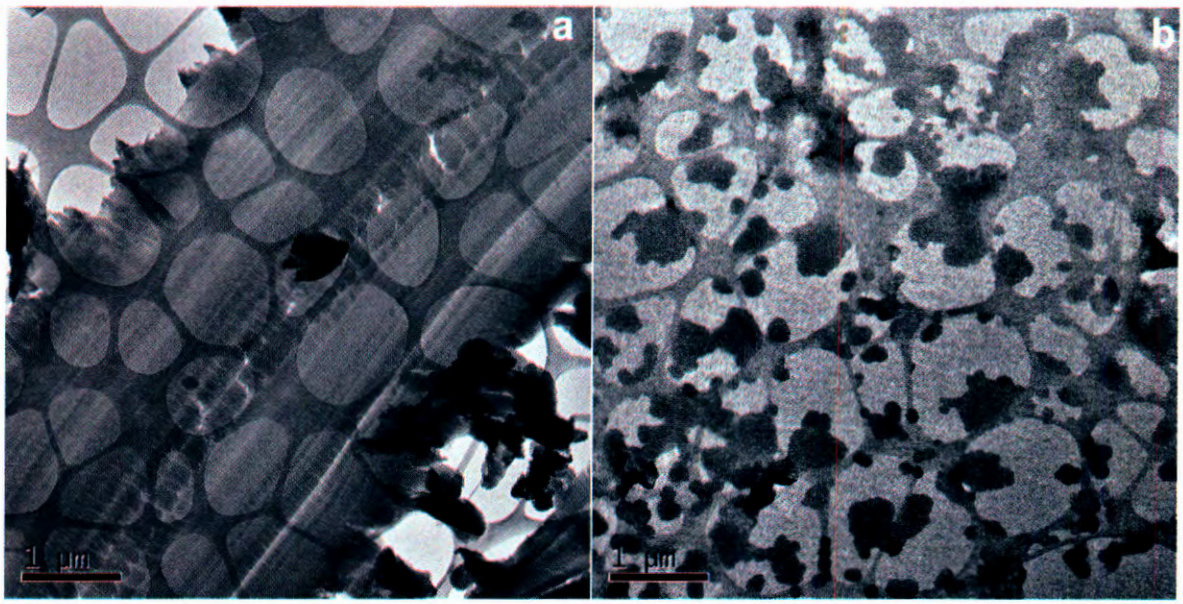

Figure 5.2 TEM micrographs of PMMA and PMMA/Ce:YAG composites with 0.5 (a) and 5 wt.% (b) Ce:YAG

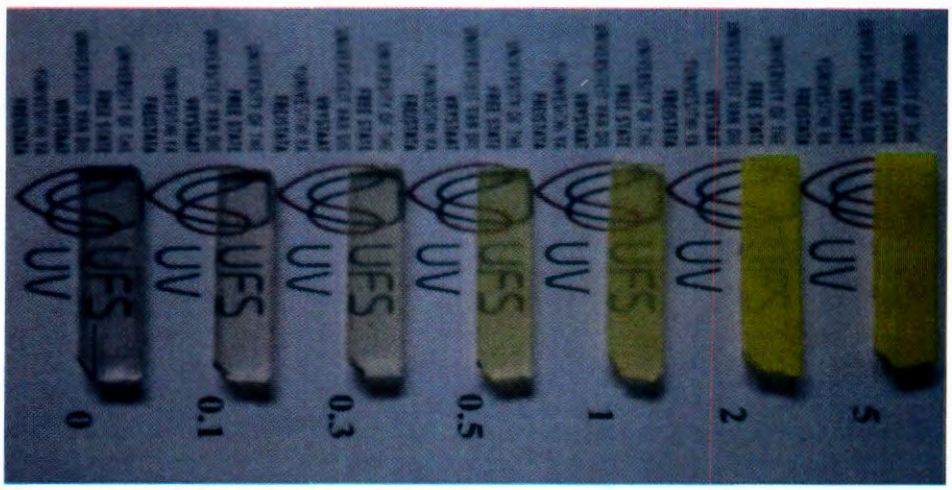

Figure 5.3 Picture of PMMA and the PMMA/Ce:YAG composites to illustrate their transparency

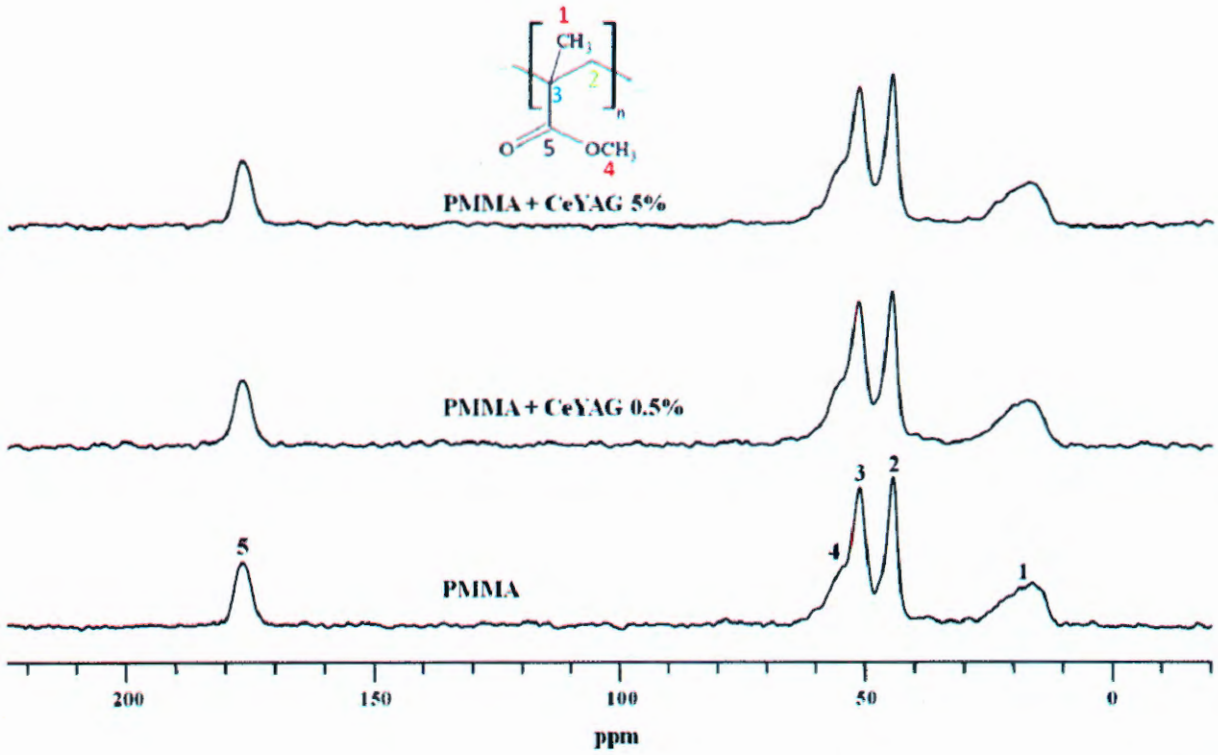

Figure 5.4 CP-MAS-NMR spectra of PMMA and PMMA/Ce:YAG composites with 0.5 and 5 wt.% Ce:YAG

The proton and carbon spin lattice relaxation times in the rotating frame, $T_{1\rho}(H)$ and $T_{1\rho}(C)$, were determined through solid-state NMR measurements in order to detect dynamic changes in the polymer induced by the presence of the filler. The spin lattice relaxation times in the rotating frame parameters ($T_{1\rho}$) are inversely proportional to the spectral density of motions in the kHz frequency, and they reflect the dynamic behaviour of a polymer chain in a range of a few nanometers. The $T_{1\rho}(H)$ and $T_{1\rho}(C)$ relaxation time values obtained from each peak in the ^{13}C spectra of PMMA and PMMA/Ce:YAG composites with 0.5 and 5 wt.% of Ce:YAG are reported in Table 5.1. The presence of 0.5 wt.% Ce:YAG shows a decrease in $T_{1\rho}(H)$ values for the quaternary carbon of the polymer chain (peak 3) and methylene (peak 2). This observation can be attributed to the increase in flexibility of the polymer chains as a result of larger free volumes caused by the presence of isolated Ce:YAG particles in the polymer matrix (Figures 5.2(a)). However, the $T_{1\rho}(H)$ values observed for the carbonyl carbon (peak 5) and methyl group (peak 1) were not significantly affected by the presence of Ce:YAG compared to those of the neat polymer, which can be due to some inhomogeneity in the sample. Furthermore, loading of

0.5 wt.% Ce:YAG in the polymer does not cause any appreciable change in this parameter, indicating that this concentration is unable to modify the dynamic behaviour of the polymer at nanometer level. The $T_{1\rho}(H)$ values of the sample containing 5 wt.% Ce:YAG increased because of the immobilization of the polymer chains, which can be attributed to the fairly well dispersed Ce:YAG particles. Longer relaxation times are ascribed to local stiffness in the polymer within a few nanometer length because of the presence of the filler [9,10].

The $T_{1\rho}(C)$ values for both composites were strongly affected by the presence of Ce:YAG particles. The addition of, and increase in filler particles significantly decreased most of the relaxation time values of the composites compared to those of the neat polymer. The electron donor-accepter interaction between yttrium and the carbonyl oxygen lone pair is a common example of a Lewis acid-base reaction. The carbonyl oxygen lone pair serves as a Lewis base which donates electrons and yttrium serves as a Lewis acid and accepts electrons. This interaction can account for the observable variation in the relaxation time due to the retrieval of electrons along the polymer chains [11]. In the study of PMMA/MCM-41 composites reported in Chapter 3 of this document we observed an increase in the $T_{1\rho}(C)$ values, in particular those of the carbonyl carbon, and we attributed it to the immobilization of the polymer chains due to hydrogen bonding interaction between the PMMA and MCM-41. In the case of PMMA/Ce:YAG composites this was clearly not the case, probably because the non-adhering particles inside the polymer increased the free volume, which then resulted in greater mobility of the polymer chains which lowered the relaxation time values [12].

Table 5.1 Relaxation time values for all the peaks in the ^{13}C spectra of PMMA and the PMMA/Ce:YAG composites loaded with 0.5 and 5 wt.% of Ce:YAG

	$T_{1\rho}H$ (ms)			$T_{1\rho}C$ (ms)		
ppm	**0 %**	**0.5%**	**5%**	**0 %**	**0.5%**	**5%**
177.9	14.3 ± 0.2	16.1 ± 0.2	33.5 ± 0.2	30.1± 0.3	24.8 ± 0.2	16.4 ± 0.3
55.4	-	21.5 ± 0.2	-	41.0 ± 0.2	4.6 ± 0.4	6.4 ± 0.3
52.3	20.5 ± 0.1	11.8 ± 0.1	54.4 ± 0.3	62.6 ± 0.4	10.7 ± 0.2	10.6 ± 0.2
45.2	13.4 ± 0.1	9.5 ± 0.3	15.8 ± 0.2	65.3 ± 0.2	14.9 ± 0.2	16.2 ± 0.1
16.6	15.2 ± 0.2	15.7 ± 0.4	10.6 ± 0.3	17.0 ± 0.1	19.6 ± 0.2	24.4 ± 0.2

5.4 Dynamic mechanical analysis (DMA)

The storage modulus curves of PMMA and the PMMA/CeYAG composites are reported in Figure 5.5, and the E' values taken at 70 and 140 °C are reported in Table 5.2. The storage modulus of all the composites is higher than that of neat PMMA throughout the investigated temperature range. However, the amount of Ce:YAG particles had little influence on the value of E', and there is no clear trend in the effect of filler on the storage modulus (Table 5.2). The increase in storage modulus above the glass transition temperature can be attributed to the immobilization of polymer chains through interaction with the filler particles, and the increase in rigidity of the composite as a result of the inherent stiffness of the filler. Musbah *et al.* [13] observed an increase in storage modulus and glass transition temperature of PMMA with the addition of europium-doped gadolinium oxide (Eu:Gd_2O_3) at 0.5, 1 and 3 wt.%. They attributed it to the reduction in the overall mobility of the polymer chains as a result of the functional physical crosslinks between the polymer and filler.

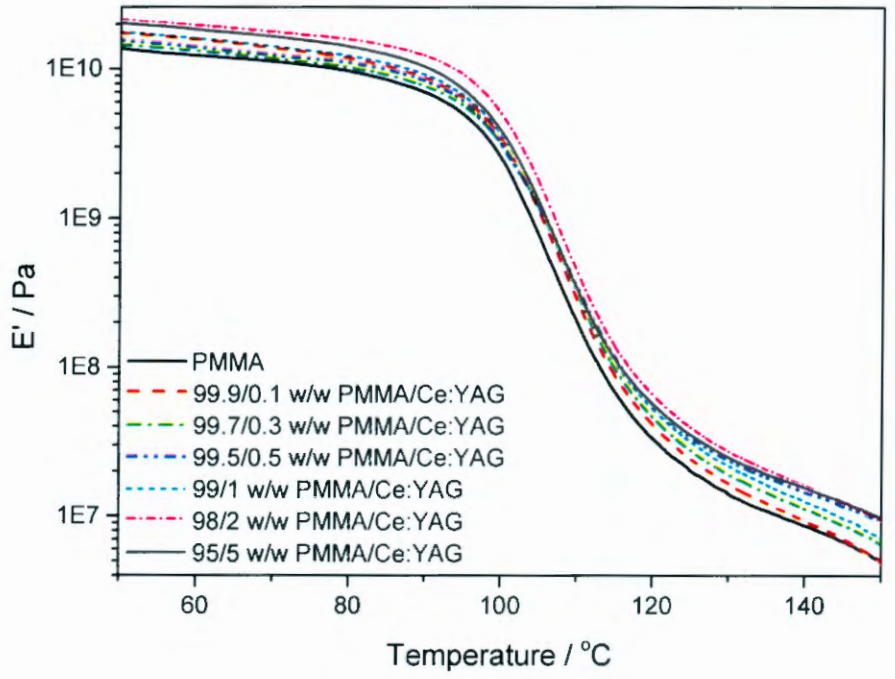

Figure 5.5 Storage modulus of PMMA and PMMA/Ce:YAG composites

Table 5.2 DMA results of PMMA and the PMMA/Ce:YAG composites

Sample	10^{-10} E' / Pa at 70 °C	10^{-7} E' / Pa at 140 °C	T_g / °C from E" curves	T_g / °C from tan δ curves
PMMA	1.3	0.8	95.3	115.7
99.9/0.1 w/w PMMA/Ce:YAG	1.4	0.9	96.7	114.8
99.7/0.3 w/w PMMA/Ce:YAG	1.2	1.1	96.3	114.5
99.5/0.5 w/w PMMA/Ce:YAG	1.2	1.5	96.5	114.5
99/1 w/w PMMA/Ce:YAG	1.4	1.2	97.5	114.1
98/2 w/w PMMA/Ce:YAG	1.7	1.6	98.1	114.1
95/5 w/w PMMA/Ce:YAG	1.6	1.5	97.7	113.9

The loss modulus curves of PMMA and the PMMA/Ce:YAG composites as function of temperature are shown in Figure 5.6, and the glass transition temperatures taken from the E" and tan δ curves are summarised in Table 5.2. The loss modulus also increased for the filler-containing samples, as was observed and discussed for the storage modulus. The addition of filler resulted in an observable increase in the glass transition temperature from the loss modulus curves (Table 5.2), which can be due to the immobilization of polymer chains which was observed earlier in the NMR results. It has been mentioned that, in particulate filled polymers, the presence of rigid fillers restricts the movement of the polymer chains, leading to a reduction in maximum value of tan δand a shift of the T_g values to higher temperatures [14]. This behaviour has been observed for PMMA with the addition of silica [15], organoclay [16], and mesoporous silica particles (Chapter 3 in this document), and has been attributed to good adhesion between the filler and the matrix, which resulted in a restriction of the mobility of the polymer chains in the composite. However, in this case the tan δ curves (Figure 5.7) do not show any significant effect of the Ce:YAG particles in PMMA. This is probably the result of the weak polymer-filler interaction, as was observed in the NMR analysis and discussed in section 5.3.

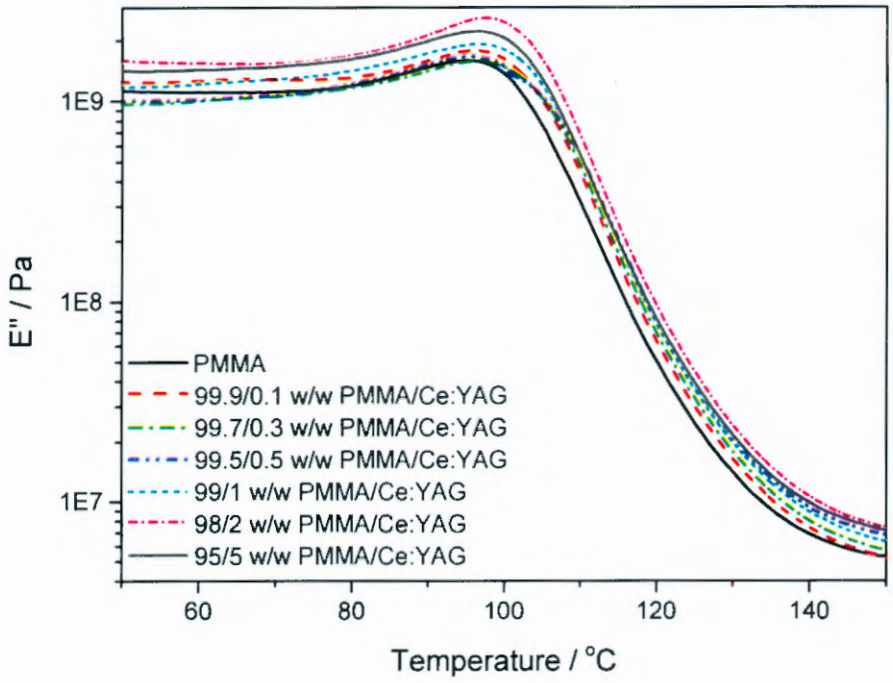

Figure 5.6 Loss modulus of PMMA and the PMMA/CeYAG composites

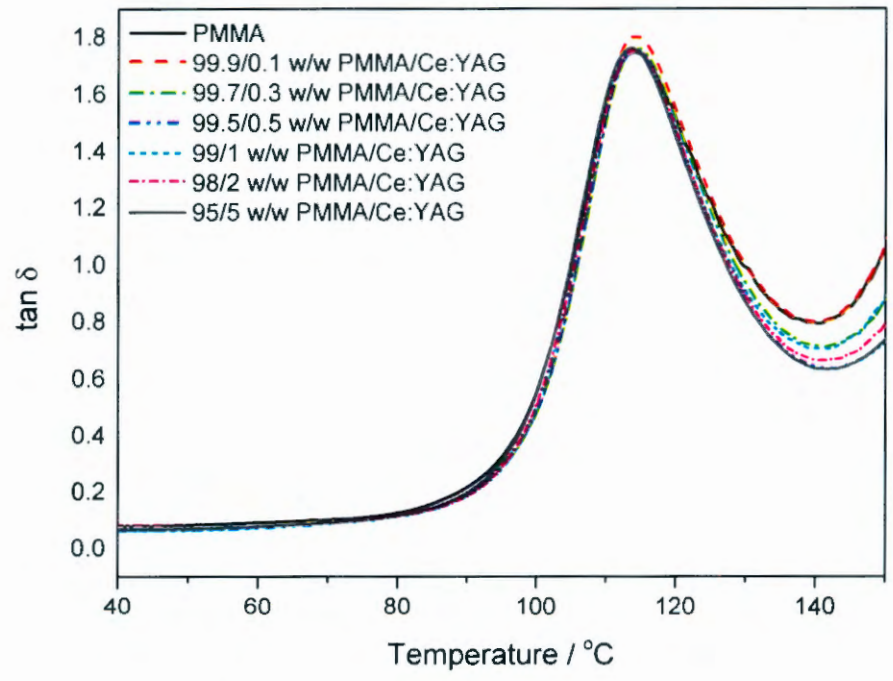

Figure 5.7 Tan δ curves of PMMA and PMMA/CeYAG composites

5.5 Impact properties

The effect of filler on the mechanical properties of polymers depends mainly on the final morphology of the composite, and how the filler is dispersed in the polymer matrix. During impact the filler particles in the composites normally act as defect centers for the formation of crazes, and the dispersion of the filler determine whether the crazes develop into cracks or becomes terminated at another particle.

The impact properties of PMMA and its composites are reported in Figure 5.8. The addition of small contents of Ce:YAG (0.1-0.5 wt.%) had no effect on the impact strength of PMMA. This can be attributed to the isolated Ce:YAG clusters in the polymer matrix (observed and discussed in section 5.2). When the particles are far apart from each other, crazes easily develop into cracks because the crazes did not effectively terminate at another filler particle, and therefore the applied stress is not effectively transferred between the polymer and the filler. Less energy is needed to break the sample. However, there was a significant increase in impact strength at higher filler loadings due to the fairly well dispersed and smaller Ce:YAG clusters (observed in Figure 5.2(b)), which allowed the transfer of the applied stress between the polymer and the filler, so that the composite requires more energy to break.

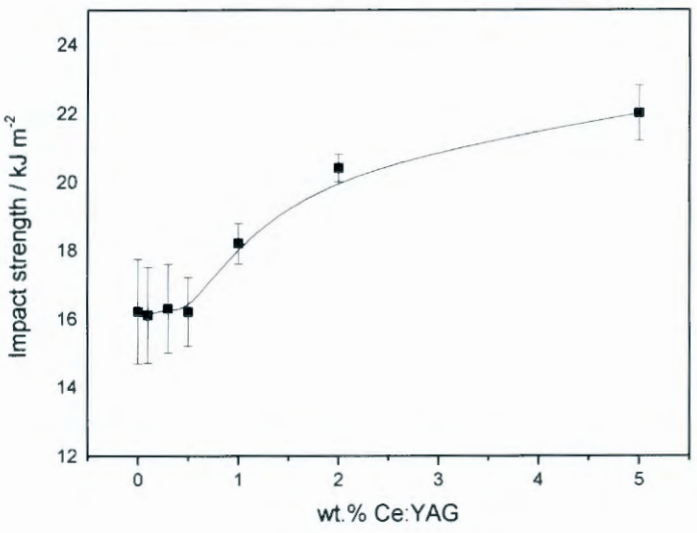

Figure 5.8 Impact strength of PMMA and the PMMA/Ce:YAG composites as function of filler content (line added to lead the eye)

5.6 Thermogravimetric analysis

The TGA curves of PMMA and the PMMA/Ce:YAG composites are shown in Figure 5.9, and some of the temperatures are summarised in Table 5.3. All the samples show one degradation step starting around 330 °C. The thermal stability of PMMA is not significantly influenced by the presence of Ce:YAG up to 2 wt.% Ce:YAG, and an observable increase was only observed for the sample containing 5 wt.% Ce:YAG. The increase in mass loss temperature can be due to the immobilisation of polymer chains (observed in the NMR results) and free radicals that took part in the degradation process, or to the volatile degradation products, that are formed during degradation, being released at higher temperatures because of interaction with the filler particles. Another possible reason for the increases in thermal stability of the composites is the difference in the thermal conductivity values of PMMA (0.19 W $m^{-1} k^{1}$) [17] and Ce:YAG (11.2 W $m^{-1} k^{-1}$). The shift in decomposition temperature can be attributed to relatively higher thermal conductivity value of Ce:YAG, which causes it to preferentially absorb heat. In this case the filler acts as a heat barrier and increases the thermal stability of the composites.

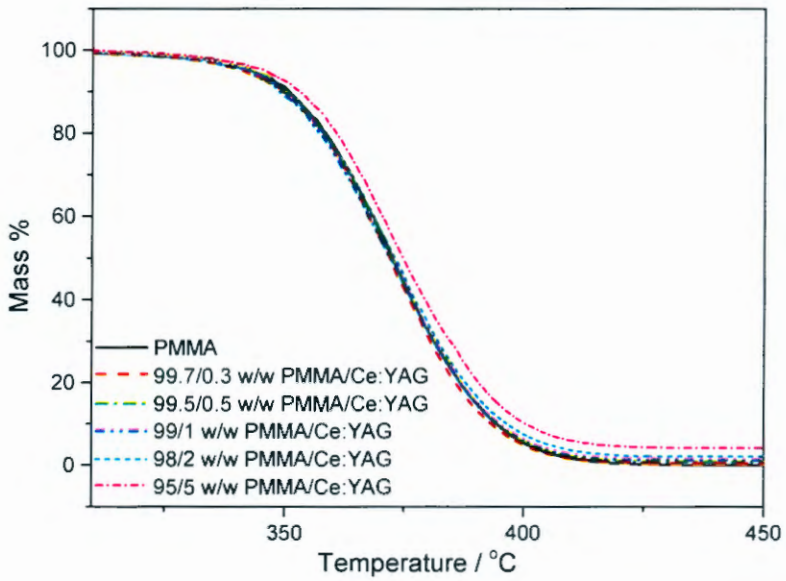

Figure 5.9 TGA curves of PMMA and the PMMA/CeYAG composites

Since the mass loss temperature is determined by the amount of filler in the composites and the interaction of the polymer chains, free radical chains, and volatile decomposition products with the filler particles, one would expect an increase in mass loss temperature with increasing filler content. This can be explained by the size of the filler clusters and the dispersion of the filler particles in the polymer. In our case the addition of small amounts of filler resulted in the formation of isolated Ce:YAG clusters (observed in the TEM images), and thus less filler surface was exposed to the polymer so that the filler had little influence on the thermal stability of PMMA. However, at higher loadings, smaller Ce:YAG clusters were fairly well dispersed in the polymer and more filler surface was exposed to the polymer. This allowed more effective interaction with the filler so that the polymer and free radical chains were immobilized and/or the volatile degradation products were trapped through their interaction with the filler particles.

The preparation method of the composites can also have a significant influence on the dispersion of the filler in the polymer matrix, and on the influence of the filler on the thermal stability of the composites. Zanotto *et al.* [11] prepared the same composites through solution mixing in the presence of the well dispersed filler, and they observed an almost 50 °C improvement in thermal stability at 5 wt.% Ce:YAG loading. They attributed this to small and well dispersed Ce:YAG nanoparticles and their strong interaction with the polymer, which not only immobilized the polymer chains but also the free radicals that took part in the degradation process. Although it is difficult to commercialize such a preparation technique, it definitely gave rise to a nanocomposite with very few clusters, which does not seem to be achievable through melt-mixing.

The amounts of residue observed at 450 °C are summarized in Table 4.3. Generally the amount of residue corresponds well with the amount of Ce:YAG initially added during the preparation of the composites, suggesting that the dispersion of the Ce:YAG clusters was fairly homogenous in the composites.

Table 5.3 TGA results for all the investigated samples

Sample	T_{40} / °C	T_{max} / °C	% Residue
PMMA	368.5	372.7	-
99.7/0.3 w/w PMMA/Ce:YAG	367.4	371.8	0.1
99.5/0.5 w/w PMMA/Ce:YAG	368.2	372.6	0.8
99/1 w/w PMMA/Ce:YAG	367.6	372.0	1.2
98/2 w/w PMMA/Ce:YAG	368.7	373.0	2.1
95/5 w/w PMMA/Ce:YAG	369.9	374.7	4.9

5.7 Thermal degradation kinetics

In order to get a better understanding of the degradation process and the effect of the Ce:YAG on the thermal stability of PMMA, the activation energy (E_a) for mass loss was determined for the degradation of PMMA and the composites filled with 0.5 and 5 wt.% Ce:YAG. The activation energy values were determined from the slope of the isoconversional plots of ln β versus 1/T (shown in Figures 5.10 to 5.12) obtained from TGA curves where the samples were respectively heated at 3, 5, 7 and 9 °C min^{-1}. The relationship between the activation energies and the extent of mass loss is shown in Figure 5.13.

The activation energy of PMMA and its composites shows a general increase with the increase in the extent of mass loss, but the composites show much higher activation energies than the pristine polymer. This can be attributed to the trapping of the free radical chains and volatile degradation products by the filler during the degradation process, so that more energy was required to initiate and propagate the degradation of the polymer, or to release the volatile degradation products adsorbed onto the filler particles. The E_a values of the two composites are very similar to each other, which suggests that the amount of Ce:YAG did not have a significant effect on the E_a values. Normally, one would expect composites with high thermal stability to require more energy to initiate degradation [18,19]. However, contrary to the TGA results, our 99.5/0.5 and 95/5 w/w PMMA/Ce:YAG samples showed similar activation energy values.

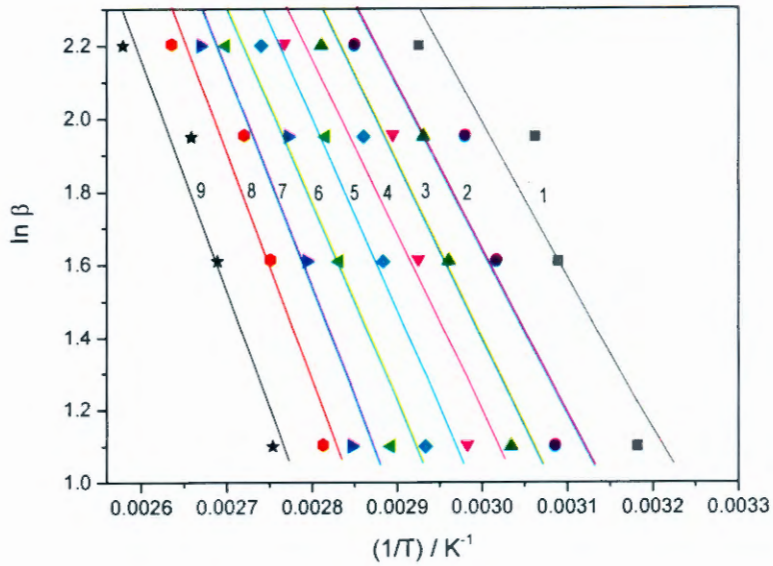

Figure 5.10 Ozawa–Flynn-Wall plots derived from the PMMA mass loss curves for the following degrees of conversion: 1) α = 0.1; 2) α = 0.2; 3) α = 0.3; 4) α = 0.4; 5) α = 0.5; 6) α = 0.6; 7) α = 0.7; 8) α = 0.8; 9) α = 0.9

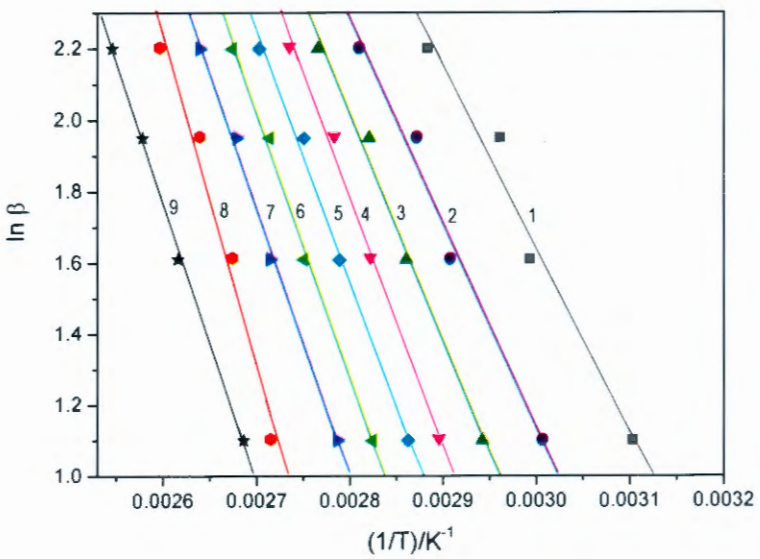

Figure 5.11 Ozawa–Flynn-Wall plots derived from the 99.5/0.5 w/w PMMA/Ce:YAG mass loss curves for the following degrees of conversion: 1) α = 0.1; 2) α = 0.2; 3) α = 0.3; 4) α = 0.4; 5) α = 0.5; 6) α = 0.6; 7) α = 0.7; 8) α = 0.8; 9) α = 0.9

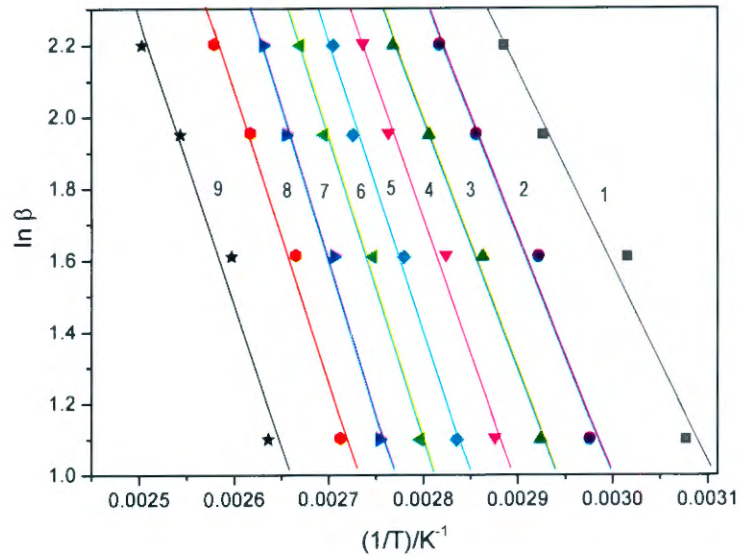

Figure 5.12 Ozawa–Flynn-Wall plots derived from the PMMA mass loss curves for the following degrees of conversion: 1) α = 0.1; 2) α = 0.2; 3) α = 0.3; 4) α = 0.4; 5) α = 0.5; 6) α = 0.6; 7) α = 0.7; 8) α = 0.8; 9) α = 0.9

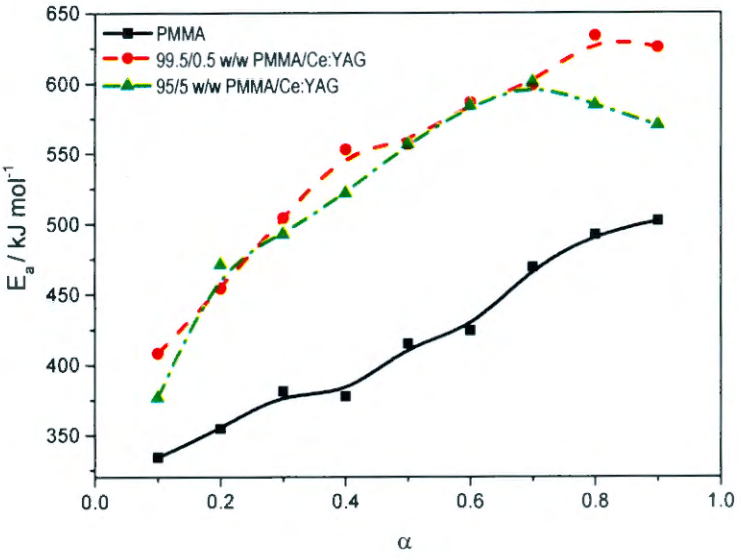

Figure 5.13 Activation energy vs. extent of degradation for PMMA and the PMMA/ Ce:YAG composites with 0.5 and 5 wt.% Ce:YAG

5.8 Luminescence properties

The photoluminescence excitation and emission spectra of PMMA and the PMMA/Ce:YAG composites are respectively presented in Figures 5.14 and 5.15. The excitation spectra of the PMMA/Ce:YAG eomposites monitored at 550 nm show a very broad band centered at 460 nm, and the emission spectra monitored at 450 nm show a band at 550 nm. Figure 4.16 shows the energy-level diagram of Ce^{3+}:YAG and its excitation (Ex) and emission (Em) processes [20]. A free Ce^{3+} ion with a $4f^1$ electronic configuration has two ground states, namely $^2F_{5/2}$ and $^2F_{7/2}$. When the electron is excited from the 4f level to the 5d state, the 5d electron of the excited $4f^0$ $5d^1$ configuration forms a ^2D term, which is split by spin-orbit coupling and the two lower energy levels of $^2D_{3/2}$ and $^2D_{5/2}$ states are formed [21,22]. The excitation band observed at 460 nm is attributed to $^2F_{5/2} \rightarrow {}^2D_{3/2}$, and the emission band can be attributed to $^2D_{3/2} \rightarrow {}^2F_{5/2}$. The luminescent intensity is related to the average distance between the luminescent centres [23]. The intensity of both the excitation and emission spectra increases with an increase in the amount of Ce:YAG in the sample, which is to be expected. The neat PMMA does not show any band in the investigated wavelength range because it is an amorphous material without luminescence centers.

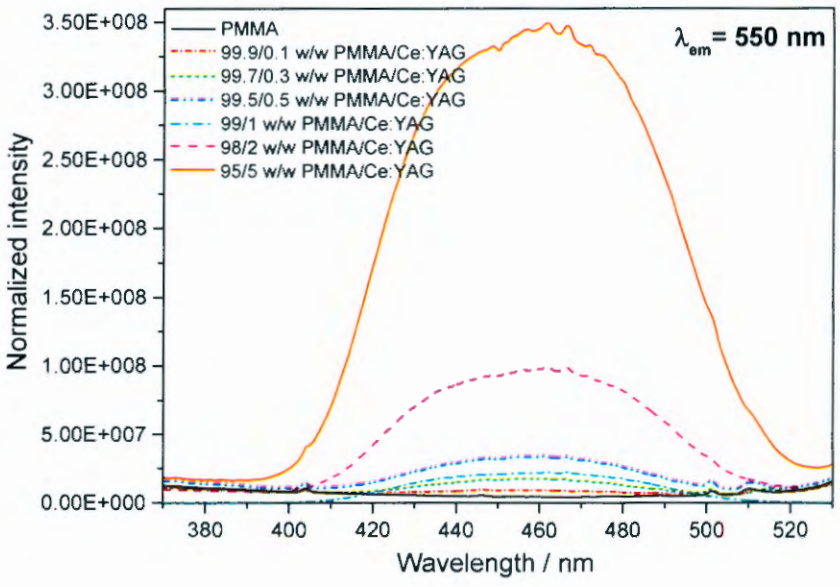

Figure 5.14 Excitation spectra of PMMA and PMMA/Ce:YAG composites

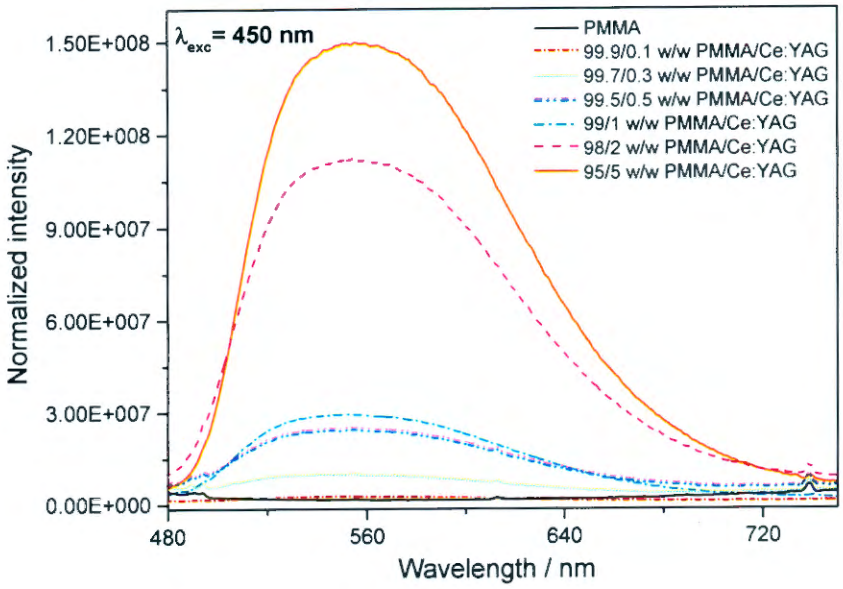

Figure 5.15 Emission spectra of PMMA and PMMA/Ce:YAG composites

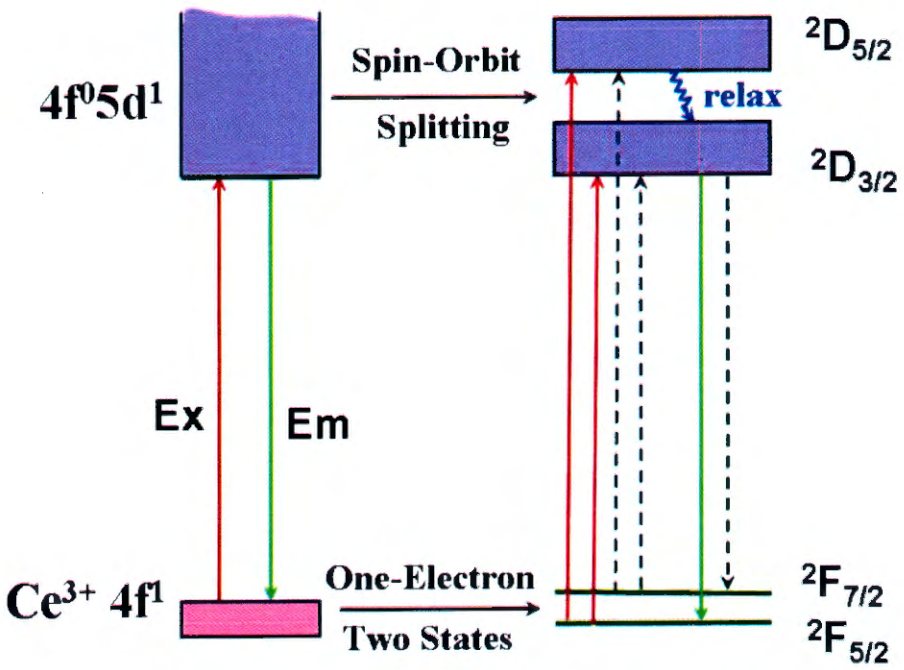

Figure 5.16 Energy-level diagram of Ce^{3+}:YAG and its excitation (EX) and emission (Em) process. The dashed lines denote the potential processes [18].

The maximum emission wavelength ($\lambda_{max = 550nm}$) reported in Figure 5.17 increases with increasing Ce:YAG loading up to 2 wt.% Ce:YAG, but it levels off for higher Ce:YAG contents in the sample. This shift is also referred to as the red shift. The red shift normally indicates that the lowest 5d electron has shifted to a higher energy level, and there is a change in the lattice parameter of the garnet phase and the crystal field around the Ce^{3+} ions [3,24,25]. The increase in Ce:YAG loading did not induce any shift in the excitation band, indicating that the red shift of the emission band does not come from any significant variations in the energy position of the 5d electronic states of the Ce^{3+} ions, both in terms of their population and type. The XRD analysis (Figure 5.1) showed no change in the cell parameter of the garnet phase when Ce:YAG was embedded in the polymer, and therefore the observed red shift in the emission band can be attributed to different environments around the Ce:YAG particles. Venkatapresad *et al.* [26] demonstrated that the emission bands of phosphors can be tuned by varying the optical properties of the matrix.

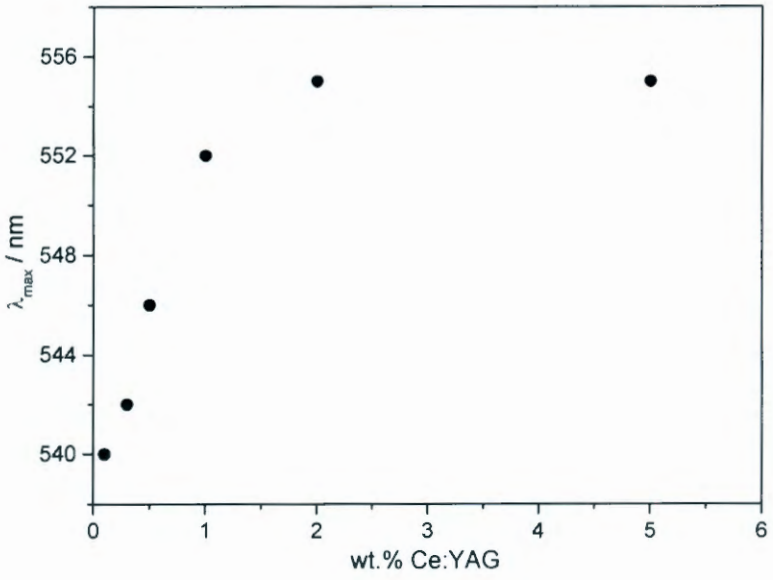

Figure 5.17 Position of the maximum of the emission band of the PMMA/Ce:YAG composites as function of Ce:YAG amount

The PMMA/Ce:YAG composites were assembled with blue light emitting diodes (LEDs) in order to test the composite efficiency and to verify its potential use as a white light source.

The emission spectra and the relative Commission Internationale de l'Eclairage (CIE) 1931 colour space of the resulting light are reported in Figures 5.18 to 5.20. The emission spectrum of the resulting light shows two peaks. The first sharp peak centered at 450 nm is attributed to the blue LEDs, and the second broad band centered at 550 nm is due to the emission of the composites (enlarged in Figure 5.19). The addition of and increase in Ce:YAG loading in the composites decreased the emission intensity at 450 nm, indicating the enhancement of the absorption ability for blue light [27].

The chromaticity coordinates, calculated from the emission spectra of the resulting lights, are reported in the CIE chromaticity diagram (Figure 5.20). The mixture of blue light and yellow light leads to the generation of white light. The CIE (x,y) coordinates of the lights, obtained when combining the blue LEDs with the composites loaded with up to 2 wt.% Ce:YAG, are located in the blue region, and for the composite containing 5 wt.% Ce:YAG they are located in the white region, which makes them more suitable for white LED devices. This behaviour can be attributed to a better balance of light between the emission from blue LEDs and the emissions from the phosphor, which is necessary to obtain white light with a proper colour rendering index and colour temperature [20]. The fairly well dispersed Ce:YAG particles can also provide better balance of light.

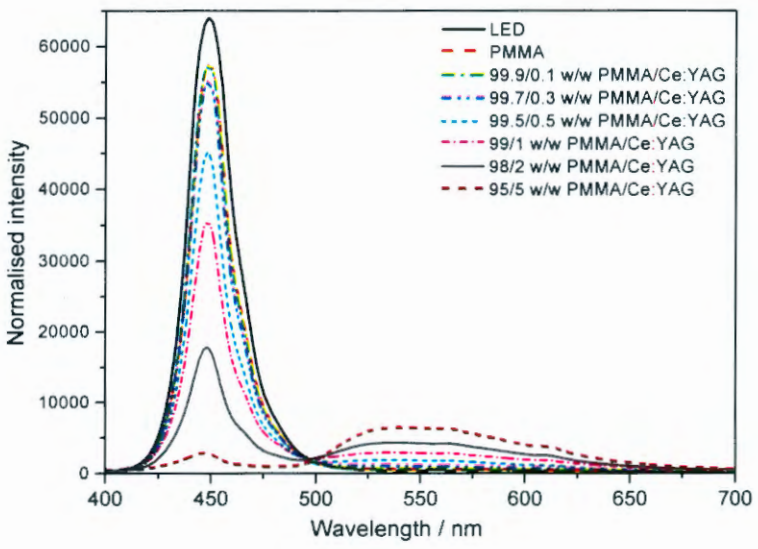

Figure 5.18 Emission spectra of PMMA and PMMA/Ce:YAG composites under blue LED

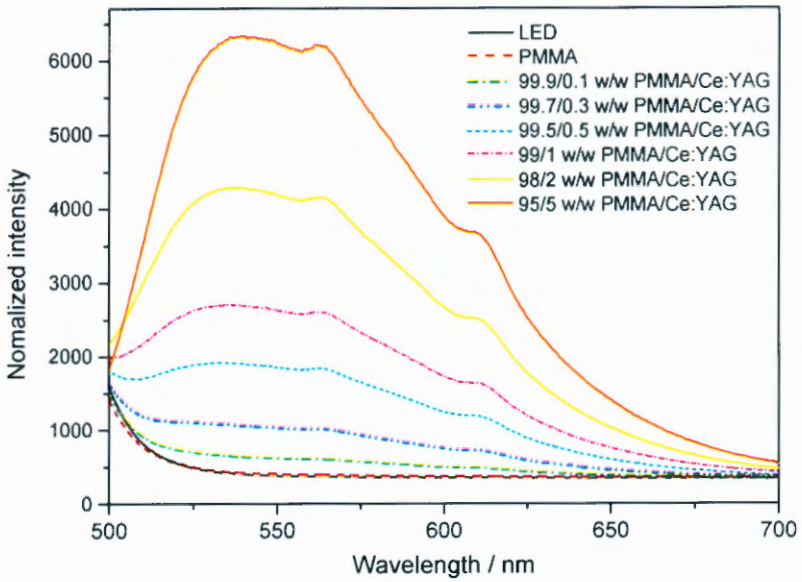

Figure 5.19 Emission spectra of PMMA and the PMMA/Ce:YAG composites under blue LED at 550 nm

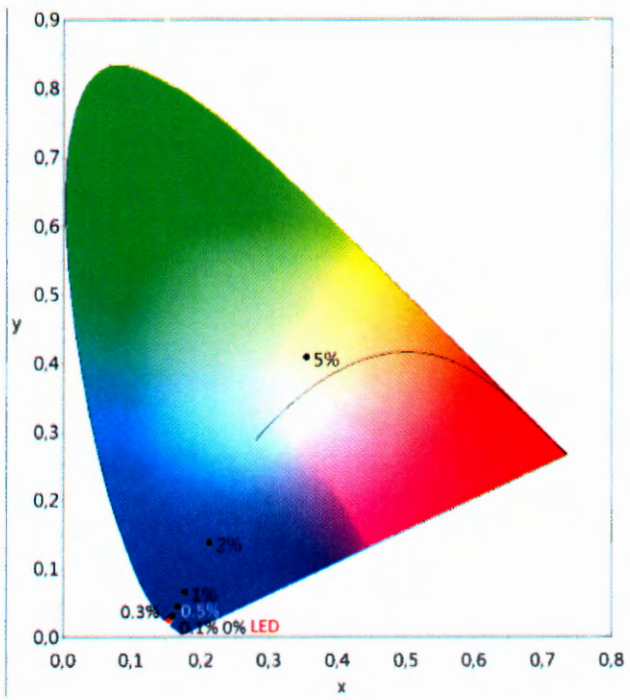

Figure 5.20 Chromaticity diagram depicting CIE colour co-ordinates for the PMMA/Ce:YAG composites

5.9 Conclusions

The purpose of the work reported in this chapter was to investigate the influence of the presence of different amounts of yttrium aluminium garnet doped with cerium (Ce:YAG) on the mechanical, thermomechanical properties, thermal degradation behaviour of PMMA as well as luminescence properties of PMMA/Ce:YAG composites. The PMMA/Ce:YAG composites maintained their transparency until 0.5 wt.% Ce:YAG loading, while higher filler loading (> 0.5 wt.%) resulted in a loss of transparency. The interaction between PMMA and Ce:YAG was through the electron donor-acceptor interaction between the carbonyl oxygen lone pair and the yttrium cation (Y^{3+}). The storage modulus, loss modulus and glass transition temperature of PMMA increased with the addition of, and increase in, Ce:YAG content as a result of the increased stiffness of the composites and immobilization of the polymer chains. The addition of Ce:YAG up to 0.5 wt.% had no effect on the impact strength of PMMA, while the samples containing more than 1 wt.% Ce:YAG showed an increase in impact strength. The increase impact strength was due to the fairly well dispersed and smaller Ce:YAG clusters which allowed the transfer of the applied stress between the polymer and the filler. The addition of Ce:YAG seemed to significantly increase the thermal stability of PMMA at 5 wt.% loading, probably due to fairly well dispersed Ce:YAG particles which formed more effective interaction with the filler so that the polymer and free radical chains were immobilized and/or the volatile degradation products were trapped through their interaction with the filler particles.The CIE (x,y) coordinates of the light obtained when combining the blue LEDs with the composites loaded with 5 wt.% are obtained in the white region, making them suitable for applications in white light emitting diodes.

5.10 References

1. H. Yang, L. Yuan, G. Zhu, H. Xu. Luminescent properties of YAG:Ce^{3+} phosphor powders prepared by hydrothermal-homogeneous precipitation method. Materials Letters 2009; 63:2271-2273.
DOI: 10.10/j.matlet. 2009.07.012

2. G. Xia, S. Zhou, J. Zhang, J. Xu. Structure and optical properties of YAG:Ce^{3+} by gel combustion method. Journal of Crystal Growth 2005; 279:357-362.
DOI: 10.1016/j.jcrysgro.2005.01.072

3 F. Yuan, H. Ryu. Ce-doped YAG phosphors prepared by co-precipitation and heterogeneous precipitation. Materials Science and Engineering: B 2004; 107:14-18.
DOI: 10.1016/j.mseb.2003.10.002

4. C.W. Won, H.H. Nersisyan, H.I. Won, J.W. Youn. Integrated chemical process for exothermic wave synthesis of high luminance YAG:Ce phosphors. Journal of Luminescence 2011; 131:2174-2180.
DOI: 10.1016/j.jlumin.2011.05.029

5. P. Rai, M.-K.Song, H.-M.Song, J.-H.Kim, Y.-S.Kim, I.-H.Lee, Y.-T.Yu. Synthesis, growth mechanism and photoluminescence of monodispersed cubic shape Ce doped YAG nanophosphor. Ceramics International 2012; 38:235-242.
DOI: 10.1016/j.ceramint.2011.06.057

6. H.P. Fu, R.Y. Hong, Y.J. Zhang, H.Z. Li, B. Xu, Y. Zheng, D.G. Wei. Preparation and properties investigation of PMMA/silica composites derived from silicic acid. Polymers for Advanced Technologies 2009; 20:84-91.
DOI: 10.1002/pat.1226

7. T.E. Motaung, A.S. Luyt, M.L. Saladino, D.C. Martino, E. Caponetti. Morphology, mechanical properties and thermal degradation kinetics of PMMA-zirconia nanocomposites prepared by melt compounding. eXPRESS Polymer Letters 2012; 6:871-881.
DOI: 10.3144/expresspolymlett.2012.93

8. G. Guerrica-Echevarria, J.I. Eguiazabal, J. Nazabal. Influence of filler on the mechanical response of an amorphous liquid-crystalline polymer. Journal of Applied Polymer Science 2003; 88:998-1003.
DOI: 10.1002/app.11759

9. N.A. El-Zaher, M.S. Melegy, O.W. Guirguis. Thermal and structural analyses of PMMA/TiO_2 nanoparticles composites. Natural Science 2014; 6:859-870.
DOI: 10.4236/ns.2014.611083

10. M.L. Saladino, A. Zanotto, D.C. Martino, A. Spinella, G. Nasillo, E. Caponetti. Ce:YAG nanoparticles embedded in a PMMA matrix: Preparation and characterization. Langmuir 2010; 26:13442-13449.
DOI: 10.1021/1a9042809

11. A. Zanotto, A. Spinella, G. Nasillo, E. Caponetti, A.S. Luyt. Macro-micro relationship in nanostructured functional composites. eXPRESS Polymer Letters 2012; 6:410-416.
DOI: 10.3144/expresspolymlett.2012.43

12. A.S. Luyt, M. Messori, P. Fabbri, J.P. Mofokeng, B. Taurino, T. Zanasi, F. Pilati. Polycarbonate reinforced with silica nanocomposites. Polymer Bulletin 2011; 66:991-1004.
DOI: 10.1007/s00289-010-0408-5

13. S.S. Musbah, V.J Radojevic, I. Radovic, P.S. Uskokovic, D.B. Stojanovic, M. Dramicanin, R. Aleksic. Preparation, characterization and mechanical properties of rare-earth-based nanocomposites. Journal of Mining and Metallurgy.2012; 48:309-318.
DOI: 10.2298/JMMB120508030M

14. L.E. Nielsen, R.F. Landel. Mechanical Properties of Polymers and Composites. Marcel Dekker, Inc.: New York (1994).
ISBN: 0 8247 8964 4

15. Y.-H. Hu, C.-Y.Chen, C.-C.Wang. Viscoelastic properties and thermal degradation kinetics of silica/PMMA nanocomposites. Polymer Degradation and Stability 2004; 84:545-553.
DOI: 10.1016/j.polymdegradstab.2004.02.001

16. S.R. Valandro, P.C. Lombardo, A.L. Poli, M.A. Horn Jr, M.G. Neumann, C.C.S. Cavalheiro. Thermal properties of poly(methyl methacrylate)/organomodified montmorillonite nanocomposites obtained by in situ photopolymerization. Materials Research 2014; 17:265-270.
DOI: 10.1590/S1516-14392013005000173

17. M.J. Assael, S. Botsios, K. Gialou, I.N. Metaxa. Thermal conductivity of polymethyl methacrylate (PMMA) and borosilicate crown glass BK7. International Journal of Thermophysics 2005; 26:1595-1605.
DOI: 10.1007/s10765-005-8106-5

18. Y.J.Y. Lee. HK. Lee, S.W. Hong, I.Y. Choi. Thermal degradation kinetics of iPP/Pd nanocomposite prepared by a drying process. Advances in Materials Physics and Chemistry 2012; 2:110-114.
DOI: 10.4236/ampc.2012.24B030

19. V.S. Aigbodion, S.B. Hassan, C.U. Atuanya. Kinetics of isothermal degradation studies by thermogravimetric data: Effect of orange peels ash on thermal properties of high density polyethylene. Journal of Materials Environment Science 2012; 3:1027-1036.

20. L. Chen L, C.C. Lin, C.W. Yeh, R.S. Liu. Light converting inorganic phosphors for white light-emitting diodes. Materials 2010; 3:2172-2195.
DOI: 10.3390/ma3032172

21. R.R. Jacobs, W.F. Krupke, M.J. Weber. Measurement of excited-state absorption loss for Ce^{3+} in $Y_3Al_5O_{12}$ and implications for tunable 5d→4f rare-earth lasers. Applied Physics Letters 1978; 33:410-412.
DOI: 10.1063/1.90395

22. Y. Dond, G. Zhou, J. Xu, G. Zhao, F. Su, L, Su, G. Zhang, D, Zhang, H. Li, J. Si. Luminescence studies of Ce:YAG using vacuum ultraviolet synchrotron radiation. Materials Research Bulletin 2006; 41:1959-1963.
DOI: 10.1016/j.materrsbull.2006.02.035

23. J.A. Capobianco, F. Vetrone, T. D'Alesio, G. Tessari, A. Speghini, M. Bettinelli. Optical spectroscopy of nanocrystalline cubic $Y_2O_3:Er^{3+}$ obtained by combustion synthesis. Physical Chemistry Chemical Physics 2000; 2:3203-3207.
DOI: 10.1039/B003031G

24. J. Zhong, W. Zhuang, X. Xing, R. Liu, Y. Li, Y. Liu, Y. Hu. Synthesis, crystal structure and photoluminescence properties of Ce^{3+}-doped $Ca_2LaZr_2Ga_3O_{12}$: New garnet green-emitting phosphors for white LEDs. The Journal of Physical Chemistry 2015; 119:5562-5569.
DOI: 10.1021/jp508409r

25. J. Wang, T. Han, T. Lang, M. Tu, L. Peng. Synthesis and photoluminescence properties of tunable green orange cerium-doped terbium-lutetium aluminum garnet. International Journal of Electrochemical Science 2015; 10:2554-2563.

26. S.V. Bhat, A. Govindaraj, C.N.R. Rao. Tuning the emission bands of nanophosphors through the refractive index of the medium. Chemical Physics Letters 2006; 422:323-327. DOI: 10.1016/j.cplett.2006.02.076

27. H. Shi, C. Zhu, J. Huang, J. Chen, D. Chen, W. Wang, F. Wang, Y. Cao, X. Yuan. Luminescence properties of YAG:Ce, Gd phosphors synthesized under vacuum condition and their white LED performances. Optical Materials Express 2014; 4: 1-7. DOI: 10.1364/OME.4.000649

Chapter 6: Morphology, mechanical, thermal and luminescence properties of polycarbonate (PC)/yttrium aluminium garnet doped with cerium (Ce:YAG) composites prepared by melt compounding

6.1 X-ray diffraction (XRD)

The XRD pattern of Ce:YAG and the PC/Ce:YAG composites are reported in Figure 6.1. The diffraction pattern of Ce:YAG shows a single YAG phase with sharp peaks that are related to its crystalline structure, typical of the garnet phase [1], while PC shows a broad diffraction band around 17° and two weak bands of lower intensity that have been reported in other studies [2,3]. The diffraction pattern of the composite loaded with 0.1 wt.% Ce:YAG is similar to the pattern of neat PC due to the small amount of filler. However, for 0.3 and 0.5 wt.% Ce:YAG loading the diffraction patterns of the composites show a low intensity diffraction peak of the garnet phase at 33°, and its intensity increases with increasing Ce:YAG loading. All the peaks related to the garnet phase are observed in the samples loaded with 1, 2 and 5 wt.% Ce:YAG, and their positions did not shift with respect to those of the powder, confirming that no structural modification occurred when the filler was embedded in the polymer, and that there was no change in the cell parameters of the garnet phase.

6.2 Transmission electron microscopy (TEM)

Figure 6.2 shows the TEM images of the PC/Ce:YAG composites filled with different amounts of Ce:YAG. The TEM images of the PC/Ce:YAG composite containing 0.5 wt.% Ce:YAG (Figure 6.2(a,b)) show isolated Ce:YAG particles in the polymer matrix. This is because of the small amount of filler in the composite which was scarcely detected in the XRD for the samples containing less than 1 wt.% filler. This composite was also less transparent than those containing smaller amounts of filler (Figure 6.3). Figure 6.2(c,d) shows a large Ce:YAG agglomerate which is the reason for the clear loss in transparancy observed in Figure 6.3.

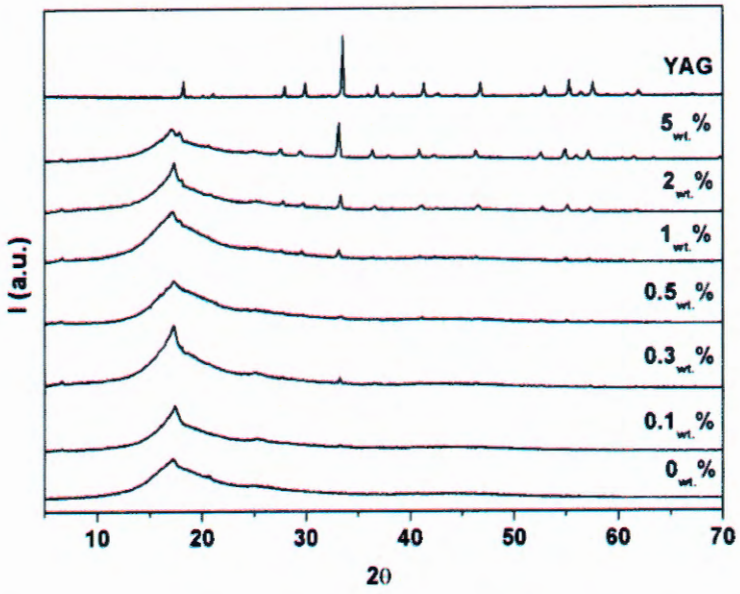

Figure 6.1 XRD patterns of Ce:YAG, PC and the PC/Ce:YAG composites

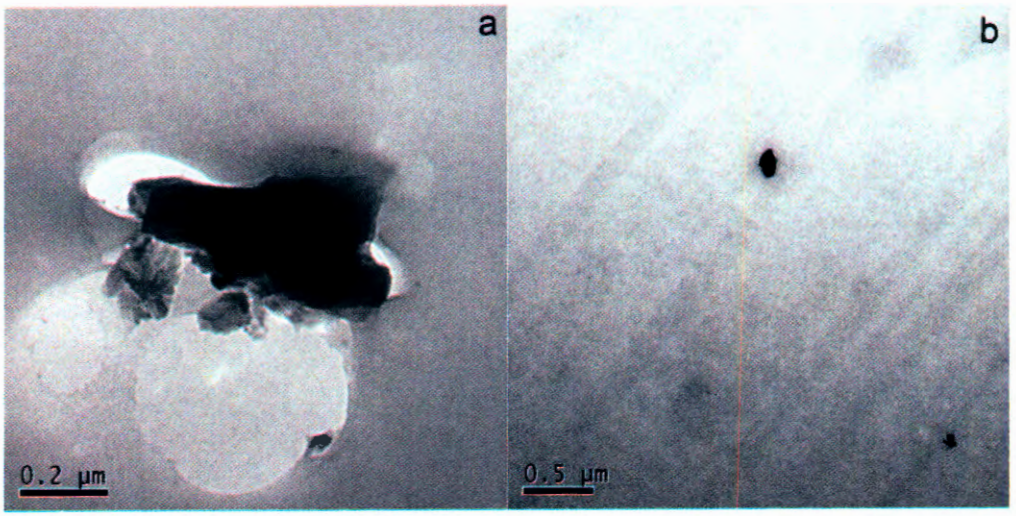

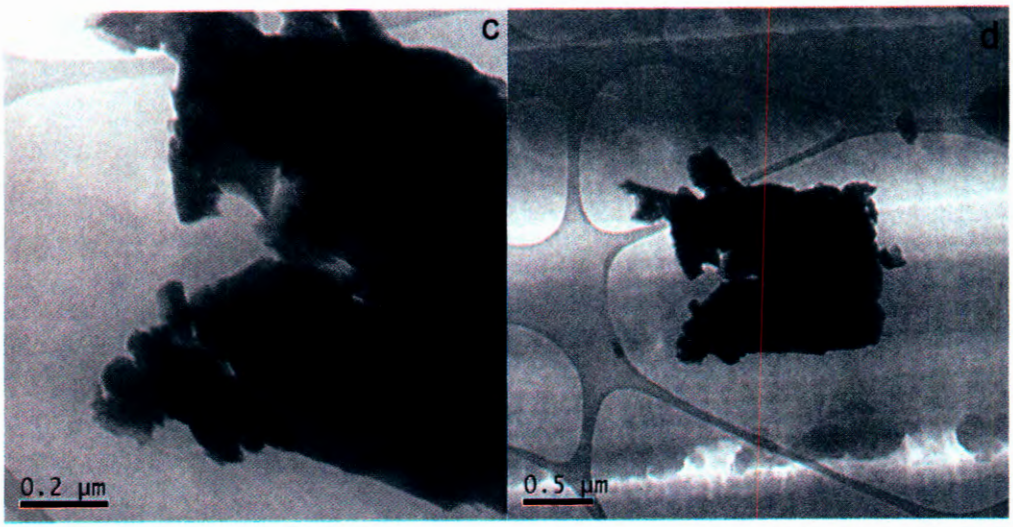

Figure 6.2 TEM images of PC/Ce:YAG composites with 0.5 (a,b) and 5 (c,d) wt.% Ce:YAG

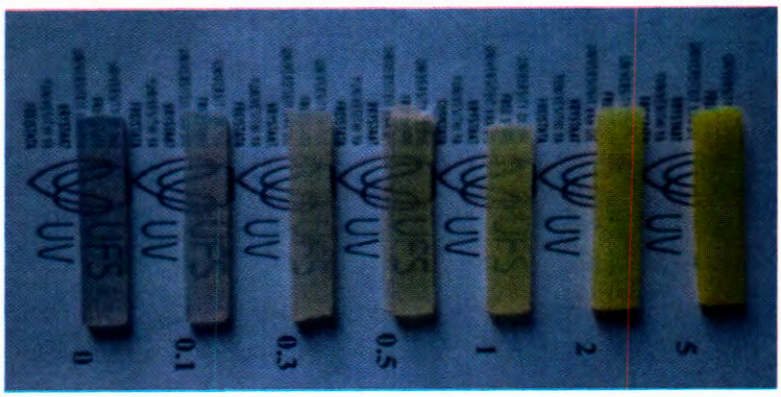

Figure 6.3 Picture of PC and the PC/Ce:YAG composites to illustrate their transparency

6.3 ^{13}C cross-polarization magic-angle spinning nuclear magnetic resonance (^{13}C {^{1}H} CP-MAS-NMR) spectroscopy

$^{13}C\{^{1}H\}$CP-MAS-NMR measurements were performed in order to investigate the interaction between PC and the Ce:YAG particles. The NMR spectra of PC and the PC/Ce:YAG composites loaded with 0.5 and 5 wt.% Ce:YAG are reported in Figure 6.4 together with the assignment of the ^{13}C chemical shifts of the polymer. The spectra show five resonances: peak 1 at 149 ppm is related to the quaternary carbons of the aromatic rings and to the carbonyl carbon, peak 2 at 127 ppm to the aromatic carbon meta to the oxygen, peak 3 at 120 ppm to the aromatic carbon ortho

to the oxygen, peak 4 at 42 ppm to the quaternary carbon bonded to the methyl groups, and peak 5 at 31 ppm to the methyl carbons [4]. In the presence of Ce:YAG there is no change in the chemical shift and in the signal shape of PC, which shows that there was no chemical interaction between the polymer and the filler so that only physical interactions were possible.

The proton and carbon spin lattice relaxation times in the rotating frame, $T_{1\rho}(H)$ and $T_{1\rho}(C)$, were determined through solid-state NMR measurements in order to detect dynamic changes in the polymer induced by the presence of the Ce:YAG. The $T_{1\rho}$ is sensitive to molecular motions in the kHz region and it is inversely proportional to the spectral density of motion. These motions reflect the dynamic behaviour of a polymer chain in a range of a few nanometers. The relaxation time values for PC and PC/Ce:YAG composites prepared with 0.5 and 5 wt.% of Ce:YAG were obtained from each peak in the ^{13}C spectra and reported in Table 6.1. The $T_{1\rho}(H)$ values of the composites containing 0.5 and 5 wt.% Ce:YAG are of the same order of magnitude and slightly higher than that of pure PC, which indicates that the material can be considered homogenous on a nanometer scale. The presence of and an increase in Ce:YAG loading did not have any influence on these values, thus the filler did not immobilize the polymer chains, probably due to the poor dispersion of the filler in the polymer.

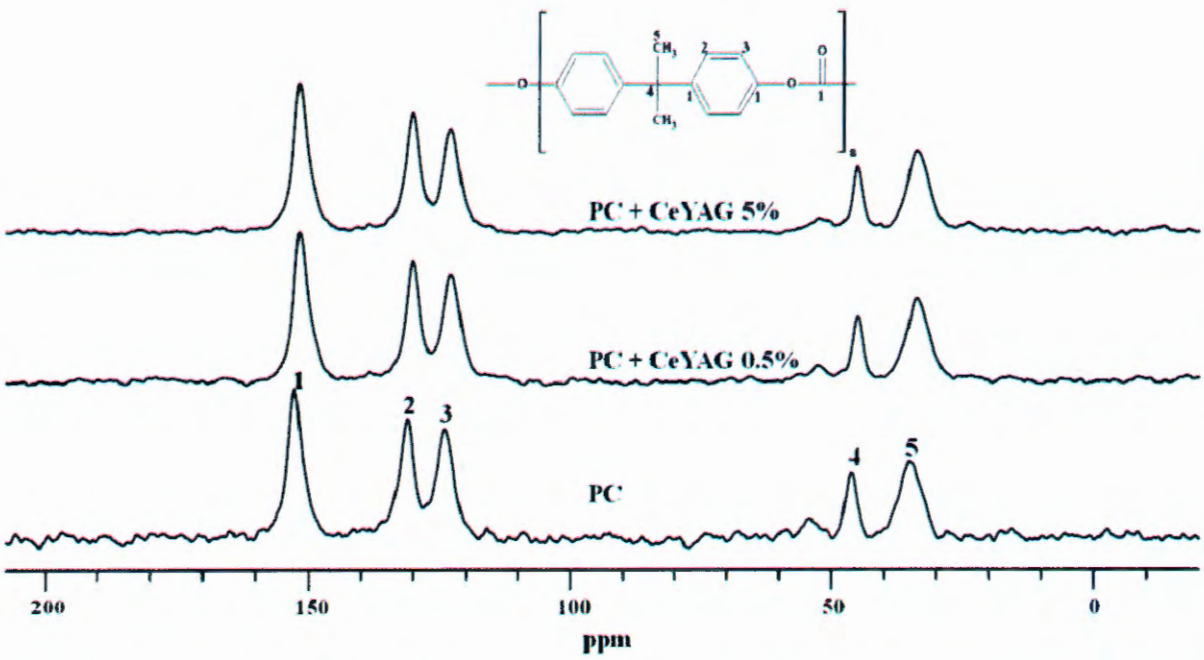

Figure 6.4 $^{13}C\{^1H\}$CP-MAS NMR spectra of PC and of PC/Ce:YAG composites with 0.5 and 5 wt.% Ce:YAG

The $T_{1\rho}(C)$ values for the different peaks in Table 6.1 vary randomly. The values for carbons 1 and 5, that are related to the quaternary carbons of the aromatic rings and to the methyl carbons, were strongly affected by the presence of Ce:YAG at 0.5 wt.% loading. For these signals, a decrease in $T_{1\rho}(C)$ values was observed, indicating that a minor contribution to the $T_{1\rho}$ relaxation arises from each molecular group that modulates the $^{1}H-^{13}C$ dipolar coupling. These variations can account for specific interactions through an electron donor-acceptor interaction between the carbonyl oxygen lone pair on the polymer chains and the yttrium cation (Y^{3+}) on the surface of Ce:YAG. This interaction was also observed between the carbonyl oxygen lone pair of PMMA and the yttrium cation (Chapter 5). The $T_{1\rho}(C)$ values of carbons 1 and 5 for the composite loaded with 5 wt.% Ce:YAG are similar to those of pristine PC. This behaviour could result from the balance between the packing of the aromatic rings in the polymer and a local disordering effect due to the electron donor-acceptor interaction.

Table 6.1 Relaxation time values for all the peaks in the ^{13}C spectra of PC and the PC/Ce:YAG composites loaded with 0.5 and 5 wt.% Ce:YAG

Carbon		$T_{1\rho}(H)$ / ms			$T_{1\rho}(C)$ / ms		
ppm		0 %	0.5%	5%	0 %	0.5%	5%
1	149	4.9 ± 0.2	5.3 ± 0.3	5.3 ± 0.3	95.3 ± 0.3	48.4 ± 0.4	100.1 ± 0.2
2	127	4.9 ± 0.2	5.6 ± 0.1	4.6 ± 0.3	10.9 ± 0.2	17.1 ± 0.2	13.0 ± 0.2
3	120	4.4 ± 0.2	4.8 ± 0.2	4.2 ± 0.2	11.2 ± 0.2	9.9 ± 0.2	11.4 ± 0.2
4	42	3.9 ± 0.2	5.2 ± 0.2	6.4 ± 0.3	28.4 ± 0.3	30.6 ± 0.2	32.2 ± 0.2
5	31	6.6 ± 0.3	5.0 ± 0.3	4.8 ± 0.2	30.5 ± 0.2	18.4 ± 0.2	27.8± 0.2

6.4 Dynamic mechanical analysis (DMA)

Figure 6.5 shows the storage modulus curves of PC and the PC/Ce:YAG composites as a function of temperature, while Table 6.2 reports the E' values at 100 and 170 °C. Below the glass transition temperature the storage modulus of PC increases with the addition Ce:YAG. However, the extent of this increase is not proportional to the amount of Ce:YAG particles in the polymer (Table 6.2). This is probably because the hard, brittle polymer and the Ce:YAG particles have very similar stiffness values in this temperature range. Above the glass transition

temperature the storage modulus was generally higher for the PC/Ce:YAG composites, but there was no clear trend in the effect of the filler on the E' values at higher loadings (Table 6.2). The maximum increase in storage modulus was observed at 0.1 wt.% Ce:YAG loading, which is probably due to the reinforcing effect of the good dispersion and small sizes of the Ce:YAG partieles, as was discussed in section 6.2. The storage modulus of the samples containing 0.3 and 0.5 wt.% Ce:YAG was lower, and at 0.5 wt.% Ce:YAG the storage modulus was almost the same as that of pure PC. At the highest filler loadings (2 and 5 wt.%) there was no clear trend on the influence of the filler on the E' values. It is therefore difficult to give a specific description and explanation of the influence of Ce:YAG on the storage modulus of PC, and a complex set of factors (e.g., weaker interaction between the polymer and the filler as a result of the presence of filler agglomerates, sample inhomogeneity) may have contributed to the observed results. Suin *et al.* [5] observed a direct increase in storage modulus of PC throughout the investigated temperature with an increase in clay loading. They attributed this to the reinforcing effect imparted by the high aspect ratio of the clay platelets which caused a greater degree of stress transfer at the interface. However, Motaung *et al.* observed a decrease in storage modulus of PC with the addition of titania [6] and zirconia [7] nanoparticles at 1 and 2 wt.% loadings, which they attributed to a plasticizing effect of the nanoparticles on the polymer matrix.

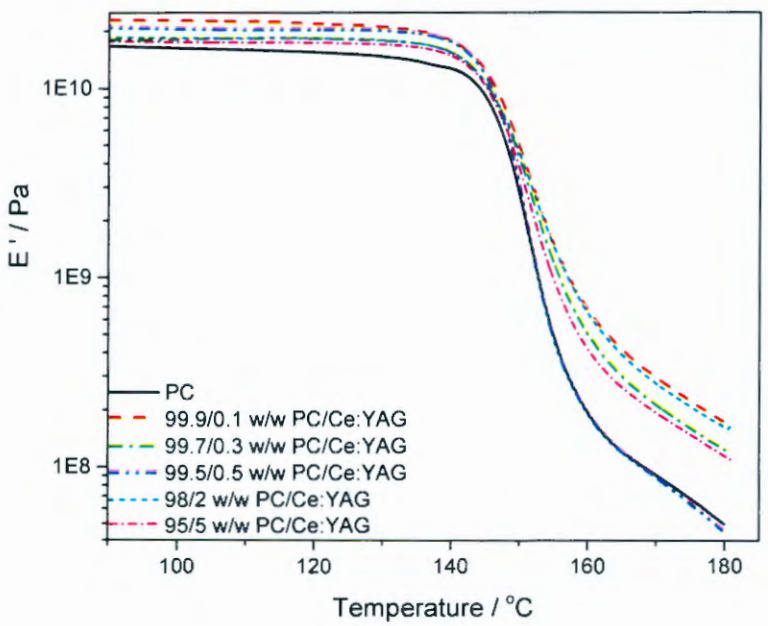

Figure 6.5 Storage modulus curves of PC and the PC/Ce:YAG composites

Table 6.2 DMA results of PC and the PC/Ce:YAG composites

Sample	10^{-10} E' / Pa at 100 °C	10^{-8} E' / Pa at 170 °C	T_g / °C from E" curves	T_g / °C from tan δ curves
PC	1.6 ± 0.1	0.9 ± 0.0	147.1	154.1
99.9/0.1 w/w PC/Ce:YAG	2.2 ± 0.0	2.8 ± 0.1	146.9	154.1
99.7/0.3 w/w PC/Ce:YAG	1.8 ± 0.0	1.9 ± 0.3	147.2	154.5
99.5/0.5 w/w PC/Ce:YAG	2.0 ± 0.1	0.8 ± 0.0	147.0	154.6
98/2 w/w PC/Ce:YAG	1.7 ± 0.3	2.7 ± 0.2	147.4	154.7
95/5 w/w PC/Ce:YAG	1.7 ± 0.0	1.6 ± 0.0	146.1	154.1

The loss modulus and tan δ curves of PC and the PC/Ce:YAG composites are shown in Figures 6.6 and 6.7, and the glass transition temperature values are reported in Table 6.2. The loss modulus curves show the same inconsistencies as was observed and discussed for the storage modulus. The addition of Ce:YAG had no influence on the glass transition temperature of PC (Table 6.2), which indicates that the filler had little effect on the polymer chain mobility, something which has also been observed from the NMR results. It is usually expected that in particulate filled polymers, the addition of rigid filler to the polymer matrix should restrict the movement of the polymer chains, thus leading to a reduction in the damping and a shift of the glass transition to higher temperatures. Figure 6.7 shows a significant reduction in the damping after the addition of certain amounts of Ce:YAG, but there was no correlation between the amount of damping and the amount of Ce:YAG mixed into PC. The absence of a change in the glass transition temperature, and the inconsistent change in the amount of damping, confirm that the dynamic mechanical behaviour of the PC/Ce:YAG composites was influenced by a complex set of factors, and that the interaction between PC and Ce:YAG was fairly weak, because a strong interaction would have dominated all the other possible contributing factors and given rise to consistently higher storage moduli and glass transition temperatures, and consistently lower damping.

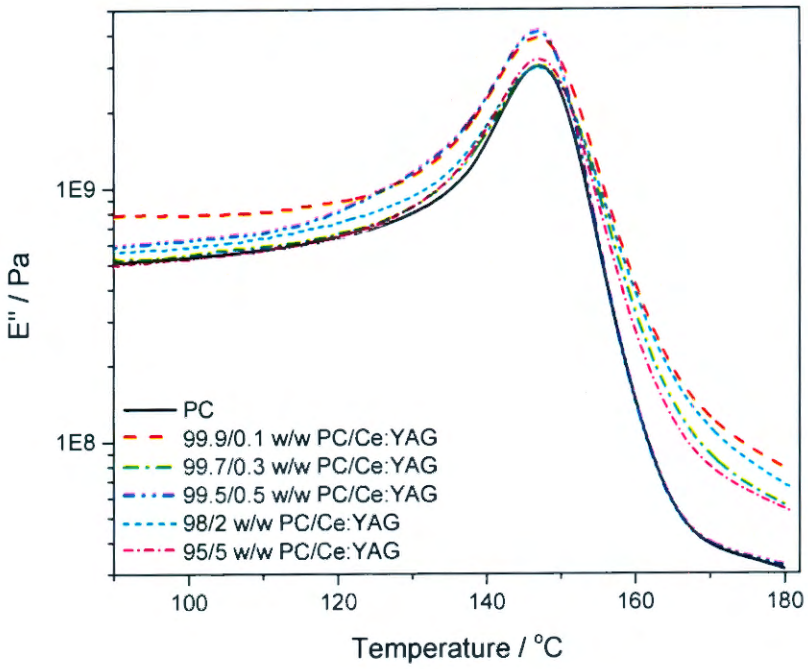

Figure 6.6 Loss modulus curves of PC and the PC/Ce:YAG composites

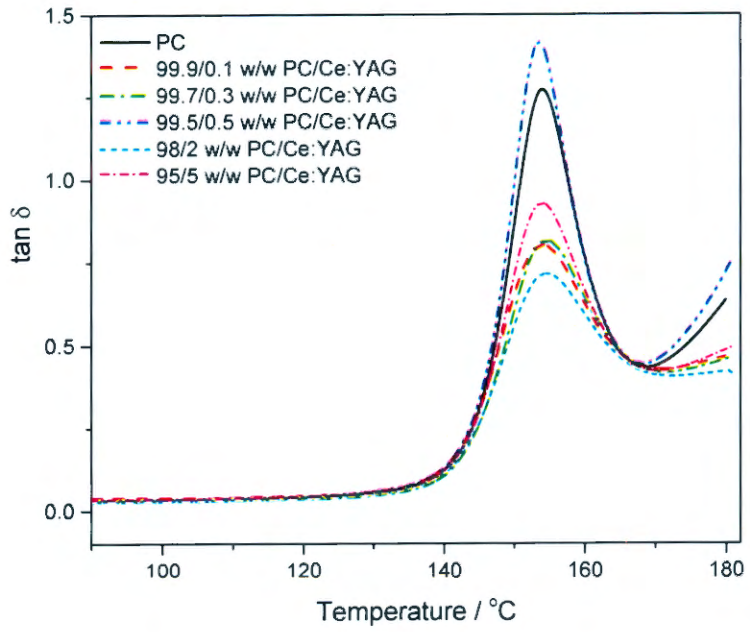

Figure 6.7 Tan δ curves of PC and the PC/Ce:YAG composites

6.5 Thermogravimetric analysis (TGA)

Figure 6.8 shows the TGA curves of PC and the PC/Ce:YAG composites at different Ce:YAG loadings, and some of the temperatures are summarised in Table 6.3. PC shows no mass loss up to 420 °C, and its decomposition occurs in a single step between 420 and 530 °C. PC leaves about 21.2% residue at 650 °C, and this has also been observed in a number of studies both in air and nitrogen atmospheres [8-10]. TGA measures mass loss, and interaction between the volatile degradation products and the filler particles would delay the volatilization of the degradation products, which would increase the temperature at which mass loss occurs. Normally at high temperatures, the long chain backbone of a polymer undergoes molecular scission and forms free radicals, which react with each other and with other polymer chains and release volatile products causing a mass loss of the polymer [11]. In our case, the free radicals and volatile degradation products did not seem to interact very strongly with the Ce:YAG particles, because little difference was observed between the TGA curves of the different samples. Other authors reported both an increase [12,13] and a decrease [14-16] in thermal stability of PC after the addition of nanoparticles. The decrease in thermal stability was related to the catalytic effect of the nanoparticles, the particle dispersion in the polymer matrix, and the preparation conditions.

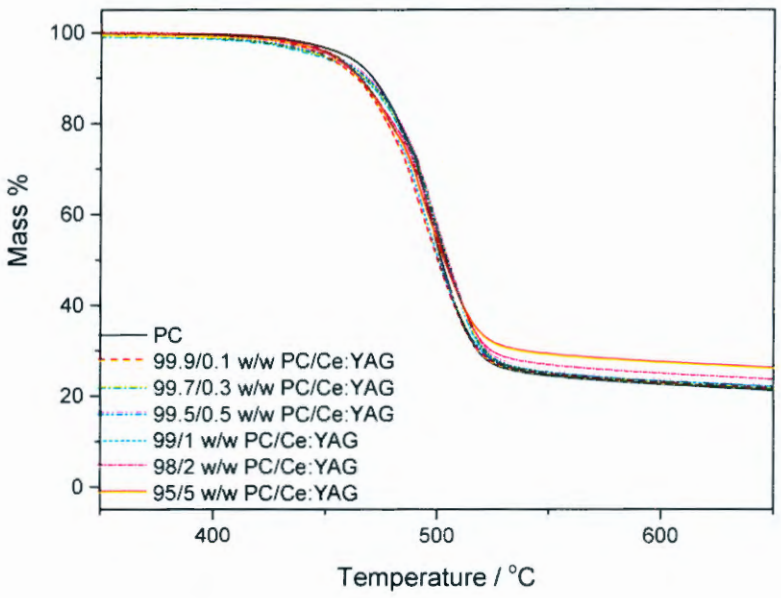

Figure 6.8 TGA curves of PC and the PC/Ce:YAG composites

Table 6.3 TGA results for all the investigated samples

Sample	T_{30} / °C	T_{max} / °C	% Residue
PC	491.6	496.3	21.2
99.9/0.1 w/w PC/Ce:YAG	486.2	494.4	21.4
99.7/0.3 w/w PC/Ce:YAG	491.2	501.8	21.6
99.5/0.5 w/w PC/Ce:YAG	492.1	502.4	21.9
99/1 w/w PC/Ce:YAG	488.3	495.7	22.4
98/2 w/w PC/Ce:YAG	489.8	501.6	23.7
95/5 w/w PC/Ce:YAG	488.4	496.2	26.5

The amounts of residue observed at 650 °C for PC and all the composites are summarized in Table 6.3. The PC/Ce:YAG composites generally left more residue than the neat PC. The differences between the residues left by the composites and that left by neat PC correspond well with the amounts of Ce:YAG initially mixed into the samples, indicating that the dispersion of the Ce:YAG particles was fairly homogenous in the composites.

6.6 Thermal degradation kinetics

In order to get a better understanding of the degradation process and the effect of Ce:YAG loading on the thermal stability of PC, the activation energy (E_a) for mass loss was determined for the degradation of PC and the PC/Ce:YAG composites filled with 0.5 and 5 wt.% Ce:YAG. The activation energy is the amount of energy that is required to initiate the thermal degradation process, and its values are determined from the slope of the isoconversional plots of ln β versus 1/T shown in Figures 6.9 to 6.11 taken at heating rates of 3, 5, 7 and 9 °C min^{-1}. The relationship between the activation energies and the extent of mass loss is shown in Figure 6.12. The activation energy increased with an increase in extent of mass loss for all the investigated samples. We observed the same behaviour for the PMMA/MCM-41 and PMMA/Ce:YAG composites, and it was also observed by other authors [17-19]. This behaviour is generally explained as changes in the degradation mechanism with an increase in the extent of mass loss. Dong *et al.* [20] investigated PC-MgO nanocomposites and they attributed the increase in the

activation energy of degradation with an increase in the extent of mass loss to the formation of a stable char which protects the polymer from further degradation.

Figure 6.12 shows that the composites have much lower activation energies than the neat PC. The activation energy is the minimum energy required to initiate the thermal degradation process, and it is related to the temperature dependence of the rate of degradation. The lower activation energy values therefore indicate that less energy was required to initiate the degradation process, and that the degradation rates of the composites were less dependent on temperature. Dong *et al.* [20] observed that the initial activation energy values of the PC-MgO nanocomposites were lower than those of the neat PC. They attributed these observations to the catalytic effect the MgO nanoparticles have on the degradation process of PC. The addition of Ce:YAG in our case may have had a similar catalytic effect on the degradation of PC. An increase in the activation energy values of similar composites was observed in a number of studies [21-24], and these were attributed to the particles acting as physical barriers, both to retard the thermal decomposition of the polymer and to prevent the transport of volatile degradation products out of the composites, both of which would require more energy to initiate the thermal degradation process.

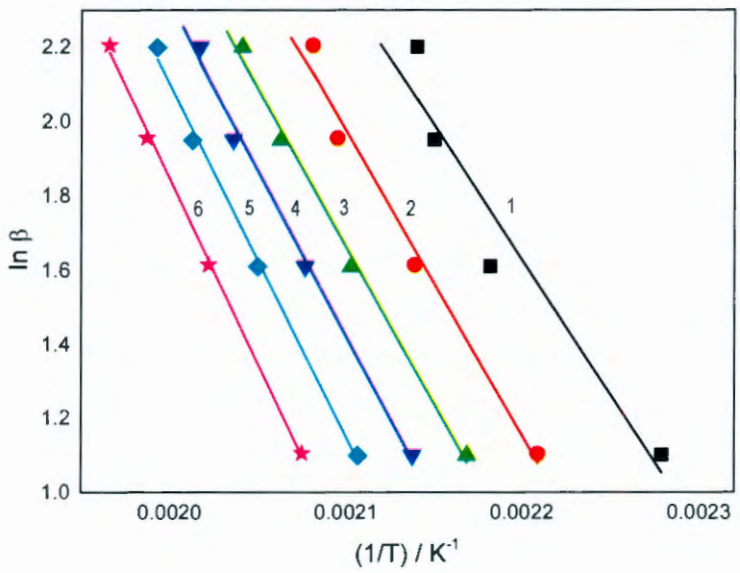

Figure 6.9 Ozawa–Flynn-Wall plots derived from the PC mass loss curves for the following degrees of conversion: 1) α = 0.1; 2) α = 0.2; 3) α = 0.3; 4) α = 0.4; 5) α = 0.5; 6) α = 0.6

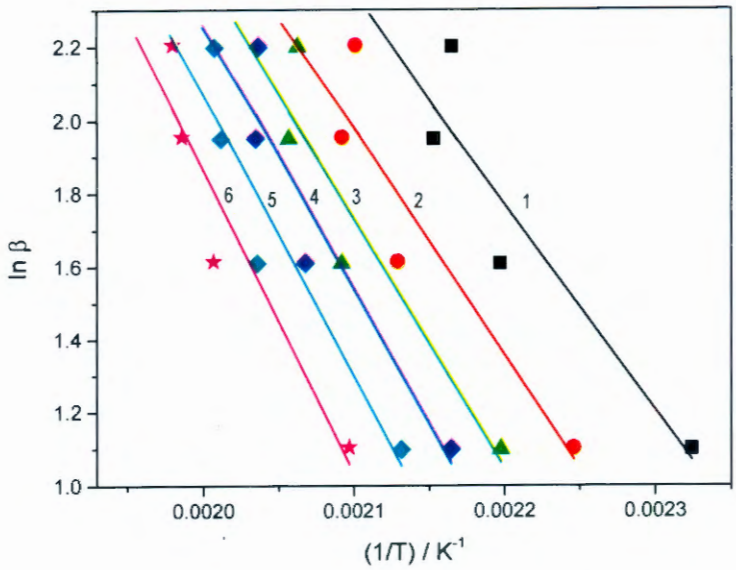

Figure 6.10 Ozawa–Flynn-Wall plots derived from the 99.5/0.5 w/w PC/Ce:YAG mass loss curves for the following degrees of conversion: 1) α = 0.1; 2) α = 0.2; 3) α = 0.3; 4) α = 0.4; 5) α = 0.5; 6) α = 0.6

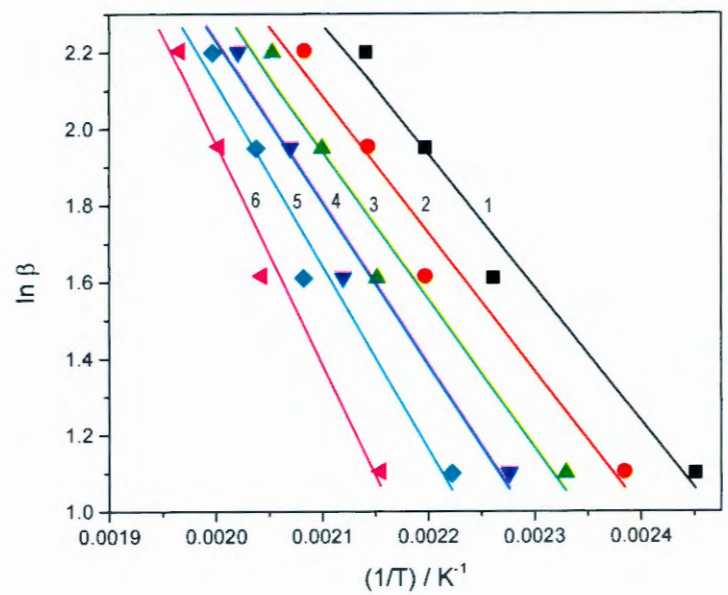

Figure 6.11 Ozawa–Flynn-Wall plots derived from the 95/5 w/w PC/Ce:YAG mass loss curves for the following degrees of conversion: 1) α = 0.1; 2) α = 0.2; 3) α = 0.3; 4) α = 0.4; 5) α = 0.5; 6) α = 0.6

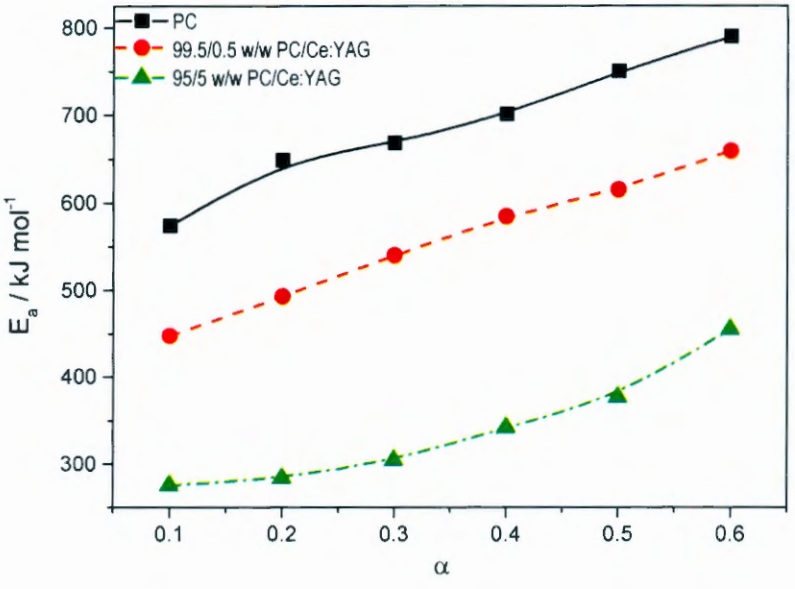

Figure 6.12 Activation energy vs. extent of degradation for PC and the PC/ Ce:YAG composites with 0.5 and 5 wt.% Ce:YAG

6.7 Luminescence properties

The excitation and emission spectra of PC and the PC/Ce:YAG composites measured at room temperature are reported in Figures 6.13 and 6.14. The energy-level diagram of Ce^{3+}:YAG, showing its excitation (Ex) and emission (Em), was shown and discussed in Chapter 5. The excitation spectra of the PC/Ce:YAG composites show a broad band centered at 460 nm, which is assigned to the $^2F_{5/2} \rightarrow {}^2D_{5/2}$ electronic transition, while the emission spectra show a band centered at 550 nm associated with the $^2D_{5/2} \rightarrow {}^2F_{5/2}$ transitions of Ce^{3+}. The intensity of both the excitation and emission spectra increased with increasing Ce:YAG content, as expected due to more Ce:YAG in the sample.

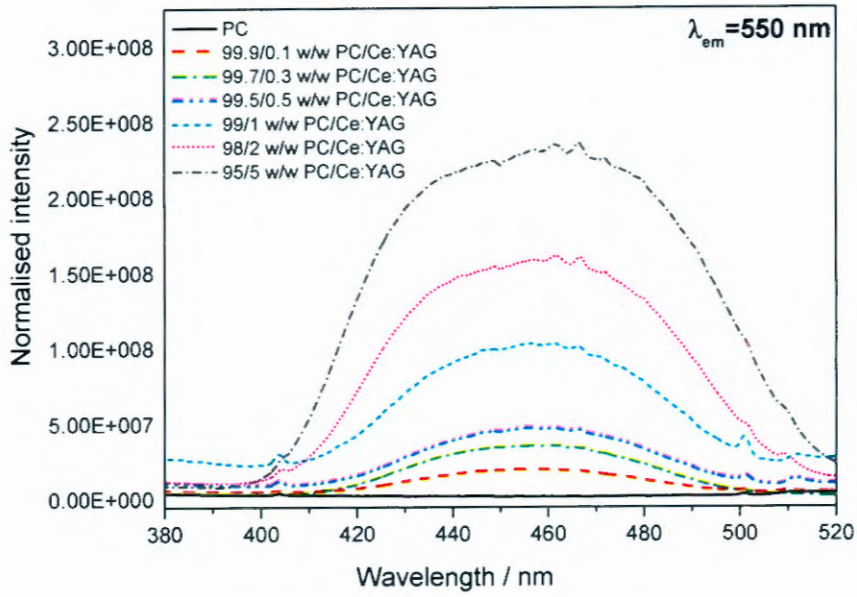

Figure 6.13 Excitation spectra of PC and PC/Ce:YAG composites

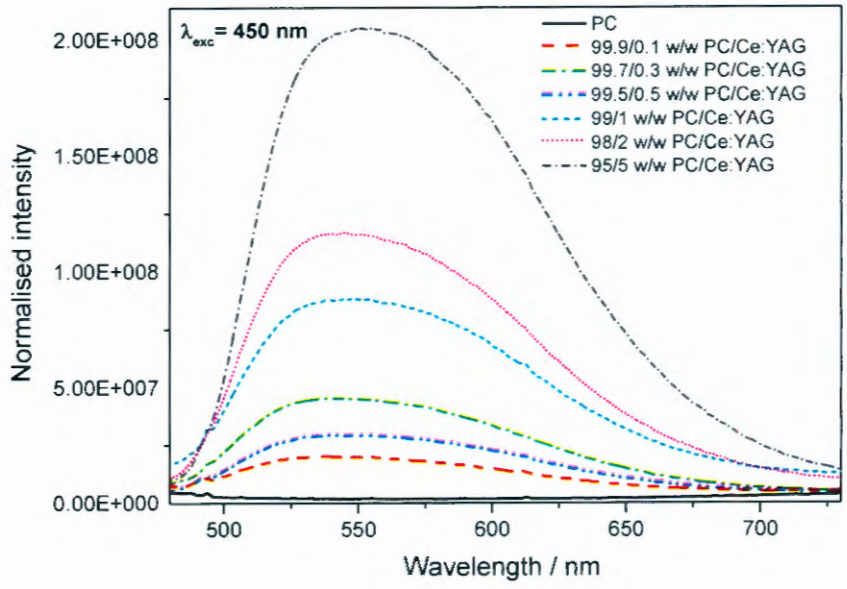

Figure 6.14 Emission spectra of PC and PC/Ce:YAG composites

Figure 6.15 shows the position of the maximum emission band of the PC/Ce:YAG composites. The increase in Ce:YAG loading resulted in a significantly shift of the maximum emission band to longer wavelengths and a red shift of 14 nm was observed. The XRD pattern of

the composites (Figure 6.1) illustrated that the presence of Ce:YAG in PMMA had no influence on the peak positions of the garnet phase, indicating that the lattice parameter of YAG was not influenced by the presence of the polymer. The observed red shift can therefore not be attributed to any change in the lattice parameter of the garnet phase. It is possible that the presence of the polymer on the surface changed the environment around the Ce:YAG as a result of the electron donor-acceptor interaction between the carbonyl oxygen lone pair of PC and the yttrium cation (Y^{3+}) on the surface of Ce:YAG (as observed from the NMR results), thus causing the observed shift. Chen *et al.* [25] suggested that the red shift in the spectrum has a significant influence on the luminescent properties of white LED. A blue shift in the photoluminescence (PL) spectrum was observed in a PMMA/Ce:YAG composite prepared by *in situ* polymerization of a mixture of methyl methacrylate (MMA) and 2-methacrylic acid (MAA) monomers [26]. However, the PMMA/Ce:YAG composites prepared by melt mixing (Chapter 5) also showed a red shift in the spectrum.

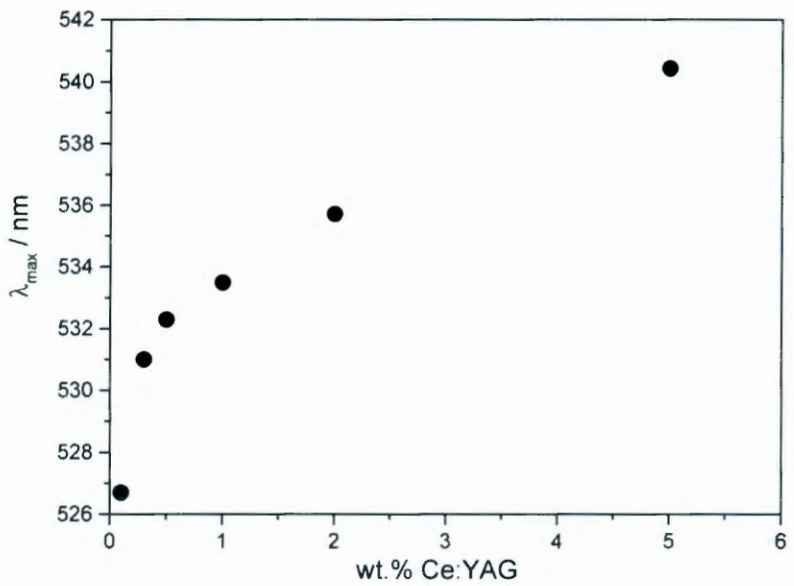

Figure 6.15 Position of the maximum emission band of the PC/Ce:YAG composites

The emission spectra of the resulting light obtained by combining the PC/Ce:YAG composites with a blue LED and the relative CIE 1931 colour space are reported in Figures 6.16 to 6.18. The emission spectrum of the resulting light consists of two bands: the first sharp band

centered at 450 nm is due to the blue LED, and the second broad band centered at 550 nm is due to the emission of the composite (enlarged in Figure 6.17). The intensity of the emission peak at 450 nm decreased, while the one at 550 nm increased with an increase in the Ce:YAG loading. The decrease in the emission peak indicates an enhancement in the absorption ability for blue light.

The chromaticity coordinates calculated from the emission spectra of the resulting lights are reported in the Commission Internationale de l'Eclairage (CIE) chromaticity diagram (Figure 6.18). The CIE (x,y) coordinates of the lights obtained by combining the blue LED, with composites loaded with up to 1 wt.% Ce:YAG, are located in the blue region, while that of the composite loaded with 2 wt.% Ce:YAG is located in the white region. The location of the composite in the white region can be attributed to a better balance of light between the emission from the blue LEDs and the emissions from the phosphor which is necessary to obtain white light with a proper colour rendering index and colour temperature. This indicates that the composite loaded with 2 wt.% Ce:YAG are suitable for white LED devices. However, the CIE coordinates of the lights obtained by combining the blue LED with the composite loaded with 5 wt.% is located in the yellow region.

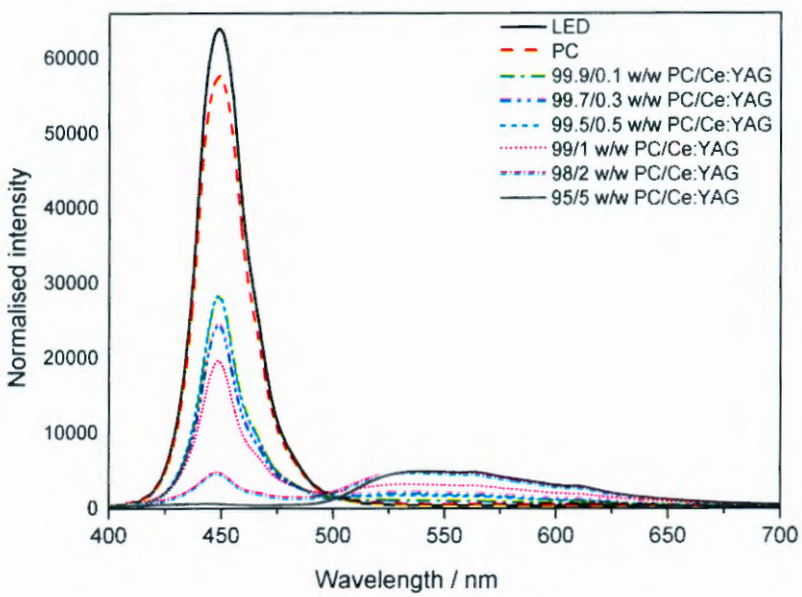

Figure 6.16 Excitation and emission spectra of PC and PC/Ce:YAG composites obtained under blue light

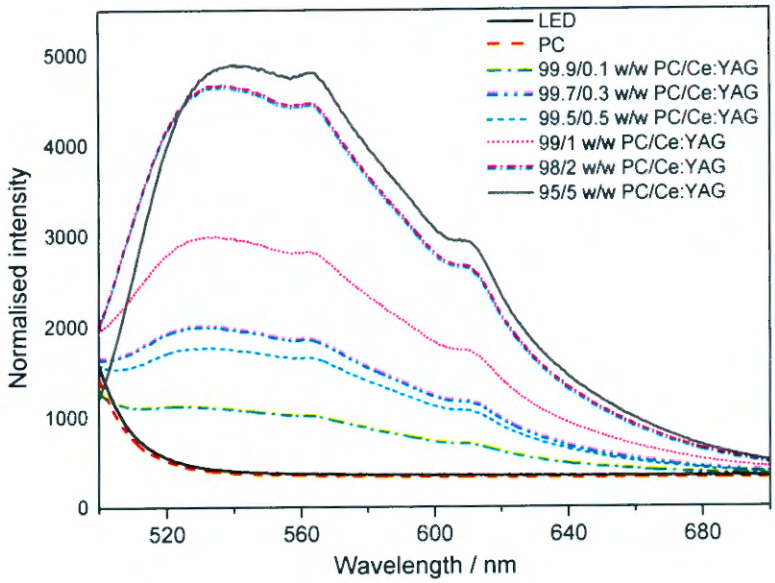

Figure 6.17 Emission spectra of PC and PC/Ce:YAG composites obtained under blue light

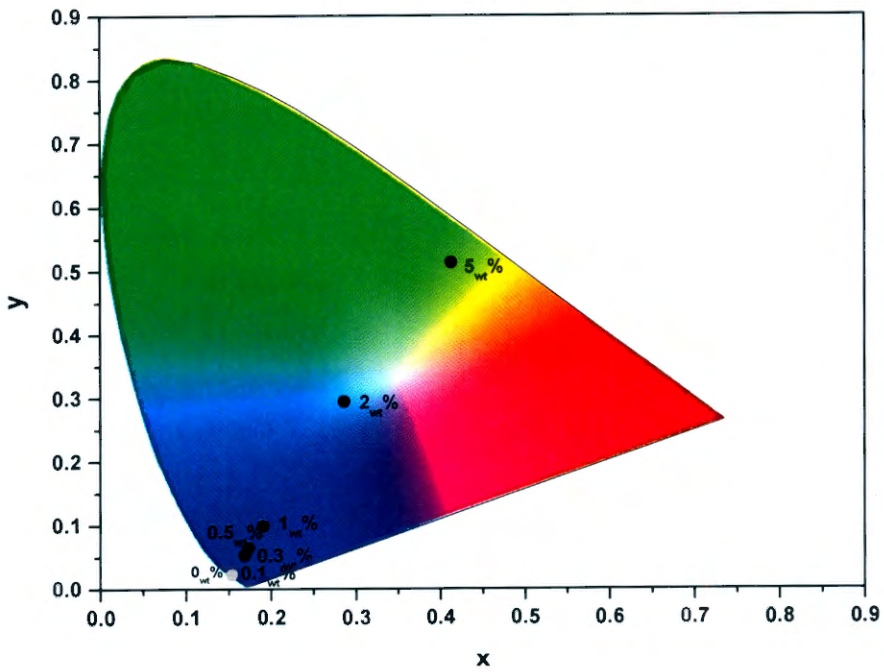

Figure 6.18 Relative CIE 1931 colour space of the resulting light

6.8 Conclusions

In this chapter we investigated the morphology, structure, thermo mechanical, thermal degradation kinetics and also the luminescence properties of PC/Ce:YAG composites prepared by melt compounding as a function of Ce:YAG content ranging from 0.1 to 5 wt.%. The transparancies of the samples decreased with increasing filler content due to the presence of larger and more agglomerated Ce:YAG particles. A weak electron donor-acceptor interaction between the carbonyl oxygen lone pair of PC and the yttrium cation (Y^{3+}) on the surface of Ce:YAG, was established. The storage and loss modulus were higher for the composite samples over the whole investigated temperature range, but the extent of increase could not be related with the amount of filler in the respective samples. The glass transition temperature was not influenced by the presence of filler, and the extent of damping changed inconsistently with the amount of filler in the samples. This supported the notion of a weak interaction between the polymer and filler. The presence of Ce:YAG accelerated the degradation process of PC, independent of the filler content, and as a result less activation energy was needed to initiate the degradation process of PC in these composites. Combination of blue LEDs with the composites loaded with >1 wt.% Ce:YAG gave off light in the blue region, while with the 2 wt.% Ce:YAG composite it gave off light in the white region, which makes the latter suitable for applications in white light emitting diodes.

6.9 References

1. S. Nishiura, S. Tanabe, K. Fujioka, Y. Fujimoto. Properties of transparent Ce:YAG ceramic phosphors for white LED. Optical Materials 2011; 33:688-691. DOI: 10.1016/j.optmat.2010.06.005
2. K.A. Vijayalakshmi, M. Melala, C.P. Yoganand, K.N. Pandiyaraj. Studies on modification of surface properties in polycarbonate (PC) film induced by DC glow discharge plasma. International Journal of Polymer Science 2011; 2011:1682-9422. DOI: 10.1155/2011/426057

3. H.M. EI Ghanem, S.A. Saqa'n, M. AI Saadi, S.M. Abdul Jawad. On the electrical and optical properties of polycarbonate/$MnCl_2$composite. Journal of Modern Physics 2011; 2:1553-1559.
DOI: 10.4236/jmp.2011.212189
4. T.E. Motaung, M.L. Saladino, A.S. Luyt, D.C. Martino. The effect of silica nanoparticles on the morphology, mechanical properties and thermal degradation kinetics of polycarbonate. Composites Science and Technology 2012; 73:34-39.
DOI: 10.1016/j.compscitech.2012.08.014
5. S. Suin, N.K. Shrivastava, S. Maiti, B.B. Khatua. Phosphonium modified organoclay as potential nanofiller for the development of exfoliated and optically transparent polycarbonate/clay nanocomposites: Preparation and characterisation. European Polymer Journal 2013; 49:49-60.
DOI: 10.1016/j.eurpolymj.2012.10.004
6. T.E. Motaung, A.S. Luyt, M.L. Saladino, E. Caponetti. Study of morphology, mechanical properties, and thermal degradation of polycarbonate-titania nanocomposites as function of titania crystalline phase and content. Polymer Composites 2013; 34:164-174.
DOI: 10.1002/pc.22389
7. T.E. Motaung, M.L. Saladino, A.S. Luyt, D.C. Martino. Influence of the modification, induced by zirconia nanoparticles, on the structure and properties of polycarbonate. European Polymer Journal 2013; 49:2022-2030
DOI: 10.1016/j.eurpolymj.2013.04.019
8. J. Bozi, Z. Czegeny, E. Meszaros, M. Blazso. Thermal decomposition of flame retarded polycarbonate. Journal of Analytical and Applied Pyrolysis 2007; 79:337-345.
DOI: 10.1016/j.jaap.2007.01.001
9. B.N. Jang, C.A. Wilkie. The thermal degradation of bisphenol A polycarbonate in air. Thermochimica Acta 2005; 426:73-84.
DOI: 10.1016/j.tca.2004.07.023
10. C. Puglisi, L. Sturiale, G. Montaudo. Thermal decomposition processes in aromatic polycarbonates investigated by mass spectrometry. Macromolecules 1999; 32:2194-2203.
DOI: 10.1021/ma981238z

11. B. Singh, N. Sharma. Mechanistic implications of plastic degradation. Polymer Degradation and Stability 2008; 93:561-584.
DOI: 10.1016/j.polymdegradstab.2007.11.008

12. S. Maiti, N.K. Shrivastava, S. Suin, B.B. Khatua. A strategy for achieving low percolation and high electrical conductivity in melt-blended polycarbonate (PC)/multiwall carbon nanotube (MWCNT) nanocomposites: Electrical and thermo-mechanical properties. eXPRESS Polymer Letters 2013; 7:505-518.
DOI: 10.3144/expresspolymlett.2013.47

13. Y. Feng, B. Wang, F. Wang, G. Zheng, K. Dai, C. Liu, J. Chen, C. Shen. Effects of modified silica on morphology, mechanical property, and thermostability of injection-molded polycarbonate/silica nanocomposites. Journal of Reinforced Plastics & Composites 2014; 33:911-922.
DOI: 10.1177/0731684413520188

14. M.C. Gupta, S.G. Viswanath. Role of metal oxide in the thermal degradation of bisphenol A polycarbonate. Journal of Thermal Analysis 1996; 46:1671-1679.
DOI: 10.1021/ie9700167

15. Y. Imai, A. Terahara, Y. Hakuta, K. Matsui, H. Hayashi, N, Ueno. Transparent (bisphenol A carbonate)-based nanocomposites with high refractive index nanoparticles. European Polymer Journal 2009; 45:630-638.
DOI: 10.1016/j.eurpolymj.2008.12.031

16. F.J. Carrion, J. Sanes, M.D. Bermudez. Influence of ZnO nanoparticles filler on the properties and wear resistance of polycarbonate. Wear 2007; 262:1504-1510.
DOI: 10.1016/j.wear.2007.01.016

17. S. Vyazovkin. A unified approach to kinetic processing of nonisothermal data. International Journal of Chemical kinetics 1996; 28:95-101.
DOI: 10.1002/(SICI)1097-4601(1996)28:2<95::AID-KIN4>3.0.CO;2-G

18. T.E. Motaung, A.S. Luyt., F. Bondioli, M. Messori, M.L. Saladino, A. Spinella, G. Nasillo, E Caponetti. PMMA-titania nanocomposites: Properties and thermal degradation behaviour. Polymer Degradation and Stability 2012; 97:1325-1333.
DOI: 10.1016/j.polymdegradstab.2012.05.022

19. T.E. Motaung, A.S. Luyt, M.L. Saladino, D. Chillura Martino, E. Caponetti. Morphology, mechanical properties and thermal degradation kinetics of PMMA-zirconia composites prepared by melt compounding. eXPRESS Polymer Letters 2012; 6:871-881.
DOI: 10.3144/expresspolymlett.2012.93

20. Q. Dong, C. Gao, Y. Ding, F. Wang, B. Wen, S. Zhang, T. Wang, M. Yang. A polycarbonate/magnesium oxide nanocomposite with high flame retardancy. Journal of Applied Polymer Science 2011; 123:1085-1093.
DOI: 10.1002/app.34574

21. V.S. Aigbodion, S.B. Hassan, C.U. Atuanya. Kinetics of isothermal degradation studied by thermogravimetric data: Effect of orange peels ash on thermal properties of high density polyethylene. Journal of Materials and Environmental Science 2012; 3:1027-1036.
ISSN: 2028-2508

22. Y.H. Hu, C.Y. Chen, C.C. Wang. Viscoelastic properties and thermal degradation kinetics of silica/PMMA nanocomposites Polymer Degradation and Stability 2004; 84:545-553.
DOI: 10.1016/j.polymdegrastab.2004.02.001

23. R. Mintao. Z. Dayu, W. Sizhu, W. Gang. Thermal decomposition of poly(ethylene terephthalate)/mesoporous molecular sieve composites. Frontiers of Chemieal Engineering in China 2007; 1:50-54.
DOI: 10.1007/s11705-007-0010-z

24. R. Pilawka, S. Paszkiewicz, Z. Roslaniec. Thermal degradation kinetics of PET/SWCNTs nanocomposites prepared by the in situ polymerization. Journal of Thermal Analysis and Calorimetry 2014; 115:451-460.
DOI: 10.1007s10973-013-3239-4

25. J. Chen, Z. Deng, Z. Liu, Lin, H. Lan, D. Chen, B. Fei, C. Wang, F. Wang, Q. Hu, Y. Cao. Optical enhancement brought by doping Gd^{3+} ions into Ce:YAG ceramics for indoor white light-emitting diodes. Optics Express 2015; 23:292-298.
DOI: 10.1364/OE.2300A292

26. M.L. Saladino, A. Zanotto, D.C. Martino D, A. Spinella, G. Nasillo, E. Caponetti. Ce:YAG nanoparticles embedded in a PMMA matrix: Preparation and characterization. Langmuir 2010; 26:13442–13449.
DOI: 10.1021/la9042809

Chapter 7: Conclusions

The aim of this study was to prepare polymer composites from poly(methyl methacrylate) (PMMA) and polycarbonate (PC) with mesoporous silica (MCM-41) and yttrium aluminium garnet doped with cerium (Ce:YAG) with various contents in the range of 0.1 to 5 wt.%. The composites were prepared through melt compounding and the morphology, polymer-filler interactions, impact and dynamic mechanical properties, and thermal degradation kinetics were investigated.

We did manage to address a number of the research questions outlined in Chapter 1. The first objective of the study was to investigate the effect of MCM-41 incorporation on the properties of poly(methyl methacylate) and polycarbonate. We established that the dispersion of MCM-41 and the trapping of the polymer chains in the pores of the filler had a significant influence on the properties of the polymer composites. The MCM-41 particles were well dispersed in both polymers at low loadings, which also helped in maintaining the transparency of the polymers, but at high filler loadings large agglomerates were observed with the resultant loss in transparency. We did establish that it was possible for part of the polymer chains in both polymers to be trapped in the pores of the filler, which contributed to the improvement in the determined properties.

We also established that the impact strength and the dynamic mechanical properties of the polymers increased with the addition of the filler, but the level of impact strength improvement depended on the filler content in the polymer. At high filler loadings the modulus of the polymers increased, but the composites had much lower impact strengths; the optimum improvement in the impact strength was observed at 1 wt.% filler content. A hydrogen bonding interaction was established between the carbonyl groups of the two polymers and the silanol group that is found on MCM-41, which contributed to the improvement in the properties. However, this interaction was obviously not strong enough to prevent agglomeration of the MCM-41 particles at higher filler contents. The thermal stability of both polymers increased with the addition of MCM-41, which was mainly due to a delayed mass loss as a result of the trapping of the volatile degradation products in the pores of MCM-41.

The second objective of the study was to investigate the effect of Ce:YAG incorporation on the properties of PMMA and PC. We found that the filler particles were not too well dispersed in both polymers at low loadings, and easily agglomerated at high filler loadings. The agglomerates, however, were fairly well dispersed in both polymers. The presence of the filler at low loadings therefore had little influence on the impact properties of PMMA and we only observed an increase at higher filler loadings, which reached a limiting value at 5 wt.% Ce:YAG content, probably because of severe agglomeration at these filler loadings. We established that the interaction between both polymers and the filler was through an electron donor-acceptor interaction between the carbonyl oxygen lone pair and the yttrium cation (Y^{3+}). However, PMMA showed stronger interaction than PC, which can be attributed to the carbonyl oxygen on PMMA having a stronger partially negative charge because the carbonyl oxygen on PC has two other oxygen atoms bonded to the carbonyl carbon compared to only one in PMMA. The presence of filler did not significantly increase the thermal stability of the PC, while an observable increase in thermal stability was only observed at higher filler loadings for the PMMA composites. This can be due to the stronger interaction between Ce:YAG and PMMA and/or its degradation volatiles. The degradation products of PC are carbon dioxide, phenol and bisphenol A, most of which should not strongly interact with Ce:YAG, while that of PMMA is methyl methacrylate, which should interact more strongly with Ce:YAG through its carbonyl oxygen. We also established that, at certain filler contents, both the PMMA/Ce:YAG and PC/Ce:YAG composites can be used in white light emitting diodes.

Due to limited research results on mesoporous silica with glassy polymers, this research can be extended by using other types of mesoporous silica, e.g. cubic MCM-48, hexagonal SBA 15, and mesocellular silica foam (MSU-F) to prepare composites using melt compounding, and to study the influence of the frame structure and pore size of the particles on the polymer-filler interactions and resultant properties. The dispersion of the nanofiller and its interaction with the polymer matrix is closely related to the properties of the composite, so the modification of the surface of the mesoporous silica with silane coupling agents and its influence on the polymer-filler interactions and resultant properties can also be investigated. It will further be interesting to see if the new type of filler, mesoporous carbon FDU-15, will have a different influence on the properties of the composites.

ACKNOWLEDGEMENTS

Firstly I would like the thank the **Almighty God**, for putting methrough this journey and giving me the strength and the courage to work hard even when I felt like giving up on everything, He always showed me the light at the end of a very dark and long tunnel. Without Him this work will not have been possible.

I would like to thank my supervisor, **Prof. Adriaan Stephanus Luyt,** for his great efforts to explain things clearly and simply, and his guidance during my research. I express my deep sense of gratitude for his guidance, and constant support all through the course of the study. Throughout my thesis-writing period, he provided encouragement, advice, and good ideas. Words cannot begin to express my gratitude, I felt like giving up a number of times but he showed me that there is always room to learn, most importantly learn from my own mistakes and I will forever be grateful.

I would also like to thank **Dr Maria Luisa Saladino** for a very beneficial collaboration, I learned a lot from you.

Special thanks to **Marlize Jackson,** thank you very much for always being the person to pick me back up when I felt like I could not get up anymore. You understood me in more ways that I never thought anyone would, thank you for always taking a moment of your time and listen to my problems and frustrations throughout the year. May god bless you even more, thank you. To my best friend **Mohanuwa Mofokeng**, it's been more than ten years and I am grateful to still have you in my life as a friend and a sister, I thank God for that. Every pain, smile and tear that I shared with you made me a stronger person.

The credit must be given to my parents and the whole Sibeko family (MAZIYA).All sense of gratitude to all my siblings Madika, Mantwa, Matseko, Manakedi, Tello, Tseko, Setjhaba, Mochakela and tebello. I am nothing without each and every one of you.

Sense of gratitude to all my fellow polymer science research group and former colleagues: Dr. Duško Dudić, Dr Julia Puseletso Mofokeng, Dr Thabang Hendrica Mokhothu, Dr Sefadi shale, Dr Mochane, Mr. Tyson Mosoabisane, Mrs. Zanele Clarke, Mr. Tsietsi Tsotetsi, Dr. Nomampondomise Molefe, Mrs Madimabe, Mr. Kgotso Mpitso, Ms. T.A. Makhetha, Ms Thandi Patricia Gumede, Mr Motloung Bennie, Mr. Mfiso Mngomezulu for all their help, support, interest and valuable inputs.